Geosynthetics '99

"Specifying Geosynthetics and Developing Design Details"

GEOSYNTHETICS 99 CONFERENCE
Boston, Massachusetts USA

Conference Proceedings

April 28-30, 1999

Organized by:

IFAI
Industrial Fabrics Association International

NAGS
North American Geosynthetics Society

GMA
Geosynthetic Materials Association

under the auspices of
IGS
International Geosynthetics Society

SPONSORED BY

Table of Contents

Testing and Design of Geosynthetics in Roads II

Slopes and Embankments

Interface Friction Testing I

PERFORMANCE OF SPREAD FOOTINGS ON SUBGRADES REINFORCED WITH GEOGRIDS AND GEOJACKS

S. M. MERRY
University of Utah, Salt Lake City, USA
C. LI
University of Utah, Salt Lake City, USA
E. C. LAWTON
University of Utah, Salt Lake City, USA

ABSTRACT

Biaxial geogrids have been shown to be an effective method of improving the ultimate bearing capacity of cohesionless soils. However, the amount of settlement required to mobilize tension in the geogrid is significant and hence, there is little difference in the initial portion of the bearing pressure versus settlement curve for unreinforced sands and those reinforced with biaxial geogrids. For example, Adams and Collin (1997) showed that using a single layer of reinforcement, the pressure producing a settlement of 0.50% of the footing diameter, B is between 92% and 119% of that for the unreinforced case. In this study, a newly developed strain-controlled loading system was used to investigate the performance of cohesionless soil reinforced multi-oriented geosynthetic inclusions, or geojacks placed over a biaxial geogrid. The investigation used 152-mm diameter rigid footings in a test 1.37-m diameter test pits. The soil was a uniformly graded 16-30 sand (>98% passing No. 16 sieve, <1% passing No. 30 sieve). As this is a preliminary study prior to full-scale tests, the geogrid-type, depth of footing (not presented herein), and number of layers of reinforcement. The results indicate that the combined reinforcement of biaxial geogrids and geojacks improves the ultimate bearing capacity even beyond that obtained with a geogrid alone. Additionally, the settlement required to mobilize tension in the geogrid (and thereby enhance performance of the foundation system) is substantially reduced. Specifically, the pressure required to produce a settlement of 0.50% of the footing diameter, B is 230% of that using a geogrid alone and about 300% of that measured in the unreinforced case.

INTRODUCTION

Rising land costs and decreasing availability of areas for urban infill has established the situation that previously undeveloped areas are now being considered for the siting of new facilities. However, these undeveloped areas often possess weak underlying foundation materials – a situation that presents interesting design challenges for geotechnical engineers. To avoid the high cost of deep foundations, modification of the foundation soil or the addition of a structural fill is essential.

Binquet and Lee (1975a, 1975b) investigated the mechanisms of using reinforced earth slabs to improve the bearing capacity of granular soils. They model tested strip footings on sand foundations reinforced with wide strips cut from household aluminum foil. An analytical method for estimating the increased bearing capacity based on the tests was also presented. Fragaszy and Lawton (1984) also used aluminum reinforcing strips and model strip foundations to study the effects of density of the sand and length of reinforcing strips on bearing capapcity. Several authors also studied strip foundations but reinforced with different materials such as steel bars (Milovic, 1977; Bassett and Last, 1978; Verma and Char, 1986), steel grids (Dawson and Lee, 1988; Abdel-Baki et al. 1993), geotextiles (Das, 1988), and geogrids (Milligan and Love, 1984, 1985; Khing et al. 1993; Ismail and Raymond, 1995). Other researchers adopted circular (Rea and Mitchell, 1978; Haliburton and Lawmaster, 1981; Carroll et al. 1987; Kazerani and Jamnejad, 1987), square (Akinmusuru and Akinbolade, 1981; Guido et al. 1985, 1986, 1987; Guido and Christou, 1988; Adams and Collin, 1997), or rectangular footings (Omar et al. 1993; Yetimoglu et al. 1994).

All of these researchers concluded that reinforcement increased the bearing capacity and reduced the corresponding settlement of the foundations compared to the unreinforced soil. However, it was also realized that an initial horizontal and vertical movement of the reinforcement is needed to mobilize the reinforcing strength. Hence, the ultimate bearing capacity of the reinforced earth would be increased but the initial settlement at small loads still could not be avoided. This is important as the design of foundation systems are usually controlled by limiting the expected settlements, which are generally about three to five percent of the settlement corresponding to the ultimate bearing capacity. Within this range, the traditional reinforced methods cannot develop their strength sufficiently and consequently the observed improvement in performance has been limited. For example, Adams and Collin (1997) showed that using a single layer of reinforcement, the pressure producing a settlement of 0.50% of the footing diameter, B is between 92% and 119% of that for the unreinforced case.

The interaction between the geogrid and soil is very complex. Jewell et al. (1985) identified three main mechanisms of interaction between soils and geogrids: (1) soil shearing on plane surfaces of the grids, (2) soil bearing on lateral surfaces of the grids, and (3) soil shearing over soils through the apertures of the grids. The first two are the skin friction and passive pressure resistance of the contact area between soils and geogrids. The third is the interfacial shear on the surface of a rupture zone created during shearing. The relative size of soil particles to the grid apertures has significant influence on the size of the rupture zone. As the ratio of this relative size (soil/geogrid) increases, the size of the rupture zone increases. Hence, the type of biaxial geogrid that should be used is dependent on the grain size distribution of the soil that will be placed around it. When supplementing the reinforcing system with geojacks, the size of the aperture depends on the size of the geojacks.

To enhance the performance of geogrid-reinforced foundation systems under small to medium loads, the geogrids were supplemented with multi-oriented geosynthetic inclusions, or geojacks (Lawton and Fox 1992; Fox and Lawton 1993; Lawton et al. 1992; Lawton et al. 1995). Figure 1 shows a close-up of a single geojack, which has a typical outside dimension of 25.4 mm (1 in). Geojacks, which were first introduced in 1990, are made with a hot-mold injection process, and can be made of almost any material that can be injection molded. Due to their high macro stiffness, geojacks made from a combination of

PP and fiberglass were used in this study. Previous studies using a layer of geojacks as the sole form of reinforcement beneath a roadway subgrade showed a decrease in rutting potential and settlements (Lawton and Fox, 1992; Lawton et al. 1992, 1995). While the exact nature of how the geojacks improve the performance is not well understood, it appears that tensile forces in the geogrid are induced at smaller deformations which allows them to be more effective at low load levels.

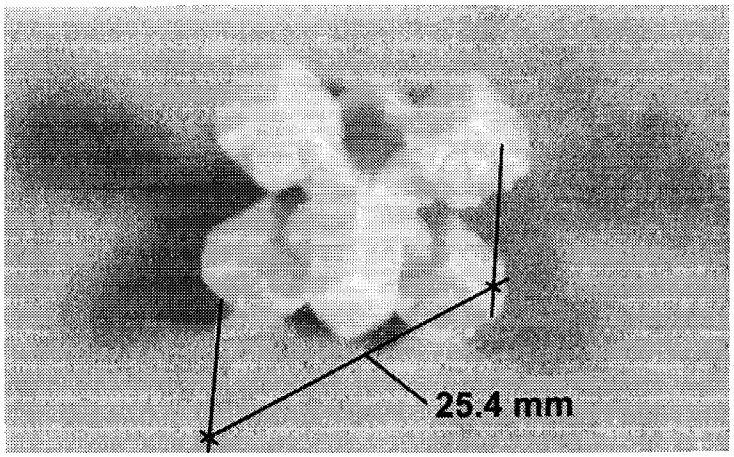

Figure 1 Detail of a single polypropylene-fiberglass geojack

MATERIAL PROPERTIES

Tests were performed on a uniformly graded 16-30 sand (>98% passing No. 16 sieve, <1% passing No. 30 sieve). Uniform sand was chosen to help control the density and fabric between tests. Drained triaxial (CD) tests and direct shear tests provided friction angles, ϕ in the range of 34° to 37°. Gravel used in one of the tests consisted of approximately 20-mm diameter, uniform, subangular particles.

Three punched and drawn, polypropylene (PP) biaxial geogrids were evaluated. Geogrid A had a nominal aperture size of 25.7-mm x 36.1-mm and a rib dimension of 3.1-mm, geogrid B had a nominal aperture size of 25.8-mm x 36.0-mm and a rib dimension of 3.1-mm, and geogrid C had a nominal aperture size of 33.0-mm x 33.0-mm and a rib dimension of 3.1-mm. Quality assurance and control results obtained from the manufacturer for these geogrids are shown in Table 1. The machine direction test results are designated as "MD", while the cross-machine direction results are designated as "XMD".

Table 1 Manufacturing quality control data on polypropylene geogrid used in this study

Geogrid	Ultimate Tensile Strength (kN/m) MD GRI-GG1	Ultimate Tensile Strength (kN/m) XMD GRI-GG1	Tensile @ 5% Strain (kN/m) MD GRI-GG1	Tensile @ 5% Strain (kN/m) XMD GRI-GG1	Tensile @ 2% Strain (kN/m) MD GRI-GG1	Tensile @ 2% Strain (kN/m) XMD GRI-GG1
A	20.1	30.7	13.4	22.0	7.0	11.0
B	13.1	20.1	9.1	15.4	4.8	7.8
C	13.5	16.1	1.2*	2.0*	5.5	7.4

* 0.5% strain

EXPERIMENTAL SET-UP

All tests were performed using the Geotechnical Load Frame at the University of Utah. The test equipment configuration can be seen in Figure 2. This system is capable of vertical loads of about 180-kN (40-kips). Although this study only provided static loads, this system can provide cyclic loads of more than one cycle per second at a full 150-mm (6-in) actuator displacement. Significantly higher frequencies are obtainable at smaller actuator displacements. The vertical load is controlled by a hydraulic actuator that is controlled with a high-performance hydraulic servo valve. The servo valve is precisely controlled with the use of closed-loop feedback at a frequency of 250 Hz by the process control software. The axial load is monitored with two electronic load cells – a 220-kN (50-kips) capacity load cell for larger loads and a 22-kN (5-kips) capacity load cell for higher precision at smaller loads. Axial deformations are monitored with a linear variable distance transformer (LVDT) mounted on the load frame. Control of the system is performed by Validyne Engineering signal conditioners, 12-bit resolution A/D and D/A cards, and a Pentium computer running Automated Testing System (ATS) software (Sousa and Chan, 1991).

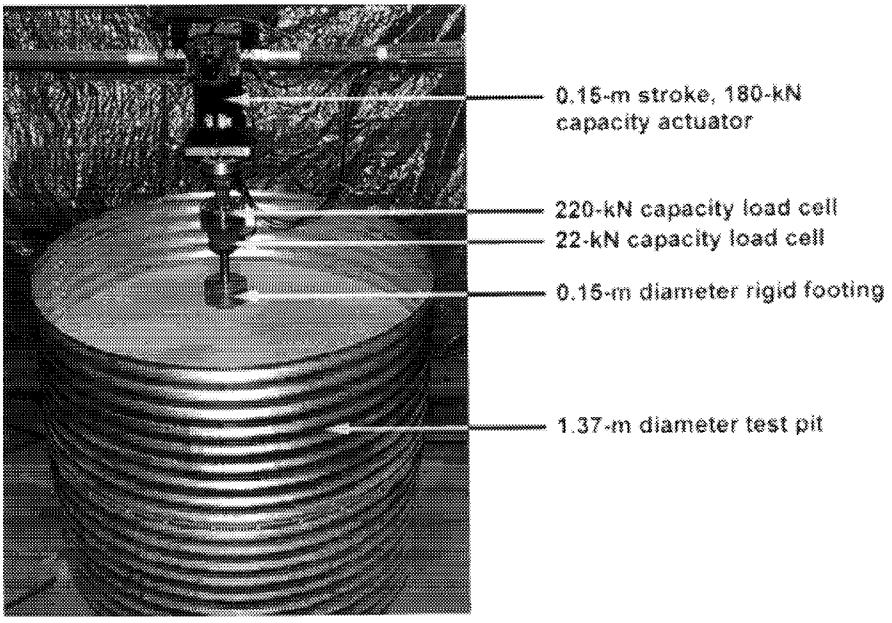

Figure 2 Strain-controlled loading system used in this study

The test pit consisted of a 1.37-m (54-in) diameter, 1.22-m (48-in) high steel drum. Using a 0.15-m (6-in) diameter (B) rigid steel footing, this test pit has a depth of more than 9B and an overall width of more than 8B. Hence, the influence of the boundaries should be minimal. Additionally, an axisymmetric system was chosen so that subsequent numerical studies will be simplified. Prior to beginning a test, the test pit was completely emptied. Sand was then uniformly deposited in the pit by hand using large scoops. This method was used to provide reasonable consistency in the void ratio, density, and fabric of the sand for successive tests. Displacement-controlled loading was performed at a constant rate of 2.5-mm (0.1-in) per minute. Data was obtained at a rate of 2 Hz for the duration of the test.

All tests were completed with the depth of the footing, D_f, equal to one-half of the footing diameter, B, the layer of geogrid reinforcement was 57.2 mm (2.25 in) below the footing (Figure 3a). Multiple layers of geogrid (where used) were separated by 50.8 mm (2.0 in). A full, but single, layer ($\cong$ 4,000 geojacks/m^2 or $\cong$ 370 geojacks/ft^2 was placed randomly on top of the geogrid and then the soil was backfilled over the reinforcement as is typically performed with geogrids alone. The geojacks have an outside dimension of 25.4 mm (Figure 1). Hence, the distance between the geojacks and the bottom of the footing remains at about 25 mm. Other than placing temporary weights around the perimeter of the geogrid to make sure it remained flat, no effort to prestretch the geogrid was made (Figure 3b). After backfilling with sand, the sand was leveled off with a screed and the footing brought down into contact with the surface. Contact was verified both visually and by monitoring the output of the load cells. After this, backfilling was continued until being leveled off at the final surface (Figure 3c). At this point, the data acquisition files were initiated and displacement-controlled loading began as previously described. Loading continued through failure (Figure 3d).

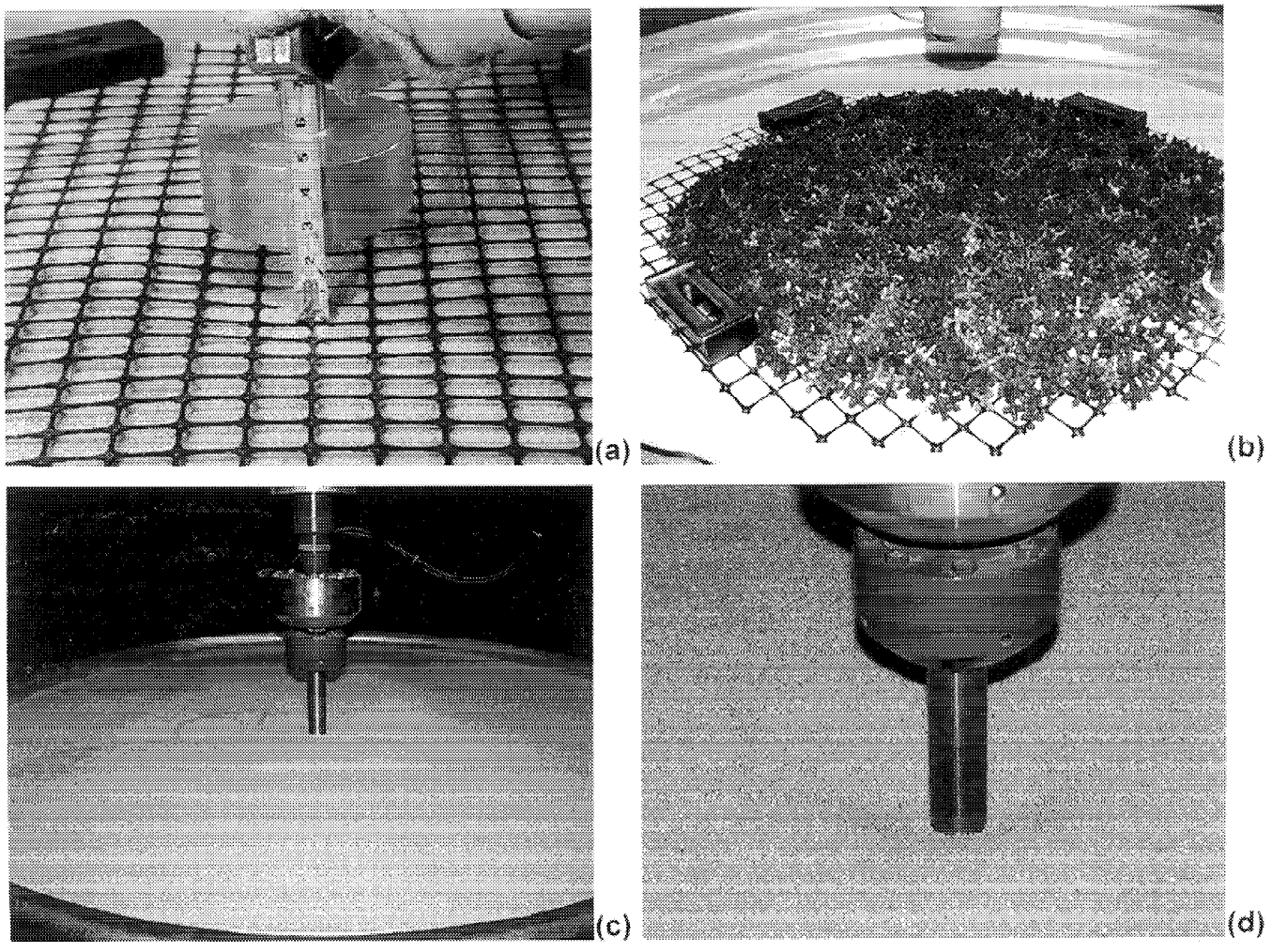

Figure 3 (a) placement of geogrid and proximity to footing above, (b) placement of geojacks on top of biaxial geogrid in 1.37-m (54-in) diameter test pit (footing is not shown, weights are to hold down geogrid and are removed as soil is backfilled), (c) system prior to initiating loading, and (d) at failure

EXPERIMENTAL RESULTS

Figure 4 shows the experimental results from varying the geogrid type. It is seen that a combination of Geogrid A and geojacks provided the greatest performance enhancement, and that this enhancement was provided at all deformation levels (e.g., initial and ultimate). This geogrid (Geogrid A) had the same aperture size as Geogrid B, but has a significantly stiffer stress-strain response (see Table 1). The geogrid with the lowest performance was Geogrid C, which had approximately the same stiffness as Geogrid B, but a different aperture. Also seen in Figure 4 is the unreinforced soil, which actually had a better initial performance than the soil reinforced with Geogrid C and geojacks. While it would seem that any reinforcement would provide some amount of improvement, it is evident that the effectiveness of the system at low loads relates to the size and shape of the aperture. It is likely that the size of the aperture of Geogrid C was too big for the size of the geojacks. This phenomenon was continually observed in four tests completed with Geogrid C and geojacks and does not appear to be a function of system preparation methods. Moreover, this indicates that the geogrid and the geojacks are a dependent system. Recommendations on the optimal configuration would be premature and requires further study.

Figure 5 shows experimental results where other parameters were evaluated using only Geogrid A. As expected, the unreinforced case is seen to have the lowest performance. Using a bilinear approach, the ultimate bearing capacity, q_{ult}, was interpreted to be in the range of 100 to 110 kPa (2.1 to 2.3 ksf). Using a friction angle of 36°, this is in reasonable agreement with a value of q_{ult} of 115 kPa (2.4 ksf) calculated using Meyerhof's method (1951). Using only Geogrid A for reinforcement, the observed ultimate bearing capacity increased to about 140 kPa and the addition of a layer of uniform (10-mm = 0.39-in diameter) gravel on top of the geogrid provided additional enhancement (q_{ult} = 240 kPa = 5 ksf). Moreover, up to a deformation of about δ/B = 0.5% (settlement = 0.77 mm = 0.03 in), all three of these cases have approximately the same pressure-settlement curve. This is more clearly shown in Figure 6 where the results in the beginning of the test have been magnified.

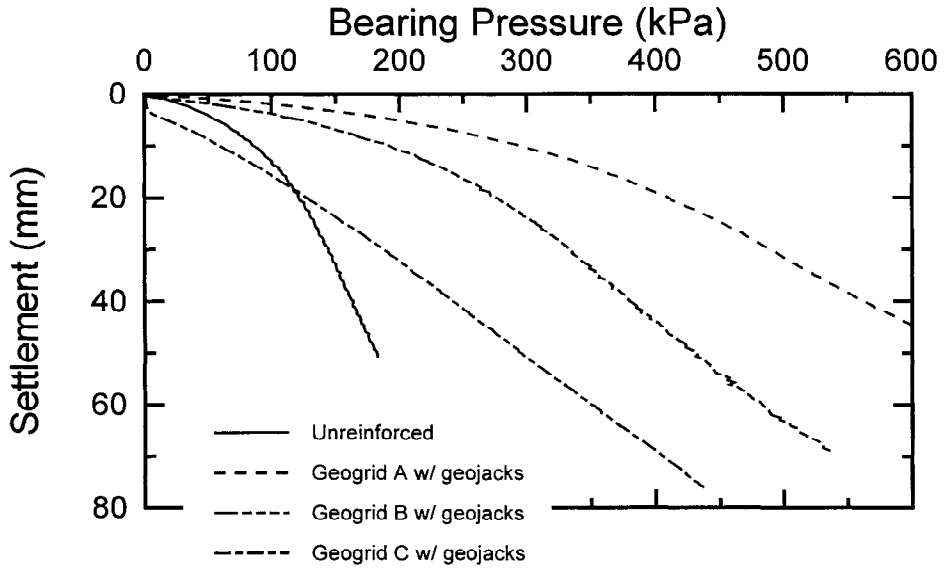

Figure 4 Results showing effect of using different biaxial geogrids

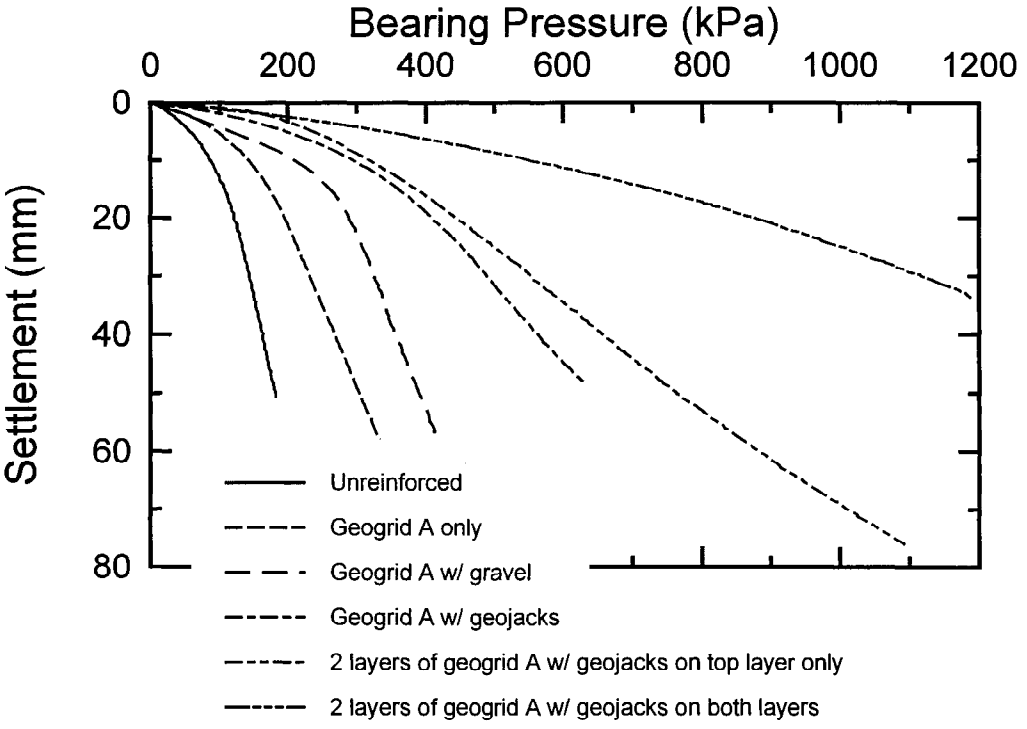

Figure 5 Experimental results showing bearing pressure vs. settlement where Geogrid A was the primary reinforcement

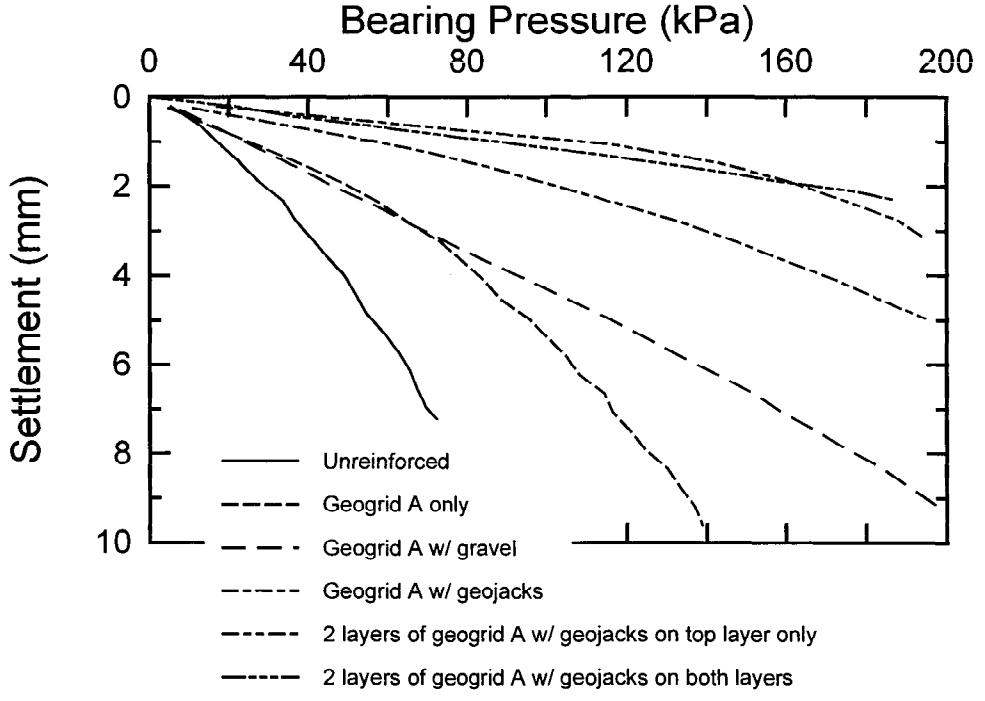

Figure 6 Detail showing initial portion of curves of bearing pressure vs. settlement where Geogrid A was the primary reinforcement

However, when the geogrid reinforcement was supplemented with geojacks, not only did the observed ultimate bearing capacity increase substantially, but the performance was also significantly enhanced. Using one layer of Geogrid A supplemented with geojacks, the bearing pressure at a deformation of $\delta/B = 0.5\%$ (settlement = 0.77 mm = 0.03 in) is 3 times greater than the unreinforced case (42.4 kPa = 0.89 ksf compared to 14.1 kPa = 0.29 ksf). As expected, using multiple layers of reinforcement provided additional enhancement. With two layers of Geogrid A and geojacks, the bearing pressure at a deformation of $\delta/B = 0.5\%$ was 4.6 times greater than the unreinforced case (65.6 kPa = 1.4 ksf compared to 14.1 kPa = 0.29 ksf). Table 2 summarizes the bearing pressures for each case at deformations of 0.5%, 1%, 2% and 5%. Except when multiple layers are used, supplementing the reinforcement with geojacks improved the performance of the foundation system. In the case of multiple layers, Table 2 suggests that the performance is better when the geojacks are not used on the second layer of geogrid. However, over the initial portion of the curves, these two pressure-settlement curves lie almost on top of each other (see Figure 6) and hence, this result needs to be substantiated with further data.

Table 2 Summary of bearing pressures at different settlements

Case	Bearing Pressure @ 0.5% B (kPa)	Bearing Pressure @ 1% B (kPa)	Bearing Pressure @ 2% B (kPa)	Bearing Pressure @ 5% B (kPa)
Unreinforced soil	14.2	23.4	39.6	73.9
Geogrid A only	18.4	38.7	69.4	122.0
Geogrid B only	5.3	29.6	57.4	101.5
Geogrid C only	2.8	5.1	12.8	49.2
Geogrid A w/ gravel	18.7	35.9	70.2	169.9
Geogrid A w/ geojacks	42.4	83.5	140.9	253.8
2 layers Geogrid A w/ geojacks on top only	81.0	144.8	192.7	281.0
2 layers Geogrid A w/ geojacks both layers	65.6	131.1	233.0	459.2

CONCLUSIONS

Facilities constructed with spread footings on marginal foundation soils may be expected to undergo fairly large deformations and hence, modification of the foundation soil is essential. Geogrid reinforcement has been shown to increase significantly the bearing capacity of structural fills. However, allowable settlements, and not ultimate bearing capacity, generally dictate the design of spread foundations on cohesionless soils. To mobilize tensile forces in the geosynthetic material, vertical movements beneath the footing must occur and hence, there was often little or no improvement in the performance of these reinforced soils at design or working loads. This study used strain-controlled laboratory tests to evaluate the performance of spread footings overlying cohesionless soil foundations reinforced with and without the use of geogrids supplemented with geojacks. It was discovered that the

performance of geogrid-reinforced foundation systems is improved when supplemented with multi-oriented geosynthetic inclusions, or geojacks.

The results of these tests indicated that the use of geojacks on top of the geogrid substantially improved the performance of the soil foundation and that the combination of geogrid and geojacks performed better than a combination of geogrid and gravel. This increased performance was observed not only at ultimate capacity, but also at smaller loads. This is significant because foundations in actual design situations are not taken to ultimate capacity, but to some fraction of ultimate (typically less than 1/3 for cohesionless soils).

Three different polypropylene geogrids as the primary reinforcement were evaluated. Two of these geogrids had about the same aperture and rib dimensions (Geogrids A and B). The third (Geogrid C) had about the same stiffness as the second (Geogrid B) but it also had a larger aperture in both the MD and XMD. The results indicated that the geogrid with the highest stiffness and smallest aperture had the best performance, both with and without geojacks supplement. Moreover, the pressure required to induce a given level of deformation increases significantly when geojacks are used. Specifically, using geojacks with Geogrid A, the pressure required to produce a settlement of 0.50% of the footing diameter, B is 230% of that using a geogrid alone and about 300% of that measured in the unreinforced case.

FUTURE STUDIES

Because the effects of scaling and confinement are significant, this technology must be verified with data from full-scale tests. As these tests will be relatively expensive, further laboratory tests are now underway to conduct a more exhaustive study of this topic including a further study of geogrid type, stiffness, and geometry. Furthermore, while the exact nature of how the geojacks improve the performance is not well understood, it appears that tensile forces in the geogrid are induced at smaller deformations. This hypothesis will be evaluated using geogrids instrumented with strain gages.

ACKNOWLEDGMENTS

Tensar Earth Technologies, Inc. supplied the biaxial geogrids and manufacturing quality control data. Dr. Nathaniel S. Fox provided the geogax used in this study. Their support is gratefully acknowledged. Finally, the authors would like to acknowledge Mr. David Plehn for his help in completing a preliminary study to this research.

REFERENCES

Abdel-Baki, S., Raymond, G.P., and Johnson, P. (1993) "Improvement of the Bearing Capacity of Footings by a Single Layer of Reinforcement," Proceedings, Vol. 2, Geosynthetics '93 Conference, Vancouver, Canada, pp. 407-416.

Adams, M.T., and Collin, J.G. (1997) "Large Model Spread Footing Load Tests on Geosynthetic Reinforced Soil Foundations," Journal of Geotechnical and Geoenvironmental Engineering, ASCE, Vol. 123, No. 1, January, pp. 66-72.

Akinmusuru, J.O., and Akinbolade, J.A. (1981) "Stability of loaded Footings on Reinforced Soil," Journal of Geotechnical Engineering Division, ASCE, Vol. 107, No. GT6, June, pp. 819-827.

Bassett, R.H., and Last, N.C. (1978) "Reinforcing Earth Below Footings and Embankments," Symposium on Earth Reinforcement, ASCE, Pittsburgh, PA, pp. 202-231.

Binquet, J., and Lee, K.L. (1975a) "Bearing Capacity Tests on Reinforced Earth Slabs," Journal of Geotechnical Engineering Division, ASCE, Vol. 101, No. GT12, December, pp. 1241-1255.

Binquet, J., and Lee, K.L. (1975b) "Bearing Capacity Analysis of Reinforced Earth Slabs," Journal of Geotechnical Engineering Division, ASCE, Vol. 101, No. GT12, December, pp. 1257-1276.

Bourdeau, P.L., Pardi, L., and Recordon, E. (1990) "Observation of Soil Reinforcement Interaction by X-Ray Radiography," in Performance of Reinforced Soil Structures, McGown, Yeo, and Andrawes, editors, Thomas Telford Publishing, London, Proceedings of the International Reinforced Soil Conference, British Geotechnical Society, Glasgow, September 10-12, pp. 347-352.

Carroll, R.G., Walls, J.C., and Haas, R. (1987) "Granular Base Reinforcement of Flexible Pavements Using Geogrids," Proceedings, Vol. 1, Geosynthetics '87 Conference, New Orleans, USA, pp. 46-57.

Das, B.M. (1988) "Shallow Foundation on Sand Underlain by Soft Clay with Geotextile Interface," Geosynthetics for Soil Improvement, edited by R. D. Holtz, pp. 112-126.

Dawson, A., and Lee, R. (1988) "Full Scale Foundation Trials on Grid Reinforced Clay," Geosynthetics for Soil Improvement, edited by R. D. Holtz, pp. 127-147.

Fox, N.S., and Lawton, E.C. (1993) "Discontinuous Structural Reinforcing Elements and Methods for Reinforcing and Improving Soils and Other Construction Materials," U.S. Patent No. 5,145,285., issued September 8.

Fragaszy, R.J., and Lawton, E.C. (1984) "Bearing Capacity of Reinforced Sand Subgrades," Journal of Geotechnical Engineering, Vol. 110, No. 10, October, pp. 1500-1507.

Guido, V.A., Biesiadecki, G.L., and Sullivan, M.J. (1985) "Bearing Capacity of a Geotextile-Reinforced Foundation," Proceedings of the Eleventh International Conference on Soil Mechanics and Foundation Engineering, Vol. 3, ISSMFE, pp. 1777-1780.

Guido, V.A., and Chang, D.K., and Sweeney, M.A. (1986) "Comparison of Geogrid and Geotextile Reinforced Earth Slabs," Canadian Geotechnical Journal, Vol. 23, pp. 435-440.

Guido, V.A., and Christou, S.N. (1988) "Bearing Capacity and Settlement Characteristics of Geoweb-Reinforced Earth Slabs," Special Topics in Foundations, edited by B. M. Das, pp. 21-36.

Guido, V.A., Knueppel, J.D., and Sweeney, M.A. (1987) "Plate Loading Tests on Geogrid-Reinforced Earth Slabs," Proceedings, Vol. 1, Geosynthetic '87 Conference, New Orleans, USA, pp. 216-225.

Haliburton, T.A., and Lawmaster, J.D. (1981) "Experiments in Geotechnical Fabric-Reinforced Soil Behavior," Geotechnical Testing Journal, Vol. 4, No. 4, December, pp. 153-160.

Ismail, I., and Raymond, G.P. (1995) "Geosynthetic reinforcement of Granular Layered Soils," Proceedings, Vol. 1, Geosynthetics '95, Nashville, TN, USA, IFAI, St. Paul, MN, USA, pp. 317-330.

Jewell, R.A., Milligan, G.W.E., Sarsby, R.W., and Dubois, D. (1985) "Interaction Between Soil and Geogrids," Polymer Grid Reinforcement, London, pp. 18-30.

Kazerani, B., and Jamnejad, G.H. (1987) "Polymer Grid Cell Reinforcement in Construction of Pavement Structures," Proceedings, Vol. 1, Geosynthetics '87 Conference, New Orleans, USA, pp. 58-68.

Khing, K.H., Das, B.M., Puri, V.K., Cook, E.E., and Yen, S.C. (1993) "The Bearing Capacity of a Strip Foundation on Geogrid-Reinforced Sand," Geotextiles and Geomembranes, Vol. 12, pp. 351-361.

Lawton, E.C., and Fox, N.S. (1992) "Field Experiments on Soils Reinforced with Small Discontinuous Multi-Oriented Geosynthetic Inclusions," Transportation Research Record No. 1369: Advances in Geotechnical Engineering, Transportation Research Board, pp. 44-53.

Lawton, E.C., Khire, M.V., and Fox, N.S. (1992) "Reinforcement of Soils by Multioriented Geosynthetic Inclusions," Journal of Geotechnical Engineering, ASCE, Vol. 119, No. 2, February, pp. 257-275.

Lawton, E.C., Schubach, J.R., Seelos, R.T., and Fox. N.S. (1995) "One Dimensional Compression Characteristics of Artificial Soils Composed of Multioriented Geosynthetic Elements," Transportation Research Record, No. 1474, Transportation Research Board, pp. 73-81.

Meyerhof, G.G., (1951) "The Ultimate Bearing Capacity of Foundations," Geotechnique, vol 2, No. 4, pp. 301-332.

Milligan, G.W.E., Fannini, R.J., and Farrar, D.M. (1986) "Model and Full-scale Tests of Granular Layers Reinforced with a Geogrid," Proceedings, 3rd International Conference on Geotextiles, Vienna, Italy, Vol. 1, pp. 61-66.

Milligan, G.W.E., and Love, J.P. (1984) "Model testing of Geogrids Under an Aggregate Layer in Soft Ground," Proceedings, Symposium on polymer Grid Reinforcement in Civil Engineering, ICI, London, England, 4.2.1-4.2.11.

Milligan, G.W.E., and Love, J.P. (1985) "Model Testing of Geogrids under an Aggregate Layer on Soft Ground," Polymer Grid Reinforcement, London, pp. 128-138.

Milovic, D. (1977) "Bearing Capacity Tests on Reinforced Sand," Proceedings of the 9th International Conference on Soil Mechanics and Foundation Engineering, Vol. 1, Tokyo, Japan, pp. 651-654.

Omar, M.T., Das, B.M., Yen, S-C., Puri, V.K., Cook, E.E. (1993) "Ultimate Bearing Capacity of Rectangular Foundation on Geogrid-Reinforced Sand," Geotechnical Testing journal, Vol. 16, No. 2, June, pp. 246-252.

Rea, C., and Mitchell, J.K. (1978) "Sand Reinforcement Using Paper Grid Cells," Symposium on Earth Reinforcement, ASCE, pp. 644-663.

Schmertmann, J.H. (1970) "Static Cone to Compute Static Settlement Over Sand," Journal of the Soil Mechanics and Foundations Division, ASCE, Vol. 96, No. SM3, May, pp. 1011-1043.

Schmertmann, J.H., Hartman, J.P., and Brown, P.R. (1978) "Improved Strain Influence Factor Diagrams," Journal of Geotechnical Engineering Division, ASCE, Vol. 104, No. GT8, August, pp. 1131-1134.

Sousa, J., and Chan, C.K. (1991) "Computer Applications in the Geotechnical Laboratories of the University of California, at Berkeley," Proceedings, Vol. 1, ASCE Geotechnical Engineering Congress, Boulder, CO, pp. 531-543.

Verma, B.P., and Char, A.N.R. (1986) "Bearing Capacity Tests on Reinforced Sand Subgrades," Journal of Geotechnical Engineering, Vol. 112, No. 7, July, pp. 701-706.

Yetimoglu, T., Wu, J.T.H., and Saglamer, A. (1994) "Bearing Capacity of Rectangular Footings on Geogrid-reinforced Sand," Journal of Geotechnical Engineering, Vol. 120, No. 12, December, pp. 2083-2099.

TENSILE BEHAVIOR OF DAMAGED GEOTEXTILE IN UNCONFINED AND CONFINED CONDITIONS

Y. BOGUSLAVSKIY
POLYTECHNIC UNIVERSITY, BROOKLYN, USA.
S. DRABKIN
POLYTECHNIC UNIVERSITY, BROOKLYN, USA
V. FAYNGOLD
POLYTECHNIC UNIVERSITY, BROOKLYN, USA.

ABSTRACT

In many practical construction applications, geotextiles are placed in soil where they experience tension in confined conditions. Often geotextiles are damaged during installation (for example, in a process of soil compaction in road building). After installation, traffic loading may cause coarse grained aggregates to do additional damage.

It is important to know the extent of damage and tensile properties of damaged materials for design purposes. The theory of elasticity was applied to investigate the effect of such damage upon the tensile properties of geotextile soil reinforcements both unconfined and confined in granular media. The exact solution of a problem of stresses on the boundaries of a hole in a finite rectangular plate was derived for unconfined and confined tensile loadings. The theoretical predictions of deformations of the damaged plate was compared with deformations observed in pullout tests with the damaged geosynthetic specimens.

INTRODUCTION

Geosynthetic products present a distinctive class of construction materials that are used as impervious barriers and for soil improvement in highways, embankments and similar projects. An important engineering problem for a designer considering the use of a geosynthetic material is to evaluate its mechanical properties in confined conditions. Manufacturers usually provide only unconfined properties specified in ASTM standards (for example, ASTM, 1993). However, these standards do not take into account that mechanical properties of geosynthetic materials depend significantly on geosynthetic-soil interaction even at low levels of confining pressure that geosynthetics experience at depths as small as 0.6 to 1.2 m. Geosynthetic materials are also vulnerable to construction damage inflicted in course of normal construction practices, e.g., soil compaction.

Previous experimental studies of construction induced damage upon short term mechanical properties of geosynthetics were performed by Watts and Brady, 1990 and 1994. They tested the effect of vibratory compaction (standard and to refusal) on 1×2 m specimens. Then they compared the tensile strength of small (0.1×0.2 m) and large (1×2 m) specimens in unconfined tensile tests. The results are valuable for quantitative assessment of compaction induced damage. However, they cannot be used to predict the effect of the damage on in situ tensile properties.

In this paper the theory of elasticity was applied to investigate the effect of holes upon the tensile properties of geotextile both unconfined and confined in granular media. The dependence of the ultimate tensile stress upon hole size has been shown. This stress increases with increased size of geotextile specimens, decreased specimens' thickness, and increased resistance to tension caused by the influence of confining media.

The exact dependence of the ultimate tensile stress on the radius of damaged area was derived. For each particular specimen size when the damaged area reached certain critical size, the tensile stress required for further deformation of the specimen significantly decreased. When the damaged area is smaller than the critical size, the tensile stress-strain characteristics of a specimen are similar to that of an undamaged specimen. The limiting parameters of multiple damages that do not influence stress-strain characteristics of specimens were estimated.

To measure the geosynthetic-soil interaction pullout tests were used. This method is widely known (e.g., Bauer et al., 1991, Juran and Christopher, 1989, Report, 1995, and Wu, 1991). This paper demonstrates that for assessing geosynthetic-soil interaction it is necessary to measure tensile stresses on opposite boundaries of a specimen in a pullout test. Constitutive laws related to tension and failure of confined geosynthetics with the damage were derived. Application to construction related damage is presented.

EQUILIBRIUM EQUATIONS FOR CONFINED UNDAMAGED GEOTEXTILE SPECIMEN

Consider a physical model of confined elastic tension of a thin finite plate $2l$ in width and $2l_0$ in length. The origin of the orthogonal coordinate system is placed in the middle of the plate as shown in Fig.1. The plane (x, y) coincides with the middle of the specimen. The thickness of the specimen is h. The tensile stress, T, is applied to the top and the bottom of the specimen. Confining media applies the external stress, $\bar{P}$, to the specimen's surface. In unconfined conditions, $\bar{P}$ is equal to zero. The stresses T and $\bar{P}$ cause appearance of the stress, σ, and strain, u, in the specimen. The following boundary conditions characterize the model in Fig. 1:

1) When external stresses are applied to the surface of the plate, $\sigma_{ik}n_k=\bar{P}_i$ where σ_{ik}, n_k, and $\bar{P}_i$ are the components of the stress tensor σ; of a unit vector n directed along the z-axis normal to the surface, and of the external stress $\bar{P}$, respectively.

2) The stress applied to the upper boundary $\sigma_{xx}(l_0)$ is T. The longitudinal deformations of a free

plate with $T = 0$ are equal to zero: $\sigma_{ik} n_k = 0$, and hence, $\sigma_{xz} = \sigma_{yz} = \sigma_{zz} = 0$.

3) For thin plates, the cross-sectional strains are uniform, the strain tensor u and stress components σ_{xx}, σ_{yy}, and σ_{xy} are functions of x and y and do not depend on z.

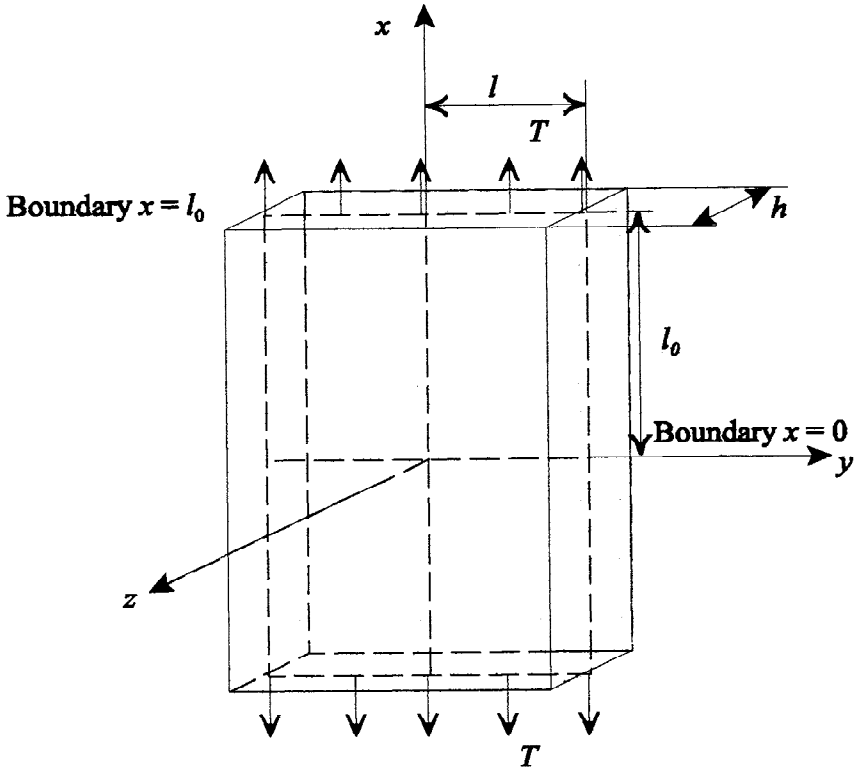

Figure 1. Pristine geosynthetic specimen

The general equilibrium equations for $T = 0$ are:

$$\frac{\partial \sigma_{ik}}{\partial x_k} = 0 \tag{1}$$

or

$$\frac{\partial \sigma_{xx}}{\partial x} + \frac{\partial \sigma_{xy}}{\partial y} + \frac{\partial \sigma_{xz}}{\partial z} = 0$$
$$\frac{\partial \sigma_{yx}}{\partial x} + \frac{\partial \sigma_{yy}}{\partial y} + \frac{\partial \sigma_{yz}}{\partial z} = 0$$
$$\frac{\partial \sigma_{zx}}{\partial x} + \frac{\partial \sigma_{zy}}{\partial y} + \frac{\partial \sigma_{zz}}{\partial z} = 0$$

In a state of equilibrium it is reasonable to assume that σ_{xz} and σ_{yz} are equal to zero when $z = 0$.

Following the first boundary condition, $\sigma_{xz} = \bar{P}_x$ and $\sigma_{yz} = \bar{P}_y$ when $z = \frac{h}{2}$. Considering the symmetry of the problem, for $z>0$ stresses inside the plate are

$$\sigma_{xz} = \bar{P}_x f(\frac{z}{h}) \approx \frac{2\bar{P}_x z}{h}$$
$$\sigma_{yz} = \bar{P}_y f(\frac{z}{h}) \approx \frac{2\bar{P}_y z}{h} \quad (2)$$

Substituting (2) in (1) and denoting $2\bar{P}_x$ as P_x and $2\bar{P}_y$ as P_y, the general equilibrium equations for a plate are derived as:

$$h(\frac{\partial \sigma_{xx}}{\partial x} + \frac{\partial \sigma_{xy}}{\partial y}) - P_x = 0$$
$$h(\frac{\partial \sigma_{yx}}{\partial x} + \frac{\partial \sigma_{yy}}{\partial y}) + P_y = 0 \quad (3)$$

The signs at P_x and P_y show that these components of $\bar{P}$ are directed opposite to the directions of specimen's deformation. These components depend upon the properties of confining media and frictional properties of geosynthetics, and the state of stresses in the plate depends on them. No other characterization of properties of confining media is necessary. The equations (3) are independent of z, which satisfies the second boundary condition.

Equilibrium equations for a free plate follow from Equations (3):

$$\frac{\partial \sigma_{xx}}{\partial x} + \frac{\partial \sigma_{xy}}{\partial y} = 0$$
$$\frac{\partial \sigma_{yx}}{\partial x} + \frac{\partial \sigma_{yy}}{\partial y} = 0 \quad (4)$$

CONSTITUTIVE LAWS OF TENSION OF DAMAGED GEOTEXTILE

In a state of uniaxial loading the stress components σ_{xy}, σ_{yx}, and $\sigma_{yy}(l)$ are equal to zero. Assuming P_x and P_y to be constant at a given confining pressure and geotextile-soil combination, the solution of (3) can be presented as:

$$\tilde{\sigma}_{xx} = \tilde{T} + P_x(x - l_0)$$
$$\tilde{\sigma}_{yy} = P_y(l - y) \quad (5)$$

where $\tilde{\sigma}_{xx} = h\sigma_{xx}$, $\tilde{\sigma}_{yy} = h\sigma_{yy}$, and $\tilde{T} = hT$. This can be checked by substituting (5) into (3). From (5)

the expression for P_x is derived as:

$$\begin{aligned}\tilde{\sigma}_{xx}(l_0)-\tilde{\sigma}_{xx}(0) &= P_x l_0 \\ P_x &= \left(\tilde{\sigma}_{xx}(l_0)-\tilde{\sigma}_{xx}(0)\right)/l_0\end{aligned} \tag{5'}$$

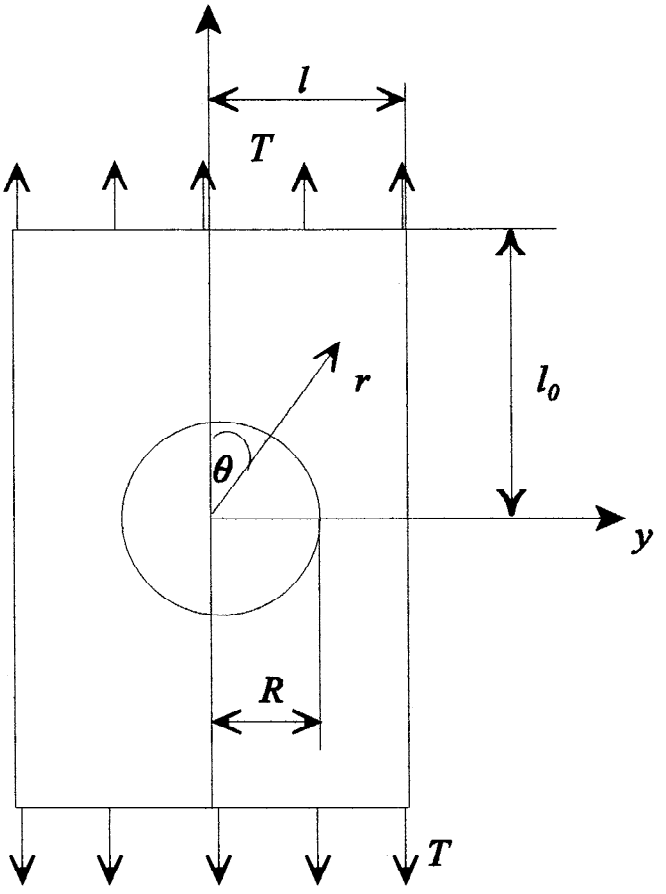

Figure 2. Damaged geosynthetic specimen.
A hole with radius, R, is cut in the middle.

Consider a plate as shown in Fig. 2. There is a circular hole with radius R with the center at $(x,y)=(0,0)$. The length of plate is $2l_0$, the width is $2l$. In a plate with a hole it is reasonable to use the polar coordinate system. Then the equilibrium equations (3) are:

$$\begin{aligned}&\frac{\partial\sigma_{rr}}{\partial r}+\frac{\sigma_{rr}-\sigma_{\theta\theta}}{r}+\frac{\partial\sigma_{r\theta}}{r\partial\theta}-\frac{P_x}{h}\cos\theta+\frac{P_y}{h}\sin\theta=0 \\ &\frac{\partial\sigma_{r\theta}}{\partial r}+\frac{2\sigma_{r\theta}}{r}+\frac{\partial\sigma_{r\theta}}{r\partial\theta}+\frac{P_x}{h}\sin\theta+\frac{P_y}{h}\cos\theta=0\end{aligned} \tag{6}$$

The boundary conditions to (6) are:

$$\sigma_{rr}(l_0,0)=T,\quad \sigma_{rr}(l,\frac{\pi}{2})=\frac{P_y}{h}l,\quad \sigma_{r\theta}(R,\theta)=0,\quad \sigma_{rr}(R,\theta)=0 \tag{7}$$

The last of these boundary conditions considers that P_x and P_y at hole's boundary $r = R$ are equal to zero.

The exact solutions of (6) considering (7) were derived as follows:

$$\begin{aligned}
\tilde{\sigma}_{rr}(r,\theta)&=2C_1\left(1-\frac{R^2}{r^2}\right)-2C_2\left(1+3\frac{R^4}{r^4}-4\frac{R^2}{r^2}\right)\cos 2\theta+r(P_x\cos\theta-P_y\sin\theta)\\
\tilde{\sigma}_{\theta\theta}(r,\theta)&=2C_1\left(1+\frac{R^2}{r^2}\right)+2C_2\left(1+3\frac{R^4}{r^4}\right)\cos 2\theta+r(P_x\cos\theta-P_y\sin\theta)\\
\tilde{\sigma}_{r\theta}(r,\theta)&=2C_2\left(1-3\frac{R^4}{r^4}+2\frac{R^2}{r^2}\right)\sin 2\theta
\end{aligned} \tag{8}$$

where $C_1=\frac{B_0 l P_y+B\tilde{T}_1}{A_0B+AB_0}$; $C_2=\frac{A_0 l P_y-A\tilde{T}_1}{A_0B+AB_0}$; $\tilde{T}_1=\frac{hT-P_x l_0}{2}$; $\tilde{\sigma}_{rr}=h\sigma_{rr}$; $\tilde{\sigma}_{\theta\theta}=h\sigma_{\theta\theta}$; $\tilde{\sigma}_{ry}=h\sigma_{ry}$; $A_0=1-\frac{R^2}{l_0^2}$;

$B_0=1+3\frac{R^4}{l_0^4}-4\frac{R^2}{l_0^2}$; $A=1-\frac{R^2}{l^2}$; $B=1+3\frac{R^4}{l^4}-4\frac{R^2}{l^2}$.

This solution can be verified by substituting it in (6) and differentiating. For unconfined conditions, when $P_x=P_y=0$ and l and $l_0\to\infty$ equation (8) gives a well known classical result for thin infinite plates (see, for example, Timoshenko and Goodier, 1970). The solutions can be verified by substitution in (6).

The Hooke's law for a plate can be expressed as:

$$\begin{aligned}
\tilde{\sigma}_{rr}&=\frac{\tilde{E}}{1-\nu^2}(u_{rr}+\nu u_{\theta\theta})\\
\tilde{\sigma}_{\theta\theta}&=\frac{\tilde{E}}{1-\nu^2}(u_{\theta\theta}+\nu u_{rr})\\
\tilde{\sigma}_{r\theta}&=\frac{\tilde{E}}{1+\nu}u_{r\theta}
\end{aligned} \tag{9}$$

where $u_{rr}=\frac{\partial u_r}{\partial r}$; $u_{\theta\theta}=\frac{\partial u_\theta}{r\partial\theta}+\frac{u_r}{r}$; $2u_{r\theta}=\frac{\partial u_\theta}{\partial r}+\frac{\partial u_r}{r\partial\theta}-\frac{u_\theta}{r}$; u_r and u_θ are displacements in polar coordinates; $\tilde{E}=hE$; E is the Young's modulus; and ν is the Poisson's ratio.

After substituting (8) in (9) and integration, the displacements u_r and u_θ were obtained as:

$$u_r = \frac{2}{\tilde{E}}\left(C_1\left(r+\frac{R^2}{r}\right) - C_2\left(r-\frac{R^4}{r^3}+4\frac{R^2}{r}\right)\cos 2\theta - \nu C_1\left(r-\frac{R^2}{r}\right) - \nu C_2\left(r-\frac{R^4}{r^3}\right)\cos 2\theta\right) + \frac{(1-\nu)r^2}{2\tilde{E}}(P_x\cos\theta - P_y\sin\theta) \tag{10}$$

$$u_\theta = \frac{2C_2}{\tilde{E}}\left(r+\frac{R^4}{r^3}-2\frac{R^2}{r}+\nu\left(r+\frac{R^4}{r^3}-2\frac{R^2}{r}\right)\right)\sin 2\theta + \frac{(1-\nu)r^2}{2\tilde{E}}(P_x\sin\theta + P_y\cos\theta)$$

The tensile strength of a pristine specimen at unconfined uniaxial loading, $\tilde{Y}$, is a material property that is usually defined in a wide strip test (D 4885) and it is often called the wide width strength. The maximum load that a specimen with a hole can withstand, T_m, occurs at the hole's boundary when $r = R$ and $\theta = \frac{\pi}{2}$ and it is:

$$T_m = \frac{\sigma_{\theta\theta}(R,\frac{\pi}{2}) - \sigma_{rr}(R,\frac{\pi}{2})}{2} \tag{11}$$

where σ_{rr} and $\sigma_{\theta\theta}$ are defined by (8). T_m decreases with the increase of R. This decrease of T_m can be observed only when finite plates are extended. At T_m the rim of the hole breaks and u_r will further increase at decreasing values of T_m. That corresponds the failure of the specimen. The process of failure is characterized with increase of u_r due mostly to the increase of the hole's radius R.

For failure conditions when $l_0 > l$, instead of (11) a simpler formula for T_m can be used:

$$T_{m*} = P_x l_0 + \frac{2}{3}\tilde{Y}\frac{1+\frac{3}{2}\frac{R^4}{l^4}-\frac{5}{2}\frac{R^2}{l^2}}{1+\frac{R^4}{l^4}-2\frac{R^2}{l^2}} \tag{12}$$

EXPERIMENTS ON UNCONFINED AND CONFINED TENSION OF DAMAGED GEOTEXTILE

The unconfined and confined tension tests were performed with rectangular geotextile specimens in a triaxial cell (Juran and Christopher, 1992), modified for tensile testing of geotextile. The measuring system is shown in Fig. 3.

A black, non-woven, heat-bounded geotextile with thickness, h, of 0.00176 m and mass per area ratio of 1.71 kg/m^2 was tested. The specimens measured 0.1 m in length by 0.2 m in width.

During the tension tests, the bottom side of the specimen was rigidly fixed. The top side was

pulled up with a strain rate of 10% of the length per minute. Two specially designed connectors ensured that a specimen was loaded within its plane. In confined tests, the geotextile specimens were extended inside the hydrostatically pressurized dry sand specimen in drained conditions. The clamps and specimens remained confined in soil during the test. The load cells measured tensile loads on the top and bottom boundaries of the specimens.

The confining sand was composed of predominantly sub-rounded grains sixty percent of which had the diameter smaller than 0.43 mm (D_{60} = 0.43 mm). Using the Unified Soil Classification System, the sand was classified as poorly graded with system group symbol SP. Specific gravity of the sand solids was 2.67. The sand in tests had the dry density of 1771 kg/m^3. This corresponds to a relative density of about 75%.

Unconfined Tension

Unconfined tension tests were performed to evaluate E, ν, and Y. Fig. 4 shows the results of unconfined tension tests of two specimens. One was pristine, the second had a hole with $R = 0.004$ m cut in the middle of the specimen before the test. The horizontal axis presents the displacement u_r of the upper boundary. The vertical axis is $\tilde{T} = hT$. Both specimens have matching load-displacement curves until the tension reaches 3 kN/m. Then a hole starts influencing the test results and the second curve lies below the first curve. As it was expected, the stresses on the upper and bottom boundaries were the same.

The experimental values of the Young's modulus, E, for both samples were 25400 kN/m^2, of the Poisson's ratio, ν were about 0.3, the strength, $\tilde{Y}$, was 13 kN/m for the pristine specimen and the ultimate $\tilde{T}_m$ was about 10 kN/m for the damaged specimen.

In Fig.5 the growth of the hole was measured in air after failure load was reached. Observed increase of the radius was compared with calculated increase using (12). There is good matching of theoretical and experimental results.

Confined Tension

Confined tension tests with pristine specimens are necessary to evaluate the influence of soil upon the confined properties of a specific geotextile. This influence was characterized with the stress P_x found in a pullout test as a difference between the tensile stress measurements at the upper ($x = 2l_0$) and lower ($x = 0$) boundaries of the specimen as shown in equation (5'). An example of deriving P_x at the confining pressure of 70 kPa is shown in Fig. 6. When loading began, no load was transferred to the bottom boundary of the specimen ($\tilde{\sigma}_{xx}(0) = 0$) because of soil's resistance. When $\tilde{T}$ reached 6.4 kN/m, $\tilde{\sigma}_{xx}(0)$ became equal to 0.1 kN/m which resulted in $P_x = 63$ kN/m^2. The tension-displacement curves measured by load cells on opposite sides of the specimen in Fig. 6 are nearly parallel when friction is fully mobilized. That confirms the assumption used for analytical derivation of constitutive laws governing tension of damaged geotextile that P_x (and therefore, P_y)

is approximately constant at a given confining pressure.

Equation (5') also shows that P_x should be directly proportional to the confining pressure. This was confirmed experimentally (Fig. 7). Therefore, only two experiments with given geotextile and soil are generally sufficient to find the effect of confinement upon tensile behavior of geosynthetics within the tested range of pressure values.

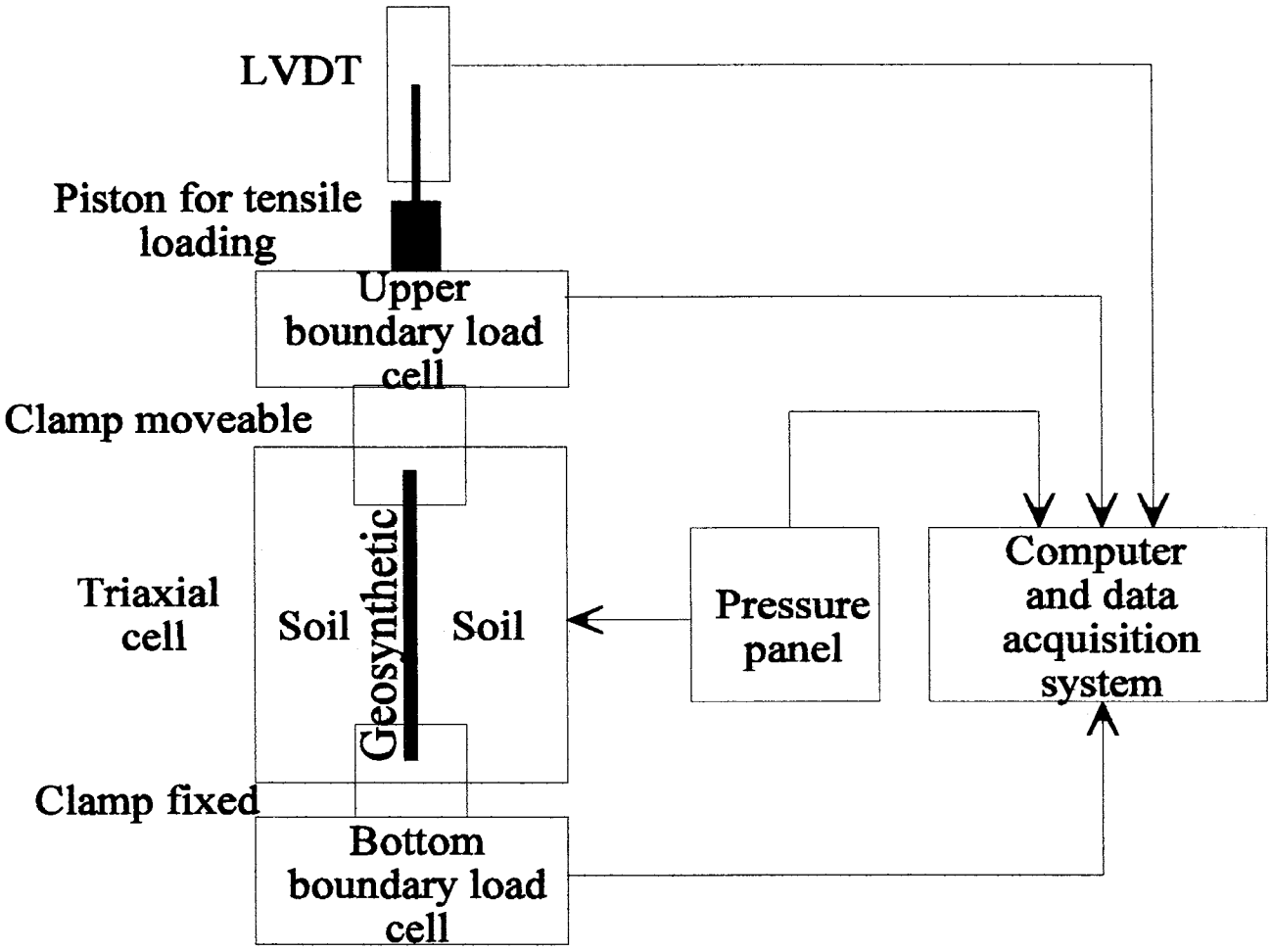

Figure 3 Triaxial system for pullout wide strip testing.

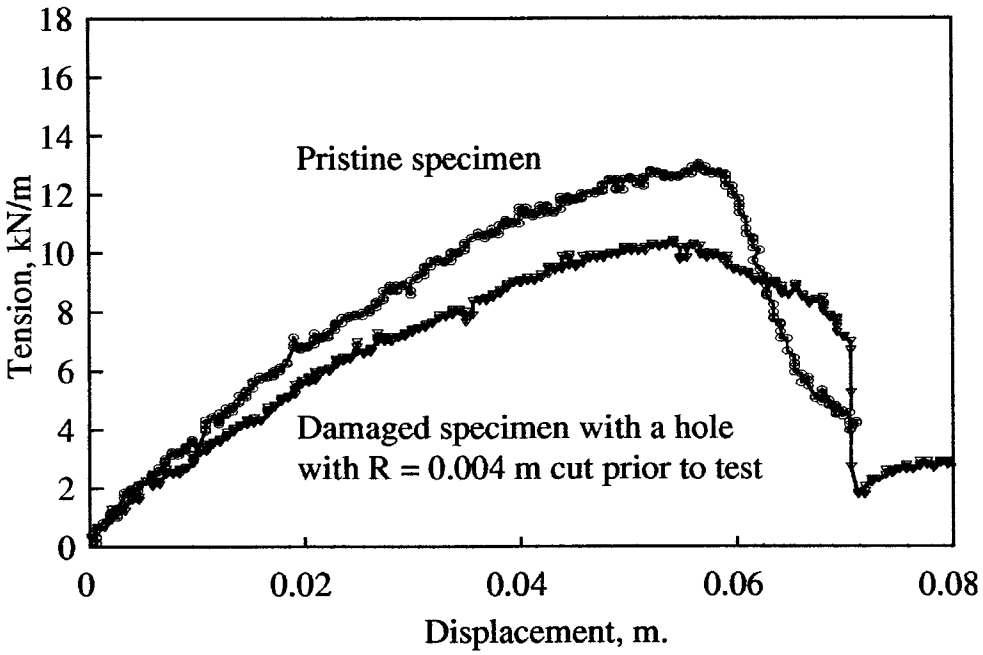

Figure 4. Wide strip unconfined test of pristine and damaged specimens.

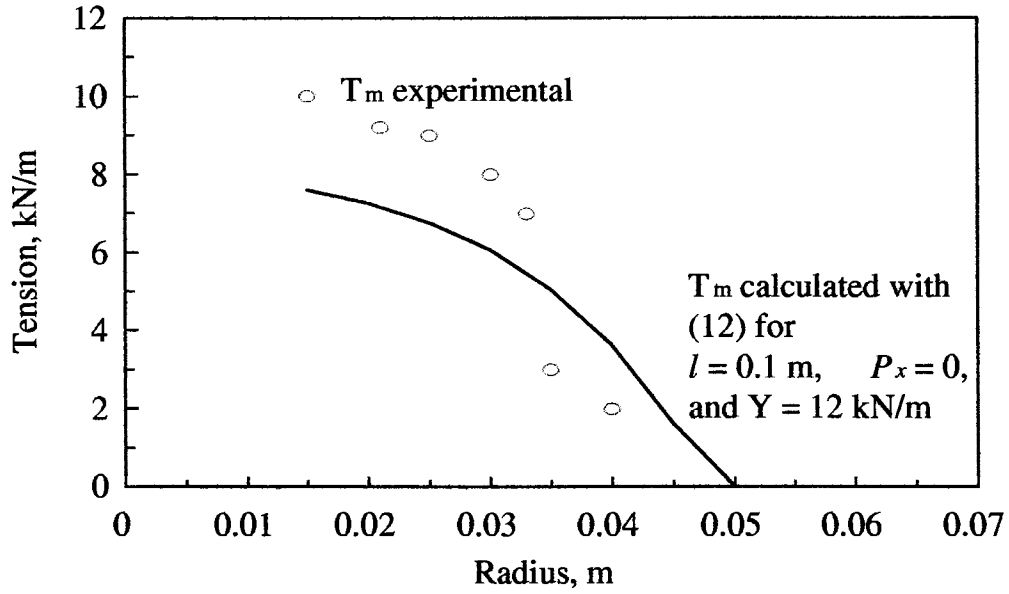

Figure 5. Change of tensile stress required for the hole's growth at failure. Unconfined conditions.

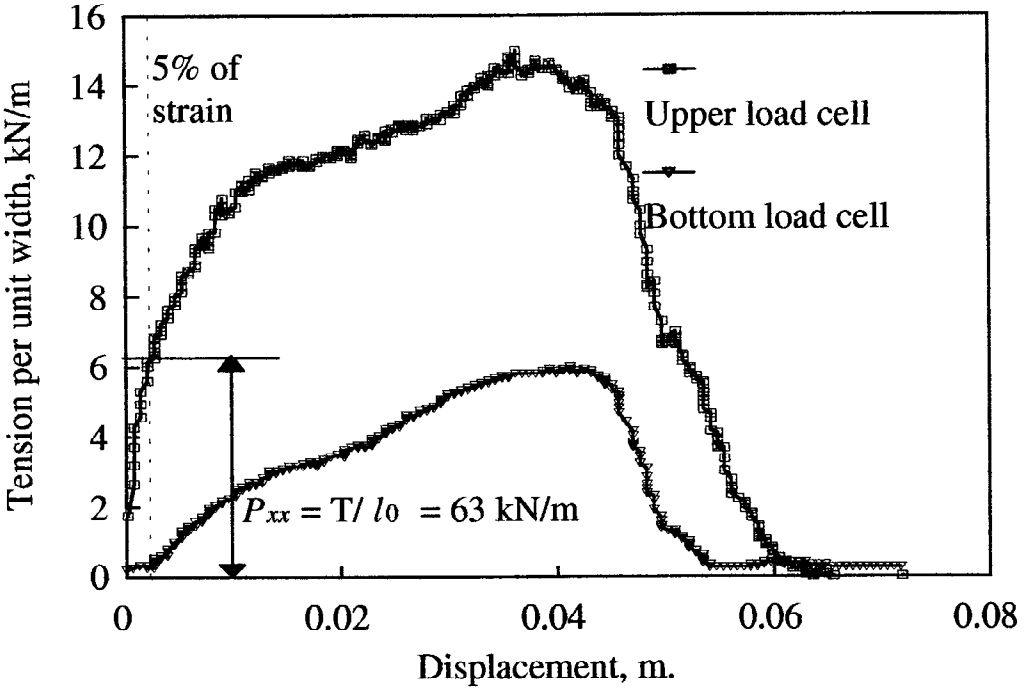

Figure 6. Testing of pristine geosynthetics at the confining pressure of 70 kPa to evaluate the effect of its interaction with soil in pullout conditions

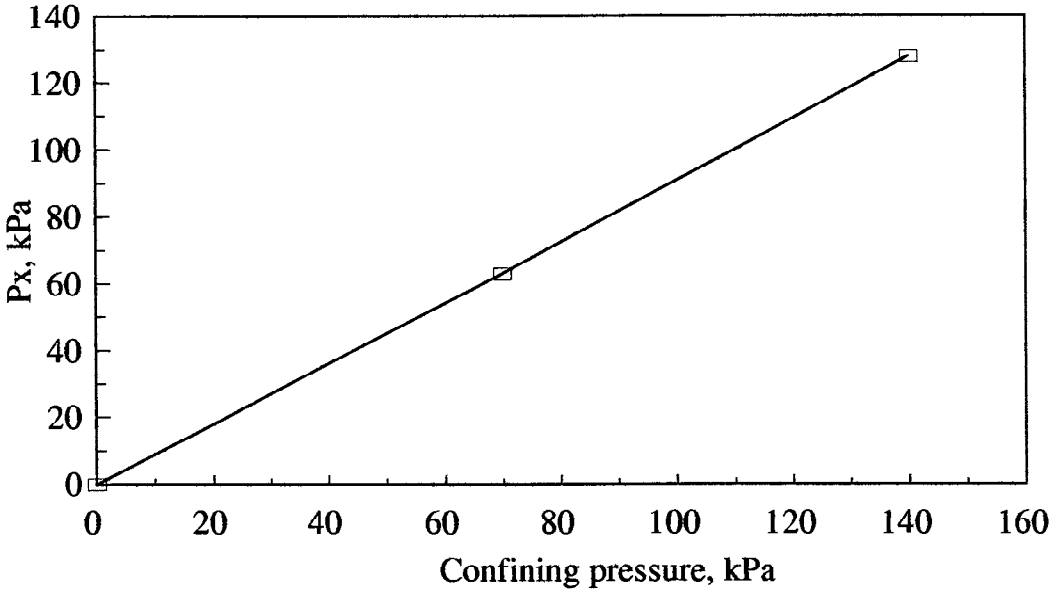

Figure 7. Experimental evaluation of the effect of confining pressure on soil-geosynthetic interaction characteristic, P_x.

Pullout test data at 140 kPa with pristine and damaged geotextile (a hole with $R = 0.004$ m in the middle cut prior to test) are displayed in Fig. 8. Then equations (11) and (12) were used to plot analytical tension-displacement curves. These characteristics of geosynthetics were predicted within 20% of error. Certain overprediction of T_m can be explained by the development of at least two holes at different weak zones in the specimen. It can be shown that when two small holes at close spacing exist in a specimen, their boundaries will move towards each other under tensile loading until one large hole develops. Therefore, $\bar{T}$ will first increase, then somewhat decrease and then increase again prior to total failure as can be seen on the damaged specimen's experimental curve.

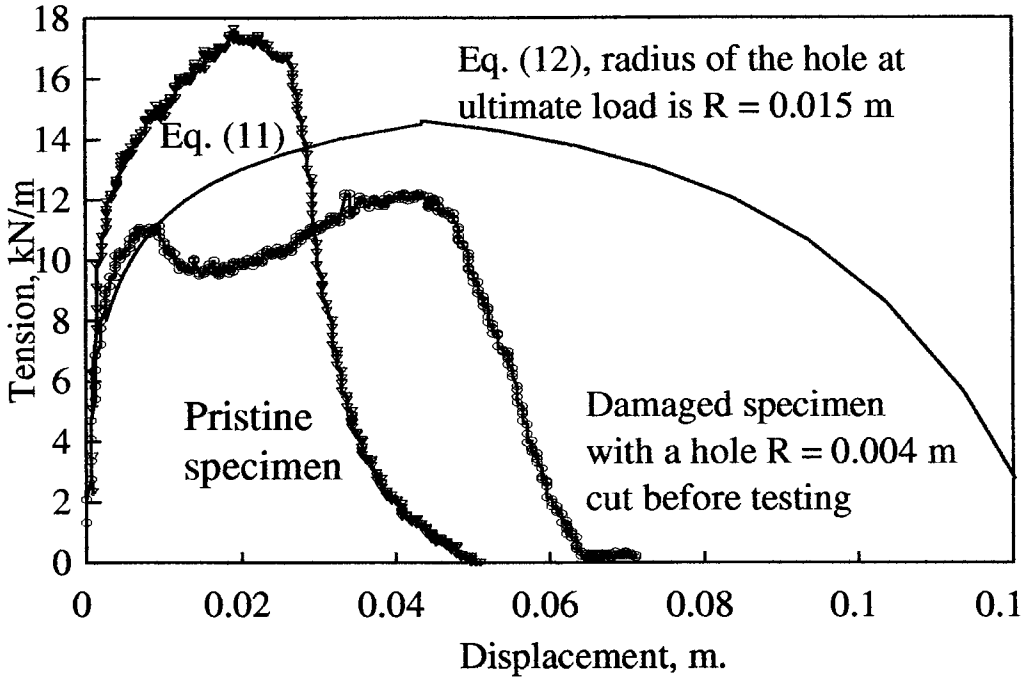

Figure 8. Pullout test of pristine and damaged specimens at confining pressure of 140 kPa. Analytical prediction of tensile behavior of a damaged specimen based on unconfined geosynthetic properties, R, and P_x.

It is important to notice that though the pristine specimen's strength in confined conditions exceeds the strength of the damaged specimen by about 1/3, the confined damaged specimen's strength is close to the strength of a pristine specimen in air. The hole did not influence the tension-displacement curve to approximately 3 to 5% of specimen's strain until the friction force was fully mobilized and the initial radius of the hole increased from 0.004 m to 0.0052 m. The failure of the specimen occurred when the radius of the hole nearly doubled. That means that for any finite geosynthetic specimen a critical radius of a hole exists when it does not influence the tensile-displacement properties. This radius should be about 1/10 of the distance from the center of the hole

to the nearest boundary of the plate. That means that it is possible to manufacture non-woven geosynthetics with the holes of mentioned size without a significant loss of the material's strength.

Another important aspect of a study dealing with the prediction of tensile properties of damaged geosynthetics is to correlate the derived results to the damaged zones of arbitrary shapes that develop due to construction process. In the study performed by Watts and Brady (1994) the damage caused by vibrational compaction was characterized with the partial factor of safety for installation damage, $f_m = \frac{\tilde{Y}}{\tilde{T}_m}$, where $\tilde{Y}$ and $\tilde{T}_m$ were evaluated in unconfined tests. Comparison of f_m for specimens damaged by standard compaction and by cutting holes as discussed in this paper showed that polypropylene and polyester samples had equal f_m, and, hence experienced similar damage. (Specimens' sizes and the rate of loading were the same in both studies). Specimens compacted to refusal had larger f_m than the specimens with the holes with $R = 0.004$ m. It is easy to cut holes in the specimens with such values of R that will give matching f_m in wide strip unconfined tests. When values of R are known, the confined properties of damaged specimens can be predicted as it was explained above.

SUMMARY

The discussed method of analysis is focused on the changes of mechanical properties of damaged geosynthetics in confined conditions. This method uses data from standard in-air wide strip tests to predict such important properties as confined strength and deformation at ultimate loads of damaged geosynthetic specimens in confined conditions. For this, it was theoretically substantiated that it is necessary to measure in pullout tests the stresses on two opposite boundaries of a specimen.

The general non-linear problem of confined tension of a finite plate with a hole was solved analytically. This solution contributed to the understanding of tension and failure mechanisms of confined geosynthetics.

It was shown that the ultimate tensile stress increased with an increase of resistance to tension caused by the influence of confining media.

For each particular specimen size, the tensile stress required for its further deformation significantly decreased when the damaged area exceeded a certain critical size. Up to that critical size, the tensile stress-strain characteristics of a specimen with holes were similar to the characteristics of a pristine specimen. Specifically, the initial stiffness of the specimens remained unaffected.

Theoretical analysis was extensively verified experimentally and showed good correlation with the test results.

REFERENCES

ASTM Standards on Geosynthetics (1993), ASTM Publication Code Number (PCN): 03435093-38, Philadelphia.

Bauer, G.E., Halim, A.O.A., and Shang, O. (1991), "Large-Scale Pullout Tests: Assessment of Procedure and Results", Proceedings of Geosynthetics '91, Vol.2, Atlanta, pp.615-628.

Juran, I. and Christopher, B. (1989) "Laboratory Model Study on Geosynthetic Reinforced Retaining Walls", Journal of Geotechnical Engineering, Vol.115, No.7, pp.905-926.

Juran, I. and Christopher, B. Closure of Discussion by Wu, J.T.H. and Tatsuoka, F. (1992) "Laboratory Model Study on Geosynthetic Reinforced Retaining Walls", Journal of Geotechnical Engineering, Vol.118, No.3, pp.496-501.

Report (1995) "Confined Creep Testing of Geosynthetics for Highway Applications", prepared by GeoSyntec Consultants for US Department of Transportation, Federal Highway Administration, Project Number GE3131.

Timoshenko, S.P. and Goodier, J.N. (1970) "Theory of Elasticity", 3rd Ed., McGraw-Hill Book Co., Inc., New York.

Watts, G.R.A. and Brady, K.C. (1990) "Site Damage Trials on Geosynthetics", Proceedings of Fourth International Conference on Geotextiles, Geomembranes and Related Products, The Hague, Balkema, Rotterdam.

Watts, G.R.A. and Brady, K.C. (1994) "Geosynthetics: Installation Damage and the Measurement of Tensile Strength", Proceedings of Fifth International Conference on Geotextiles, Geomembranes and Related Products, Singapore, 5-9 September, 1994 (Compact Disk).

Wu, J.T.H., "Measuring Inherent Load-Extension Properties of Geotextiles for Design of Reinforced Structures", ASTM Geotechnical Testing Journal, Vol. 14, No.2, 1991, pp.157-165.

GEOTEXTILES TO STABILIZE THAWING, LOW-BEARING-CAPACITY SOILS: A COMPARISON OF TWO DESIGN METHODS FOR USE BY THE US ARMY

KAREN S. HENRY
US ARMY COLD REGIONS RESEARCH AND ENGINEERING LABORATORY, HANOVER, NH, USA

ROBERT D. HOLTZ
UNIVERSITY OF WASHINGTON, SEATTLE, WA, USA

ABSTRACT

Thawing fine-grained soils are often saturated and have extremely low bearing capacity. Geotextiles reinforce unsurfaced roads on weak, saturated soils and therefore are good candidates for stabilization of thawing soils. To stabilize the soil, a geotextile is placed on it, then the geotextile is covered with aggregate. Design involves selection of aggregate thickness and geotextile. The US Army uses one of two commonly used design techniques for geotextile reinforcement of low-volume roads. The other method, which offers potential to reduce aggregate thickness over the geotextile by accounting for the tensile properties of the geotextile, was compared with the Army method. Although it offers considerable aggregate savings over the current method, it may be unconservative with respect to stresses estimated at the subgrade surface. Future work should consider adopting a method that provides realistic estimates of stresses at the subgrade as well as aggregate savings through accounting for the tensile properties of geotextiles.

INTRODUCTION

Thawing fine-grained soils are often saturated or even supersaturated and thus have extremely low bearing capacity. Geotextiles have been used in the construction of low-volume, unsurfaced roads on weak, saturated soils to reinforce the aggregate/subgrade interface and they are therefore good candidates for use in stabilization of thawing soils. To stabilize weak soil with a geotextile for trafficking, the geotextile is placed on it and then covered with aggregate. The design involves selecting aggregate thickness and the geotextile for the specific soil bearing capacity. There are two commonly used techniques for geotextile reinforcement of low-volume, unsurfaced roads, one of which is prescribed in US Army guidance.

The current Army design technique for static loading (defined as up to 100 passes of a vehicle at the maximum wheel load and a minimum rut depth of 0.10 m) of low-volume roads on soft, cohesive soils was

examined for ease of use and applicability to the reinforcement of thawing soil. Another design method that offers the potential to reduce required aggregate thickness over the geotextile (and thus cost) was compared with the Army method. Theory and results from both design methods are presented. Although both design methods include traffic loading for up to 1000 vehicle passes, this report deals only with the techniques for static loading. This situation often applies to the military in theaters of operation.

METHOD CURRENTLY USED BY THE ARMY (TM5-818-8)

The design method for the stabilization of low-bearing-capacity soils with geotextiles for low-volume roads currently used by the US Army was developed by the US Forest Service (Steward et al., 1977) based on the theory of Barenberg et al. (1975). The design method, which generally applies to soft, cohesive soils, is presented in US Army Manual TM5-818-8 (1995) as soil bearing capacity vs. aggregate thickness curves for various wheel loads, each at a tire pressure of 552 kPa (80 psi) (e.g., Fig. 1). (The aggregate is usually crushed rock.) The design procedure includes (1) converting soil strength to an equivalent cohesion, c; (2) selecting a maximum wheel load; (3) selecting a value for the bearing capacity factor, N_c. (N_c values used with design curves for static loading are 6.0 with geotextile and 3.3 without geotextile); (4) using cN_c in the appropriate design chart (e.g., Fig. 1), determining the depth of aggregate required with and without a geotextile; (5) determining which section is less costly to build; and (6) if use of a geotextile is advantageous, specifying one according to geotextile construction survivability requirements.

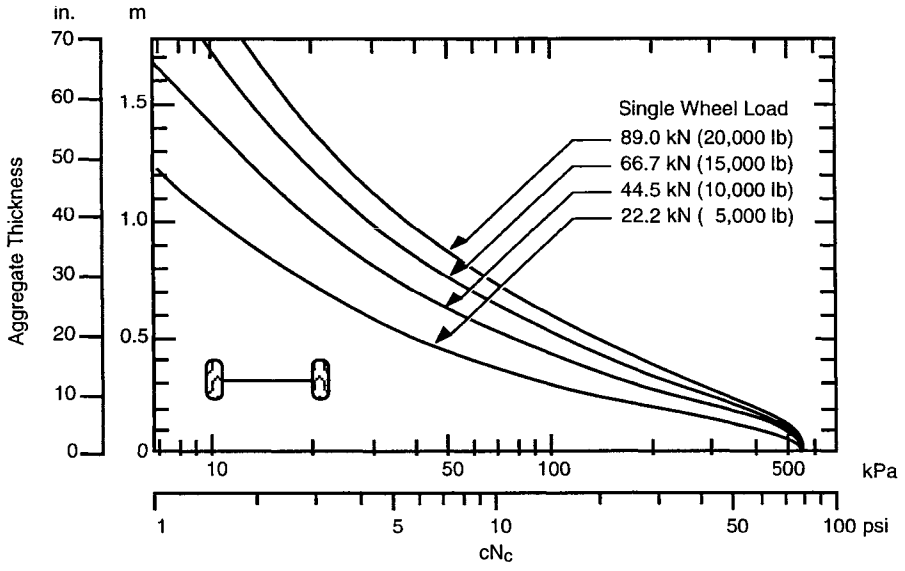

Figure 1: Aggregate thickness design curve for single-wheel load on gravel-surface roads (from TM5-818-8).

Guidance on selecting wheel loads and contact pressure is provided here for easier use of TM5-818-8. For single and dual wheels on a single axle, the wheel load is defined as the total load on either the left or right side of the axle. The axle load, a quantity used in other design methods, is defined as the total load on the axle. For tandem axles, Barenberg et al. (1975) use a wheel load of 0.66 times the sum of the loads on one side of the tandem axles, whereas others, such as Giroud and Noiray (1981), use a factor of 0.60. Contact pressures for use in design are approximately 0.9 to 1.0 times the tire inflation pressure for single-tired vehicles and 0.70 to 0.75 times the tire inflation pressure for dual tires (Barenberg et al., 1975). For the design method presented in TM5-818-8, there is negligible difference in the design curves for actual tire inflation pressure vs. contact pressure (Barenberg et al., 1975).

Bender and Barenberg (1978) summarize the theory and tests that led to the design method of TM5-818-8. For soft clay subgrades at or near saturation, wheel loads are transient, therefore undrained loading applies, the angle of internal friction is zero, and the shear strength of the soil is equal to its cohesion. Based on the theory of plastic equilibrium, the ultimate bearing capacity, q_d, for soil in this condition is

$$q_d = (2 + \pi)c \ . \tag{1}$$

However, plastic deformation that can cause localized shear failure begins at

$$q \approx \pi c \ . \tag{2}$$

Barenberg et al. (1975) conducted laboratory tests (two-dimensional, cyclic loading) with geotextiles placed between crushed stone and a saturated clay subgrade. Stress levels on the subgrade were estimated by a Boussinesq stress distribution beneath a circularly loaded area (e.g., Newmark, 1942), and ratios between the calculated subgrade stress and measured soil strength were developed. The allowable stress with geotextile on the subgrade, σ_z, was found to be

$$\sigma_z = 6c \ . \tag{3}$$

However, without geotextile, the allowable stress was

$$\sigma_z = 3.3c \ . \tag{4}$$

These numbers are very close to the theoretical values of general and local bearing capacity failure (Eqs. 1 and 2). Therefore, Barenberg et al. (1975) constructed design charts for aggregate thickness vs. soil strength by assuming that the allowable pressure at the subgrade is 6c without geotextile and 3.3c with geotextile (Fig. 2). For the design charts, stress at the subgrade was calculated using Boussinesq stress distribution beneath a circularly loaded area (Newmark, 1942), and the

contact area, A, was determined by dividing the wheel load by the contact pressure. The radius, r, needed for determination of the stress as subgrade, was obtained from $A = \pi r^2$. Barenberg et al. (1975) did not consider tensile modulus or strength of the geotextile in developing their design method.

The Barenberg et al. (1975) design method is based on the assumption that the subgrade is uniform and that full plastic failure zones can develop, the depth of which depend on the geometry and magnitude of the loading. Thus, this method would be conservative for shallow thawed layers. Bounds on the depth of the thawed layer for full development of the plastic zone are discussed in the following section.

GIROUD AND NOIRAY DESIGN METHOD

Giroud and Noiray (1981) developed a design method for geotextile placement between the aggregate and subgrade of unpaved roads. The Giroud and Noiray (1981) design method is widely used (e.g., Holtz et al., 1995) and accounts for the load support and soil confinement provided by the geotextile itself. Therefore, thinner aggregate layers over the geotextile are allowed, compared with the method presented in TM5-818-8. Design curves for dual wheels on a single axle, with an axle load of 80 kN (18,000 lb) are shown in Figure 3. The curves are used to determine aggregate layer thickness without geotextile (h_o') and reduction of thickness with geotextile (Δh).

Giroud and Noiray (1981) assumed a soft, saturated cohesive subgrade in undrained loading, and that the effect of the geotextile placed between the aggregate and the subgrade is to change the bearing capacity

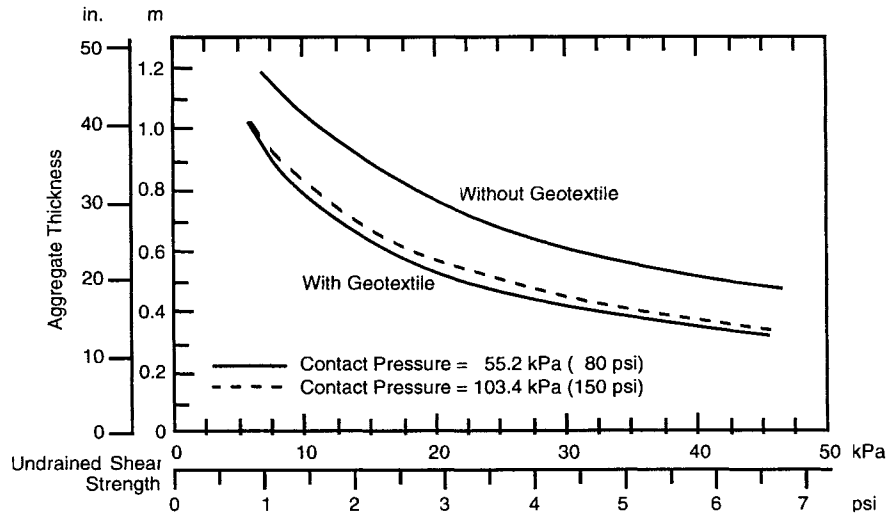

Figure 2: Design aggregate thickness chart for an 88.95-kN (20,000-lb) wheel load (from Barenberg et al., 1975).

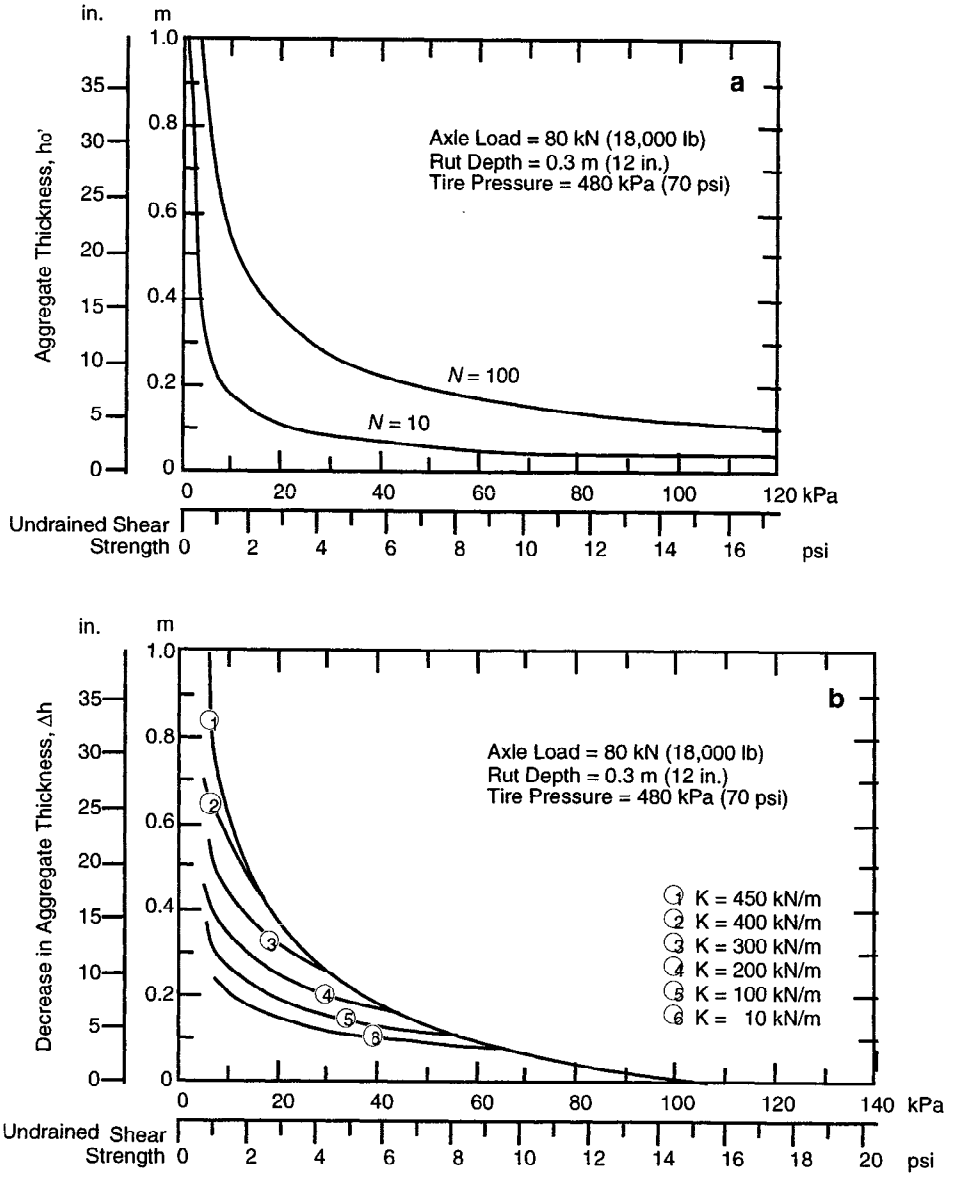

Figure 3: (a) Aggregate thickness, h_o', without geotextile (N is number of applications of axle-load to unsurfaced road); and (b) reduction of aggregate thickness, Δh, resulting from use of geotextile as function of soil cohesion (from Giroud and Noiray, 1981).

failure from local (which occurs near the elastic limit; see, e.g., Whitman and Hoeg, 1965) to general (plastic). Thus, the soil mechanics principles were the same as those used by Barenberg et al. (1975). However, Giroud and Noiray (1981) extended this concept to account for the "membrane effect" of the geotextile, which refers to the fact that the material contained by the concave side of a stretched, flexible

membrane is at a higher pressure than the material on the outside of it. As the subgrade deforms, the geotextile also deforms, which puts it in tension. The tensile strength of the geotextile then helps both to support the load and to confine the soil, making it stronger. The modulus, K, of the geotextile is increasingly influential as the rut depth increases.

Like that of Barenberg et al. (1975) this theory and design technique is based on the assumption that the subgrade soil is of a sufficient depth, H_{min}, to allow the plastic zones associated with bearing capacity failure to develop. For the stress distribution assumed by Giroud and Noiray (1981), this amounts to

$$H_{min} = \frac{B + 2h \tan\alpha}{\sqrt{2}} \tag{5}$$

where B is the width of the loaded area as shown in Figure 4, h is the thickness of the aggregate layer, and $\alpha = (\pi/4) - (\phi/2)$, where ϕ is the friction angle of the aggregate expressed as radians (Fig. 5). The value of tan α is assumed to be 0.6. Assuming a dual-tired truck with an axle load, P, having tire pressures P_c, the width, B (m), of the wheel load is given by:

$$B = \sqrt{\frac{P\sqrt{2}}{P_c}} \text{ (off-highway), and } B = \sqrt{\frac{P}{P_c}} \text{ (on-highway)} \tag{6}$$

The values for H_{min} for a minimal aggregate cover of 0.15 m (6 in.) are given in Table 1.

Thus, the Giroud and Noiray (1981) technique is not generally applicable to thawed layers less than 0.4 m (16 in.) thick, and the same is assumed for the current US Army design technique. If a geotextile is used to reinforce relatively thin thawed layers, the tension in the geotextile will not be fully mobilized. However, assuming that the subgrade

Table 1: Thickness of plastic zone in a subgrade for dual-tired truck loading and aggregate layer of thickness 0.15 m (6 in.).

Wheel load, kN (lb)/ tire pressure, kPa (psi)	Plastic zone thickness, on-highway truck, H_{min} (m/in.)	Plastic zone thickness, off-highway truck, H_{min} (m/in.)
80 kN (18,000 lb)/ 480 kPa (70 psi)	0.42/16.5	0.47/18.5
60 kN (13,500 lb)/ 480 kPa (70 psi)	0.38/15	0.43/17

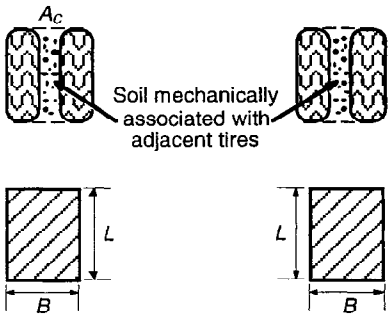

Figure 4: Definition of equivalent contact area used in analysis (Giroud and Noiray, 1981).

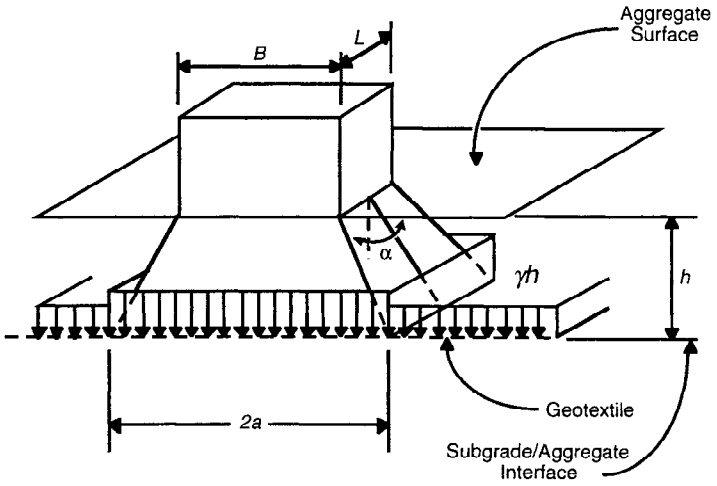

Figure 5: Wheel load distribution by the aggregate layer to the subgrade (Giroud and Noiray, 1981).

soil underlying the thawed soil is stronger than the thawing soil, the support required of the geotextile will also be less than if the subgrade were uniformly weak, and therefore, geotextile reinforcement design is conservative. In this case, the geotextile will probably provide important separation between the thawing soil and the aggregate that will likely lead to longer use of the road without maintenance.

Other assumptions pertaining to the geotextile include that (1) the geotextile does not fail, (2) the aggregate will not slide along the geotextile surface, (3) the secant tensile modulus of the geotextile is the mechanical property of interest, and (4) the shape of the deformed geotextile consists of parabolas. These assumptions are generally reasonable for high-quality aggregate and geotextiles that meet survivability criteria overlying a weak subgrade. (See Henry [in press] for more discussion of the assumptions made by Giroud and Noiray, 1981.)

In addition to including the tensile support provided by the geotextile, the Giroud and Noiray theory differs from that presented by Barenberg et al. (1975) in the assumed shape of the stress distribution through the aggregate layer to the subgrade. Giroud and Noiray (1981) used a trapezoidal distribution of the stress beneath a loaded rectangle (Fig. 5), as opposed to the Boussinesq distribution beneath a circular plate. The assumed shape of the load and the stress distribution through the aggregate layer to the subgrade results in significant differences in the estimated stresses at the subgrade for certain loading and soil conditions, especially for relatively thin aggregate layers (less than approximately 0.3 m or 12 in.), as will be demonstrated below.

It is also noted that Giroud and Noiray (1981) assumed that the aggregate had "the properties required to ensure a proper distribution of the applied load," or a minimum CBR value of 80. Similarly, Barenberg

et al. (1975) assumed the aggregate to be capable of transmitting stresses to the subgrade in a manner modeled by Boussinesq. This topic will be discussed in more detail later.

COMPARISON OF THE GIROUD AND NOIRAY METHOD WITH THE ARMY METHOD

The tensile reinforcement advantages offered by high-strength geotextiles may offset the increased cost by allowing thin aggregate layers. Therefore, the currently used Army design technique was compared with the design technique of Giroud and Noiray (1981). Design equations from both methods were programmed using MathCad 6.0 (Mathsoft, 1995) to generate design curves. Details are given in Henry (in press). Design curves provided in Barenberg et al. (1975) and Giroud and Noiray (1981) for static loading were first reconstructed, and the calculation techniques used for this work were verified to be accurate (Henry, in press).

Figure 6 shows the soil strength vs. aggregate thickness curves for both design techniques without geotextiles for dual wheels on a single axle for wheel loads of 60 and 115 kN (13,500 and 25,850 lb) and tire pressures of 414 kPa (60 psi) (representative of 10-ton and 20-ton trucks typically used by the US Army). The Barenberg et al. (1975) method is considerably more conservative at these loading conditions, and this stems from the load distribution assumptions pertaining to the spreading of the load beneath the wheels. Table 2 shows the vertical stress at various depths below the load for a wheel load of 115 kN and

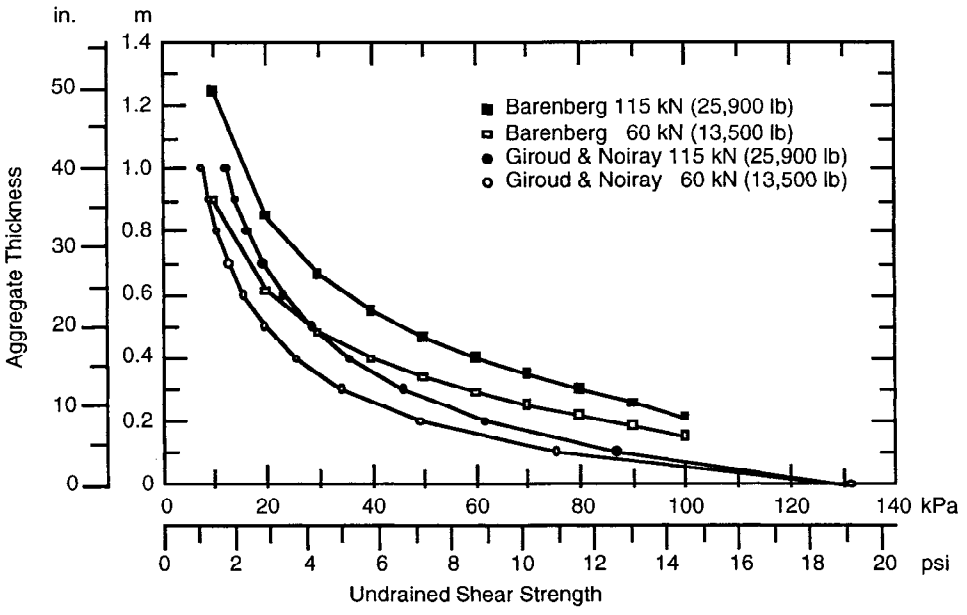

Figure 6: Design curves for static loading adapted from Giroud and Noiray (1981) and Barenberg et al. (1975): soil strength vs. aggregate thickness with no geotextiles.

Table 2: Vertical stress at various depths below applied wheel load of 115 kN and contact pressure of 414 kPa according to Newmark (1942) and trapezoidal stress distribution used by Giroud and Noiray (1981).[1]

Depth below applied stress z (m/in.)	Stress acc. to trapezoidal stress distribution (kPa/psi)	Stress acc. to Boussinesq (Newmark) method (kPa/psi)	Ratio of trapezoidal stress to Boussinesq stress
0.1/4	275.4/39.9	400.1/58.0	0.69
0.2/8	198.1/28.7	342.1/49.6	0.58
0.3/12	151.0/21.9	265.7/38.5	0.57
0.4/16	120.4/17.5	210.0/30.5	0.60
0.5/20	99.7/14.5	151.1/21.9	0.66
0.6/24	85.2/12.4	116.2/16.9	0.73
0.7/28	74.8/10.8	91.2/13.2	0.82
0.8/32	67.3/9.8	73.0/10.6	0.92
0.9/36	61.9/9.0	59.6/8.6	1.04
1.0/40	57.9/8.4	49.4/7.2	1.17

contact pressure of 414 kPa using the Boussinesq stress distribution beneath a circularly loaded area (Newmark, 1942) and the trapezoidal stress distribution beneath a rectangular load used by Giroud and Noiray (1981).

Barenberg et al. (1975) stated that they used the Boussinesq stress distribution because experimental and field work of others show that stress distribution through a granular layer to the subgrade follows the same pattern as that given by the Boussinesq theory. Indeed, Yoder and Witczak (1975) also refer to the use of Boussinesq distribution of stresses below traffic loading for pavement design. Mobility models also incorporate Boussinesq stress distributions (Blaisdell, 1997, personal communication). Although trapezoidal stress distribution below rectangular-shaped loads is commonly used in shallow foundation design (e.g., Perloff, 1975), Giroud and Noiray (1981) did not reference other work that uses trapezoidal stress distribution to estimate traffic loading stresses through aggregate.

The significant difference in estimation of stresses at the subgrade surface used by the two methods warrants further investigation. In addition, there is limited field evidence suggesting that the Giroud

[1] The Boussinesq method used to generate results in this report did not add the pressure due to the weight of the overburden (= γz) whereas the trapezoidal method used did. The calculations were carried out in this manner in order to be consistent with how the original researchers presented them. If the weight of the overburden were added to the stresses estimated by the Boussinesq method, the differences in stresses at depths of up to 1 m would be even greater than those listed in Table 2.

and Noiray (1981) design method is unconservative for static loading conditions at rut depths of 0.05 to 0.10 m in both reinforced and unreinforced test sections when the aggregate layers are 0.25 to 0.50 m thick and the subgrade strength ranges from 30 to 40 kPa (Fannin and Sigurdsson, 1996). Thus, until further investigation, use of the guidance in TM5-818-8, which incorporates the Boussinesq stress distribution through the aggregate, is recommended.

Because the potential for aggregate savings is of interest to the US Army, and the Giroud and Noiray (1981) method shows promise for large savings over the current Army design method, design curves for Army vehicles were developed according to both methods for comparison of aggregate thickness required. Design curves generated by both design methods for the US Army's 10- and 20-ton trucks are presented in Figures 7 and 8, respectively. A geotextile tensile modulus of 200 kN/m (1143 lb/in.) was used for Figures 7b and 8b because this value is easily obtained for commercially available products. Considerable aggregate savings may be realized with the Giroud and Noiray (1981) method.

DISCUSSION AND RECOMMENDATIONS FOR FUTURE WORK

Using the Giroud and Noiray (1981) method may lead to unconservative design because the stress distribution through the aggregate layer to the subgrade may be underestimated. However, the Giroud and Noiray method should be further investigated because it promises large aggregate savings, compared with the method presented in TM5-818-8, due to its ability to account for tensile properties of the geotextile reinforcement. These benefits are particularly useful at large rut depths, a situation that can be tolerated by military vehicles on thawing soils. It may be worthwhile to develop and test a design method that uses a Boussinesq stress distribution through the subgrade with the membrane support mechanism presented by Giroud and Noiray (1981). Furthermore, if a Boussinesq stress distribution is used, the load at the surface is not necessarily best modeled as a circular area; other wheel load geometries should be considered. For example, the length-to-width ratio for an HEMTT wheel load is estimated as L = 1.6B (Richmond et al., 1990).

Even though soils are usually only temporarily in a weakened state when they thaw, they will sometimes have to carry more than 100 vehicles during thawing. Thus, a method that accounts for repeated traffic loading is desirable, and this should also be included in future development efforts.

Recall that Giroud and Noiray (1981) assumed that the aggregate had properties required to ensure proper distribution of load. By assuming Boussinesq distribution through the aggregate layer, Barenberg et al. (1975) implicitly assumed a high-quality aggregate (similar to the crushed rock that they tested). McMahon and Yoder (1960) found that crushed limestone distributed stresses to a subgrade that were very closely approximated by Boussinesq theory. However, Herner (1955) demonstrated that stress distribution through an aggregate layer is significantly influenced by the aggregate and that gravel and sand concentrated

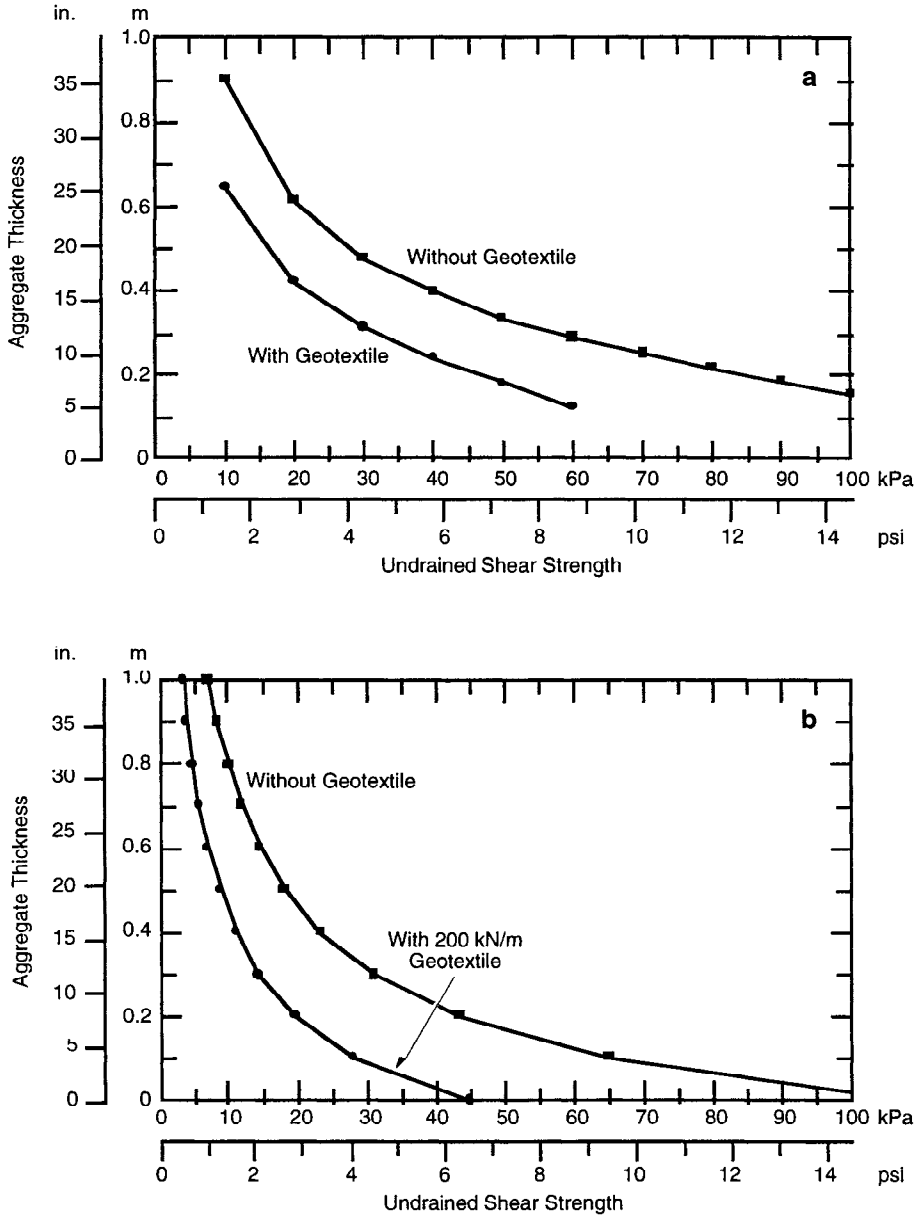

Figure 7: Design curves for static loading for (a) 10-ton dump truck, according to Barenberg (1975) method and (b) Giroud and Noiray (1981) method.

stresses into a smaller area on the subgrade than did crushed limestone (and were therefore larger in magnitude). This should be borne in mind in working with either of these design methods. If aggregate of poorer quality than crushed rock is used, stresses are likely to be more concentrated at the subgrade surface than those estimated by the Boussinesq method; in extreme cases, a failure might occur in the aggregate or it may slide along the geotextile. Future work, especially for theater-of-

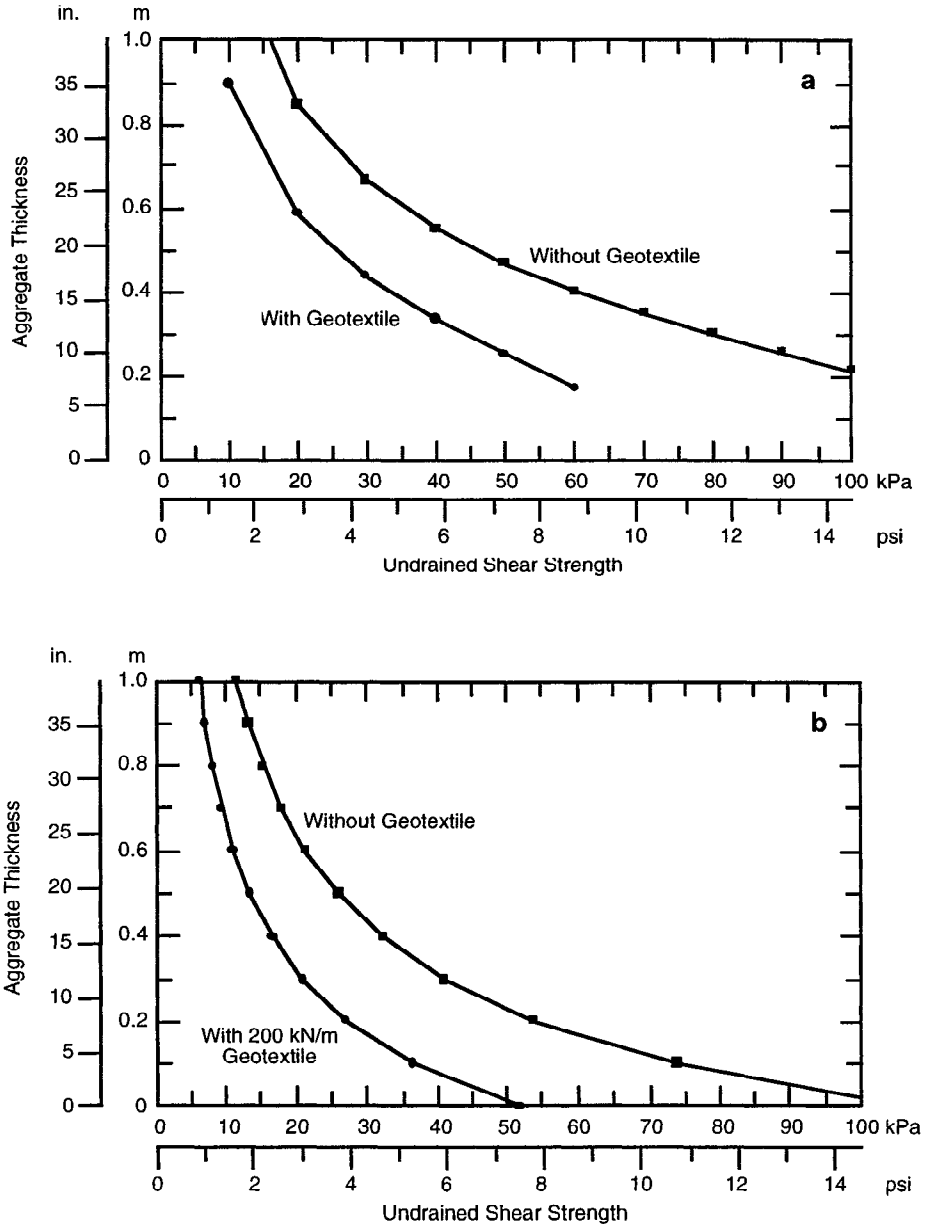

Figure 8: Design curves for static loading for (a) 20-ton dump truck, according to Barenberg (1975) method and (b) Giroud and Noiray (1981) method.

operation military applications (when time and aggregate sources may often be limited), should focus on adapting this design technique for lower quality material.

Finally, the tensile modulus values of some commercially available geotextiles far exceed those used in Figures 7b and 8b. Future work should consider the use of available products with higher modulus values. This could result in substantial aggregate savings.

CONCLUSIONS

If 10- or 20-ton trucks are expected to exert the maximum wheel loads on thawing or other low bearing capacity subgrade soils for less than 100 passes, Figures 7a or 8a can be used as design charts, respectively. These are much easier to use than the charts currently published in TM5-818-8. If the thawed layer is less than 0.4 m (16 in.) thick, this design is likely to be conservative. However, the geotextile will probably still provide benefit, as a separator, which will lengthen times between maintenance of the aggregate surface.

Considerable aggregate savings for the US Army would be realized by using the Giroud and Noiray (1981) design method. However, since their method may be unconservative due to underestimation of stresses reaching the subgrade in certain cases, it should not be used by the U.S. Army until further study is completed. A hybrid method, combining a Boussinesq stress distribution through the aggregate with a membrane support mechanism as presented by Giroud and Noiray (1981), might be an optimum design technique. When this design approach is further developed, it should also include repeated traffic loading, the shape of the wheel load, properties of the overlying aggregate, and geotextiles with representative modulus values.

ACKNOWLEDGMENTS

This work was funded by the US Army Corps of Engineers under the 4A762784AT42 program project 62784-AT-42, The Cold Regions Theater of Operations Technology work package.

REFERENCES

Barenberg, E.J., J. Hales and J. Dowland (1975), "Evaluation of soil-aggregate systems with MIRAFI fabric," University of Illinois Report No. UILU-ENG-75-2020, prepared for Celanese Fibers Marketing Company, 52 p.

Bender, D.A. and E.J. Barenberg (1978), "Design and behavior of soil-fabric-aggregate systems," Transportation Research Record 671, pp. 64-75.

Blaisdell, G.L. (1997), Research Civil Engineer, U.S. Army Cold Regions Research and Engineering Laboratory, Hanover, NH 03755-1290, personal communication.

Fannin, R.J. and O. Sigurdsson (1996), "Field observations on stabilization of unpaved roads with geosynthetics," American Society of Civil Engineers Journal of Geotechnical Engineering, Vol. 122, No. 7, July, pp. 544-553.

Giroud, J.P. and L. Noiray (1981) "Geotexile-reinforced unpaved road design," Proceedings of the American Society of Civil Engineers Journal of the Geotechnical Engineering Division, Vol. 107, No. GT9, September, 1981, pp. 1233-1254.

Henry, K.S. (in press) "Geotextile reinforcement of low bearing capacity soils: A comparison of two design methods applicable to thawing soils," CRREL Special Report 888, U.S. Army Cold Regions Research and Engineering Laboratory, Hanover, NH.

Holtz, R.D., B.R. Christopher and R.R. Berg (1995) "Geosynthetic design and construction guidelines," participant notebook, FHWA HI-95-038, US Department of Transportation, Federal Highway Administration, Washington, DC.

Mathsoft (1995) "Mathcad PLUS 6.0," MathSoft Inc., Cambridge, MA.

McMahon, T.F. and E.J. Yoder (1960) "Design of a pressure-sensitive cell and model studies of pressures in a flexible pavement subgrade," Proceedings, Highway Research Board, pp. 650-682.

Newmark, N.M. (1942) "Influence charts for computation of stresses in elastic foundations," University of Illinois Bulletin, Vol. 40, No. 12, 28 p.

Perloff, W.H. (1975) "Pressure distribution and settlement," Foundation Engineering Handbook, H.F. Winterkorn and H.Y. Fang, eds. Chapter 4, Van Nostrand Reinhold, NY, pp. 148-196.

Richmond, P.W., G.L. Blaisdell and C.E. Green (1990) "Wheels and tracks in snow: Second validation study of the CRREL shallow snow mobility model," CRRELl Report 90-13, CRREL, Hanover, NH, 39 p.

Steward, J.E., R. Williamson and J. Mohney (1977) "Guidelines for use of fabrics in construction and maintenance of low-volume roads," US Forest Service, Portland, OR, Division of Engineering, 172 p.

TM5-818-8/AFJMAN 32-1030 (1995) "Engineering use of geotextiles," Headquarters, Departments of the Army and the Air Force, Washington, DC.

Whitman, R.V. and K. Hoeg (1965) "Two-dimensional analysis of stress and strain in soils: Report No. 2, Development of plastic zone beneath a footing," Waterways Experiment Station Contract Report No. 3-129, Vicksburg, MS, 47 p.

Yoder, E.J. and M.W. Witczak (1975) "Principles of pavement design," Second edition, John Wiley and Sons, NY, 711 p.

GEOMEMBRANES AND THE CONTROL OF EXPANSIVE SOILS

MALCOLM L. STEINBERG, P.E., F.ASCE
STEINBERG AND ASSOCIATES, UNITED STATES

ABSTRACT

The geomembrane is a member of the family of geosynthetics. It is a manmade fabric, a hydrocarbon compound treated to generally provide a substantially waterproof material. Geomembranes have been used to create a barrier to minimize moisture changes in expansive soils. These moisture changes cause volumetric changes in the swelling and shrinking clays and shales. Expansive soils are found on all the earth's continents with the exception of the polar ones. These soils have been identifies in forty of the fifty United States. Damage estimates to transportation facilities, homes, and businesses exceed $10 billion annually in the United States. Case studies using geomembranes examine primarily Texas highways. The work of Wyoming Department of Transportation on more than fifty highway projects is reported. In these and other states the geomembrane barriers have been used horizontally and vertically, often both ways. Mention is made of highway treatment in Israel and railroad lines in China. The past and current impact of the expansive soils on buildings are considered in Australia and the United States. Durability results indicate the geomembrane will last decades. Geomembrane costs have decreased and placement rates have increased. The geomembrane moisture barrier generally can decrease damages caused by expansive soils.

GEOMEMBRANES

Geomembranes are manmade hydrocarbon compounds; their usage grows annually around the world. The geomembrane is a part of the geotextile family familiar to many of us from our earliest days when its identifiable use was for diapers. The manufacturing of the geomembrane has become so generalized; a variety of fabric companies are marketplace providers. In some cases one company will manufacture the geotextile, another will do the coating to transform the cloth to geomembrane, receiving a variety of tests confirming its suitability to serve as a water barrier. (Froebel, 1977)

Geomembranes were developed in Germany in the mid 1800's. Commercial production did not take place until a century later. Reputedly, they were used first by the Dutch as

protective fabrics on their dikes. The geomembrane was brought to the United States by the DuPont Company. Tests by DuPont on roads found the geomembrane to provide added strength to the section. DuPont's, Dr. Harry Tan, observed the work being done in Colorado to minimize destructive pavement movements caused by moisture changes in the soils. He concluded the geomembrane could minimize these changes. (Tan, 1975)

The geomembrane is a spun bonded polypropylene coated with polyethylene, had weights from 82 to 170 grams per square meter (2.4 to 5.1 ounces per square yard). Thicknesses ranged from 0.2 to 0.5 millimeters (7 to 20 mils). Other manufactures entered the market with products in the geomembrane category. Among their properties were thicknesses to 1.5 millimeters (60 mils) and weights to 300 grams per square meter (9 ounces per square yard). Some High Density Polyethylene (HDPE) geomembranes have thicknesses up to 3.0 millimeters (120 mils).

EXPANSIVE SOILS

Expansive soils were the cause of the destructive movements Dr. Tan proposed to address. Soil mechanics have come a long way. The early studies by Atterberg led to tests bearing his name. Atterberg's Limits focused on determining liquid, plastic, and shrinkage limits, leading to plasticity indices. Dr. Karl Terzaghi's development of soil studies earned him the title of the Father of Soil Mechanics and his text with Dr. Ralph Peck is called the Bible of Soil Mechanics. (Terzaghi & Peck, 1967)

Early conferences including the one at Harvard University in 1936 gave further insights into the expansive soil challenge. A presentation by Wooltorton offered an analysis of the cause of damages to over 100 buildings in the Mandalay District of Burma. His study revealed that structural design and construction procedures were not the cause of the buildings' distress. Wooltorton laid the blame on the region's expansive clays. (Wooltorton, 1936)

Henry Porter, Texas Highway Department research engineer, in 1942 presented results of studies on a highway between Houston and San Antonio. The wide moisture variations in the clay subgrades coupled with the volumetric changes resulted in severe pavement irregularities. The ponding of the clay subgrade also offered some indications of efforts to control these destructive movements. Ponding uses dikes built with subgrade material to create areas to be filled with water to increase the soil's moisture content and accelerate volumetric changes. Willard Simpson, a consulting engineer from San Antonio, Texas, offered additional information on the need to carry foundations beneath the area of significant moisture changes.

Following the forties, Professor Spencer Buchanan of Texas A & M University organized the first International Conference on Expansive Soils. Subsequent international and regional meetings have shown the universality of the expansive soil challenge. These soils are found on all the earth's continents except the polar ones. A study conducted by the U. S. Army Corps of Engineers (USACE), Waterways Experiment Station (WES), for the Federal Highway Administration (FHWA) found evidences of these expansive soils in 40 of the 50 states. (Snethen & Johnson, 1969) Reports of studies presented at recent technical meetings, the American Society of Civil Engineers (ASCE) conferences, and the Transportation Research Board (TRB) meetings, indicate the breadth as well as the timeliness of the problem.

EARLY CONTROL ATTEMPTS

Early efforts to control destructive movements from expansive soils included ponding the subgrade on highway projects. Paul Teng, Mississippi Highway Department, followed Porter's early effort with the drilling holes filled with pervious material prior to ponding the site. Similar efforts without the drilled holes were conducted by the Texas Highway Department. Post construction testing on the Texas project determined moisture change in the clay subgrade tended to be most pronounced from the surface to a 1.8 to 2.4 meter (6 to 8 foot) depth. This was named the zone of activity. (Watt & Steinberg, 1972)

The lime treatment of highway and airport expansive clay subgrades began over 50 years ago in the United States. It continues to this day. Treatment was initially just 15 centimeters (6 inches) deep, but now in the more active areas, depths range up to 61 centimeters (24 inches). One Belgium project had 1.5 meters (5 feet) of subgrade lime treatment. China's history of using lime in construction probably extends over many centuries.

Electro-osmotic treatment used by L. Casagrande while building German submarine pens was repeated on an Arizona Highway Department test. It was not viewed as a success in Arizona and has not been done since. Removal and replacement of swelling clays has been used repeatedly. Some reports have indicated satisfactory results. The recently completed Denver International Airport has used this technique as part of addressing their expansive soil challenge. Heavy asphalt applications have also been used.

USING GEOMEMBRANES

Geomembranes first were used on highway projects in the 1960's. The use of heavy asphalt applications to the Mancos Shale on a Colorado highway attracted Dr. Harry Tan. He felt the geomembrane could do the sealing of the expansive subgrade from moisture intrusion better than the asphalt's heavy application of 4.5 liters per square meter (one gallon per square yard). Tan provided the Colorado Highway Department (CDOT) with the fabric for a test project. The geomembrane was placed between 15 centimeter (6 inch) sand layers. Initial reports from B. A. Brakey, CDOT Research Engineer, indicated that the geomembranes were doing the job. Several years later CDOT reported the sand layers were water saturated. They concluded the geomembranes didn't help and continued using the blasting of their expansive Mancos Shale prior to recompaction.

About the same time South Dakota DOT research and materials engineer, E. B. McDonald, used a geomembrane vertically 1.2 meters (4 feet) deep along the shoulder of a highway built over an expansive shale. His report stated the geomembrane section showed improvement compared to the unprotected adjacent roadway. More importantly he conjectured that had it been placed twice as deep it would have stopped all the movement. (McDonald, 1973)

TEXAS GEOMEMBRANE EXPERIENCES

These two geomembrane studies were reported at the Expansive Soils Technical Advisory Group (ESTASG) meeting formed by Dr. Donald Snethen and Dr. Lawrence Johnson of the WES study for the FHWA. The Texas Department of Transportation (TxDOT) put the information to use. Their first project was on General Clements McMullen Drive an urban

arterial street on San Antonio's westside. A test section 183 meters (600 feet) used the geomembrane offered by the DuPont Company. It was placed horizontally on the subgrade followed by base, bladed, watered, and compacted. Though there was some movement of the geomembrane during those operations no fabric tearing was observed. Considerable pre- and post construction tests on the geomembrane and adjacent unprotected sections indicated the geomembrane provided a stronger, smoother riding section. The testing included spreadability and serviceability indices, potential vertical rise, and photo logging.

These results encouraged TxDOT to place the geomembrane vertically 2.4 meters (8 feet) deep along the shoulders of a 0.8 kilometer (one-half mile) section of Interstate Highway (IH) 410 in southwest San Antonio. In the Valley Hi Drive interchange area the highway is in a cut section. The pavement had distortions including exposure of the base course and repeated asphalt level ups. The northbound lane of the four lane freeway received the geomembrane with the adjacent southbound lane serving as the control section. The 2.4 meter (8 foot) depth placement was chosen as the lower elevation of the zone of activity. This was determined on a nearby TxDOT ponding project. As the geomembrane supplied was 3 meters (10 feet) wide it provided a 0.6 meter (2 foot) lap to the roadway's paved shoulder.

Though some difficulty was initially experienced in placing the geomembrane in the vertical trench, a utility subcontractor used a backhoe for the excavation. The challenge of the trench wall movements was solved by using a sliding shoring pulled by the backhoe. Extensive pre- and post construction testing was involved including the placement of moisture sensors. The sensors had a short life but preliminary indications showed the geomembranes minimized moisture change inside the protective subgrade. Serviceability and photo logging provided continuing data. The test results indicated the geomembrane provided a method to control the expansive clay's destructive movements. The roadway maintained a smoother riding surface when protected by the geomembrane. Much of the testing on these two TxDOT projects was conducted by the University of Texas' Center for Transportation Research.

Sand backfill was specified on this IH 410/Valley Hi Drive project for the vertical geomembrane trench. Shortly after the project opening reports were received that a vehicle had gotten off the paved shoulder and was stuck in the sand backfill. When another vehicle had the same problem a few weeks later a request came for a remedy. Mixing cement with the top 0.3 meter (one foot) of the sand was recommended. This was not done since no further vehicles were reported stuck. The trench width was not specified on the plans. If the contractor could keep it narrower they were entitled to the benefits. (Steinberg, 1981)

IH 37 in southeast San Antonio was rehabilitated in the late 1970's. A 3.2 kilometer (two miles) cut section had required $50,000 to $100,000 a year in maintenance expenses. The repeated level ups with asphalt concrete had attracted considerable attention from local residents including a state legislator. A revision of the section providing positive drainage from the eight lane divided highway's median to the outside ditches included placing the geomembrane 2.4 meters (8 feet) deep along both outside shoulders. This time the contractor used a trenching machine for the excavation. A conveyor belt carried the excavated material to a dump truck. A cement stabilized base poured from a portable batching plant moving along the pavement capped the trench. Again pre- and post construction testing was extensive. Serviceability indices showed the geomembrane provided a smoother riding surface than the adjacent untreated control sections. Moisture sensors initially indicated the geomembrane minimized moisture change but their effectiveness was short lived. No maintenance was

required on this project for 12 years. These results made the engineers happy and didn't hurt their public image at all. Many of these tests and subsequent TxDOT geomembrane projects were conducted by Texas A & M University's Texas Transportation Institute, usually directed by Professor Robert L. Lytton.

An additional 21 TxDOT projects have used geomembranes. Generally placement was vertically 2.4 meters (8 feet) deep along the shoulders. Where city street rehabilitation was involved placement was horizontal. Another IH 10 rehabilitation project on San Antonio's eastside, awarded shortly after the IH 37 contract, used the geomembrane vertically. By the time of its plan preparation a generic geomembrane specification had been developed. The contractor used a trenching machine and in areas where original construction had placed underdrains to deal with seeps, trench wall sliding developed. The solution was to move the trench further away from the shoulder and place additional geomembrane horizontally to tie to the shoulder. The horizontal material required a subgrade cover due to the geomembrane's ultraviolet light sensitivity. As the years went by with no pavement maintenance expenses on the project, the resident engineer commented it had made a believer out of him.

A series of rehabilitation projects were awarded on IH 10 between San Antonio and Seguin. These projects were usually in cut sections where the expansive clays were changing the initially smooth riding pavements to ones providing the typical distorted section. On these projects the contractors generally used a trenching machine to excavate the material where the geomembrane would be placed vertically. One of the projects specified base scalpings as trench backfill. When they were used up the contractor suggested a finer material. It was found later these fines didn't compact very well. Cracking developed on the paved shoulders. Nondestructive testing revealed voids in the backfill. Pumping grout into those areas solved the problems. On the subsequent projects the engineer specified a concrete gravel.

On a project north of Snyder in west Texas the engineer and contractor experimented using different types of backfill material. They concluded that using the excavated material for the trench worked just as well as any of the other materials. On a major rehabilitation and widening of IH 45 the highway linking Dallas and Houston, the deep vertical moisture barrier, a geomembrane, was used along the outside shoulders of both mainlanes. The contractors bid for the geomembrane work on the 20.9 kilometer (13 mile) project for excavation, fabric, and backfill totaled over $1 million.

Not all geomembrane projects were considered a success. Two farm to market highways north on IH 10 between San Antonio and Houston had recurring pavement distortions after geomembrane placements of 2.4 meters (8 feet). Another project south of San Antonio in Atascosa County has considerable post construction cracking. One theory suggested a subsurface fault was causing the movement. On TxDOT geomembrane projects pre- and post construction testing was not as extensive as their first three locations. (Steinberg, 1985)

One privately owned project in Texas was the Laredo tire test track. The expansive soils there had caused considerable distortion to the pavement sections. Placement of the geomembrane vertically created a way of dealing with the destructive movements. Some of the proposed geomembrane sections were reduced by the owner's interests resulting in the question as to whether this limitation impaired the geomembrane's effectiveness. Overall the geomembrane vertical and horizontal moisture barriers on Texas highways were considered a success.

WYOMING'S EXPERIENCES

Probably the state highway department placing the most geomembranes is Wyoming. Over 50 highway rehabilitation projects by the Wyoming Department of Transportation (WyDOT) have used geomembranes. These projects extend from one corner of the state to the other. Prior to using the geomembranes WyDOT had used the method recommended by their neighbors to the south, Colorado. There they blast and recompact the shale. In Wyoming it didn't seem to solve the expansive soil's destructive movements. WyDOT in the early 1980's started using the geomembrane vertically 1.2 meters (4 feet) deep.

WyDOT's current procedure is placing the geomembrane horizontally across the roadway subgrade and then vertically along the outside shoulders. Depth of vertical placement will vary from 0.9 to 1.5 meters (3 to 5 feet) generally reaching a rock condition. Over 3,344,000 square meters (4 million square yards) of the geomembranes have been placed. Testing has indicated the results are usually very good and continues to be used.

OTHER STATES' EXPERIENCES

Ten other state highway departments in the United States have used the geomembranes to control these expansive soils. Mississippi's placement pattern was different. On a test section they placed the geomembrane horizontally starting 2.7 meters (9 feet) from the roadway centerline extending to the ditch backslope. Early indications were a lack of satisfaction with the results. (Browning, 1992)

AUSTRALIAN GEOMEMBRANE EXPERIENCES

The use of geomembranes to control the expansive soil's destructive movements is not limited to the United States. Australia has used it on their highways and on building sites in the state of Victoria. Much of the work there was led by Dr. James Holden, then at Victoria Roads Authority (VICRoads), now at Swinburne University. Working there with the Civil Engineering Department Director, Kerry McManus, significant developments have taken place.

Initial highway placements by VICRoads involved cutting a trench 1.8 to 2 meters (6 to 6.5 feet) deep, placing and backfilling the geotextile. The process was viewed as effective in controlling the moisture and volumetric changes in their expansive soils. Since the expansive soils in Australia seem most prevalent in that subcontinent's coastal area where 80% of their population live, efforts to control costs were a prime consideration. This resulted in narrowing the trench width and reducing cost.

The solution developed a special trenching boom cutting the 1.8 to 2 meter (6 to 6.5 foot) depth with a width of 7.6 to 8.9 centimeters (3 to 3.5 inches). A flowable backfill of cement, fly ash, sand, and water has further reduced the cost. The Australians are using these developments on several of their highways in Victoria. In addition they have worked with several municipal councils in addition to the city of Melbourne in using this technique to reduce building damages from the expansive soils. Results are assessed as very satisfying. (Evans, Holden & McManus, 1997)

OTHER COUNTRIES' EXPERIENCE

Other countries outside of the United States using the geomembranes to control the destructive movements of their expansive soils are China and Israel. The Chinese have reported 20% of their rail system is built over expansive soils. They have noted the intrusion into their rail ballast of the clays causing severe problems for train movement. Success has been achieved by placing geomembranes horizontally over the expansive subgrades. While unprotected sections have required continuing high maintenance expenses, the geomembrane protected areas are spared delays and costs.

Israel has used the geomembranes on several of its highways. They were used on roads in the northern part of the country. Later placements were used on widening and improving the highway between Tel Aviv and Jerusalem. Testing has been conducted and results are awaited.

PLACEMENT

Placement of the geomembrane horizontally has never been a problem. On the early Texas urban street rehabilitation the geomembrane was unrolled by hand using TxDOT District maintenance personnel. On many of the later projects the fabric is unrolled from the framework attached to the front end of a tractor.

Placement vertically was once described by a contractor as impossible. The District Engineer, Raymond Stotzer, cleared the air by reminding the man he bid it and he would build it. A utility subcontractor came in with a backhoe and did the job. Trenching machines were usually the equipment of choice. The Australians development of the special boom attachment to a trencher seems to be the most economical. With a 7.6 centimeter (3 inch) wide trench the flowable backfill should provide an efficient, low cost placement operation.

Early geomembrane installation rates have increased from 91 to 122 meters (300 to 400 feet) a day to 0.8 kilometer (one-half mile) a day. In Wyoming where geomembrane was placed horizontally and vertically the ability to get the fabric on the roadway section covered with base was a governing force. The 0.8 kilometer (one-half mile) a day seemed the usual. Australia reports 610 meters (2,000 feet) a day is a reasonable goal.

COSTS

There has been a considerable decrease in cost. Early Texas projects had bid prices for the entire vertical geomembrane placement operation at $65 to $82 per meter ($20 to $25 per foot). On the big IH 45 TxDOT contract the bid price for the geomembrane work complete was $20 per meter ($6 per foot). WyDOT with its horizontal and vertical placements gets bids of $1.20 to $1.50 per square meter ($1.00 to $1.25 per square yard). As the work becomes more usual the prices have come down considerably.

DURABILITY

Durability is a lingering question. How long will a geomembrane last in the ground under a base and pavement? Twenty years after a coated polypropylene was placed on a highway project, its manufacturer found it to still be in good shape. An independent

geotechnical consultant reports similar results as did a WyDOT study. This latter work indicated, despite some damage evidenced in the placement of the base on top of the geomembrane and some loss of the original design strengths, the roadway continued to have a smooth undistorted pavement. Durability poses no problem if minimal precautions are taken.

TESTING

A cautionary note is appropriate here. Failures frequently focus on the lack of preconstruction testing; not drilling enough test holes; not looking at the site soil conditions. Some failures occur for lack of testing. Others may be assessed negatively when in actuality no geomembrane was placed there.

CONCLUSION

The future can only be viewed brightly. It is safe to say geomembranes, when used after appropriate preconstruction site testing, can control the destructive movements of expansive soils.

Many of the details not fully covered here are found in a McGraw-Hill book published in July, 1998 written by this author.

ACKNOWLEDGEMENTS

Fu Hua Chen, Bill Hawkins, Raymond Stotzer, Doc Morris, Bob Lytton, Mike Hager, Gdalyah Wiseman, Amos Komornick, Gerald Hewitt, Jim Holden; and to all those from Atterberg, Terzaghi, Casagrande, Peck; and to all who passed their knowledge along.

REFERENCES

Browning, G.S.,(1992) "Evaluation of Soil Moisture Barrier", Mississippi Department of Transportation, Vicksburg, Mississippi.

Evans, R., Holden, J.C., and McManus, K., (1997) " Application of a New Vertical Moisture Barrier Construction Method for Roadway Pavements", Swinburne University, Melbourne, Victoria, Australia.

Froebel, R.K.,(1977) "Geosynthetics Technology, Manmade Fabrics and Textile Dictionary", Celanese Corporation, Charlotte, North Carolina.

McDonald, E.B., (1973) "Experimental Moisture Barrier and Waterproof Surface", South Dakota Department of Highways, Pierre, South Dakota.

Snethen, D.R. and Johnson, L.D., (1969) "Technical Guidelines for Expansive Soils on Roadway Subgrades", U.S. Army Corps of Engineers (USACE), Waterways Experiment Station (WES), Washington, D.C.

Steinberg, M.L., (1985) "Monitoring the Use of Impervious Fabrics, Geomembranes, in the Control of Expansive Soils", Department Research Report No. 187-12, State Department of Highways and Public Transportation, Austin, Texas.

Steinberg, M.L., (1981) "Deep Vertical Fabric Moisture Barriers in Swelling Soils", Transportation Research Record 790, Washington, D.C.

Tan, S.S., (1975) "Drainage Under Pavements", E.I.DuPont de Nemours, Wilmington, Delaware.

Terzaghi, K. and Peck, R.B., (1967) "Soil Mechanics in Engineering Practice", Second Edition, John Wiley and Sons, Inc., New York, N.Y.

Watt, G. and Steinberg, M.L., (1972) "Measurements of Swelling Clay in a Ponded Cut", Research Report 118-6, Center for Transportation Research, University of Texas, Austin, Texas.

Wooltorton, D., (1936) "A Preliminary Investigation into the Support of Foundations in the 'Black Cotton' and Kyatti Soils of the Mandalay District, Burma", Proceedings of the International Conference on Soil Mechanics and Foundation Engineering, Harvard University, Cambridge, Massachusetts.

DESIGN & ANALYSIS OF A GEOSYNTHETIC REINFORCED LEVEE TEST SECTION

RICHARD J. VARUSO
U.S. ARMY CORPS OF ENGINEERS, USA

JOHN B. GRIESHABER, PH.D., P.E.
U.S. ARMY CORPS OF ENGINEERS, USA

M. S. NATARAJ, PH.D., P.E.
UNIVERSITY OF NEW ORLEANS, USA

ABSTRACT

Reinforced levee test sections have been constructed and monitored in southern Louisiana since the late 1980's. Although the results of these test sections indicated that the anticipated stresses were never realized by the geosynthetic reinforcement, each test section has provided the geotechnical industry with some very important information about the effectiveness of using geosynthetic reinforcement. The most important information acquired from these previous test sections was the fact that the foundation soils experienced significant gains in shear strength due to the consolidation of the soft foundation material during and immediately following embankment construction. The New Orleans District of the U.S. Army Corps of Engineers (NOD) is researching the viability of a new design methodology that would adequately account for these gains in shear strength resulting from consolidation. This new methodology was derived via the results from the NOD's latest geosynthetic reinforced levee, discussed herein.

INTRODUCTION

Background

Earthen embankments located on foundations of low strength high water content clayey soils are quite common in southern Louisiana. These foundations have made it necessary for the design engineer to specify embankments with very large cross-sections in order to maintain stability and an adequate factor of safety. This has resulted in high construction costs for river and hurricane protection levees due to the enormous expense of embankment fill, land taken by the levee base, and wetland acquisition. These requirements have prompted geotechnical engineers to come up with new, innovative ways to construct these protection levees with lower design, real estate, and construction costs. Designing earthen embankments, reinforced with geosynthetics (namely geotextiles and geogrids) has become one of the most common and cost effective innovations used by the NOD. This paper presents the results from a reinforced levee

test section designed by the NOD which was incorporated into the mainline levee system of the Westwego to Harvey Canal Hurricane Protection Project, near New Orleans, Louisiana.

Previous Test Sections

The NOD has been utilizing geosynthetic reinforcement for levees on soft foundations since the late 1980's. In order to observe and document the performance of geosynthetics used in earthen embankments, the NOD has previously designed and monitored four (4) levee test sections, namely: The Westminster North-South Test Section (Hadj-Hamou et.al., 1987), The Empire "Reach A" Test Section (Bakeer et.al., 1988), The Bonnet Carre Test Section (Chiu et.al., 1989), and the St. Charles Test Section (Pinner, 1993). The stability analyses for the levee sections were completed using the current NOD design methodology, i.e. Wedge Method analysis (Caver, 1973) assuming soil strengths derived from unconfined-undrained (UU) triaxial test, with the stress of the geosynthetics at 5% strain incorporated as a horizontal resisting force in the stability equation. The instrumentation utilized in these test sections typically included strain gages installed on the reinforcement along with other various instruments to determine subsurface foundation conditions. One significant fact that has been learned from these previous test sections is that the design stresses assumed in the stability analyses were never realized by the reinforcement. The strain results (with respect to the design factors of safety) acquired from these test sections is illustrated in Table 1 below:

TABLE 1. STRAIN VALUES FROM PREVIOUS TEST SECTIONS

TEST SECTION	STRAIN (ϵ)	FACTOR OF SAFETY
Westminster North-South	1.67	1.3
Empire "Reach A"	2.30	1.3
Bonnet Carre	2.90	1.1
St. Charles	3.40	1.2

The reinforcement used in these test sections never experienced the design strain of 5% and therefore, never experienced the stresses for which the geosynthetics were designed. This indicates that, in these levee sections, the geosynthetics were not utilized to their fullest potential and the levee sections were somewhat over designed.

Further analysis of the previous test sections indicate that when an embankment is constructed on a soft foundation, this material experiences a significant increase in soil strength due to consolidation during and immediately following construction. This information was derived by monitoring the dissipation of excess pore water pressures as well as the consolidation of the foundation soils. The low strain readings recorded by the previous test sections have been attributed to this gain in shear strength.

Objectives

It is the goal of the subject test section to determine how to more efficiently utilize geosynthetic reinforcement in the NOD's levee embankments. The information derived from this test section will be used to derive a new design methodology which will account for the anticipated gains in shear strength due to consolidation during and immediately following construction.

DESIGN OF TEST SECTION

Site Geology

The test section is located south of the Mississippi River between the towns of Westwego and Harvey, LA. Elevations in the study area are less than +5 feet National Geodetic Vertical Datum (NGVD). The upper 25.0 meters of the foundation consist of Holocene deposits, which contain swamp, interdistributary, and prodelta deposits . Swamp deposits are approximately 2.5 meters thick and range in elevation from 0 to -23 feet NGVD. These deposits consist of soft to medium clays with some silt lenses and organics that have relatively high water contents. Beneath the swamp deposits are interdistributary deposits that are approximately 3.5 meters thick and range in elevation from -14 to -63 feet NGVD. Interdistributary deposits consist of soft to very soft clays with relatively high water content and contain some silts, organics, and shells. Prodelta deposits underlie interdistributary deposits and are approximately 6.0 meters thick, ranging in elevation from -57 to -78 feet NGVD. Prodelta deposits generally consist of massive clays of medium consistency with some silt.

Foundation Soil Properties

One hundred and fifteen (115) borings were taken along the proposed alignment of the entire Westwego to Harvey Canal Hurricane Protection Project. Of the 115 borings, eight (8) were taken along the Westminster East-West Levee, including one within the test section reach, see Figure 1. Soil laboratory tests consisting of consolidation (C), unconfined compression (UCT), unconsolidated-undrained triaxial (UU), and consolidated-undrained triaxial (CU) tests were performed on representative soil samples from all eight undisturbed borings taken in the area. Other related tests, such as natural water content, unit weight, and Atterberg liquid and plastic limits tests, were also performed on selected samples. Based on the boring and soils test data, the foundation soils were determined to be predominately fat clays varying in consistency from very soft to stiff. In some locations, organic clays and peat appear in the top 6.0 meters of the foundation and have a very soft consistency. The design values for cohesion and wet density are illustrated in Figure 2.

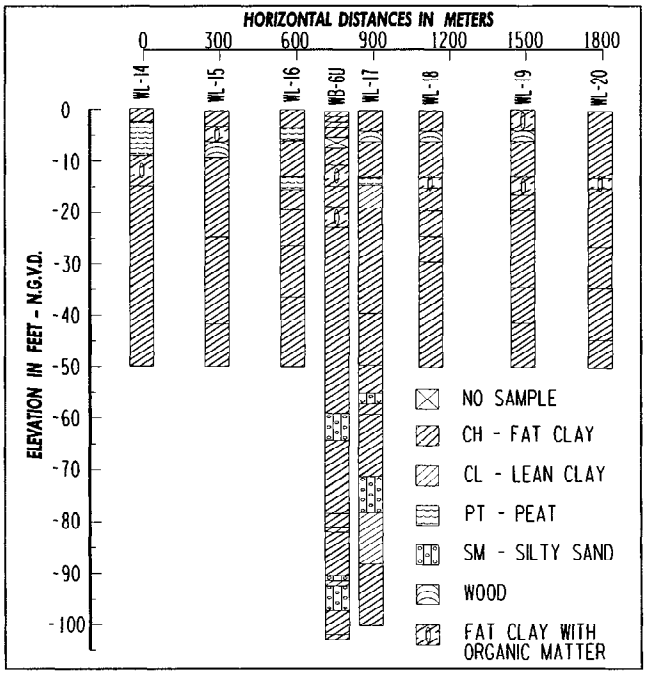

FIGURE 1. Soil Boring Logs

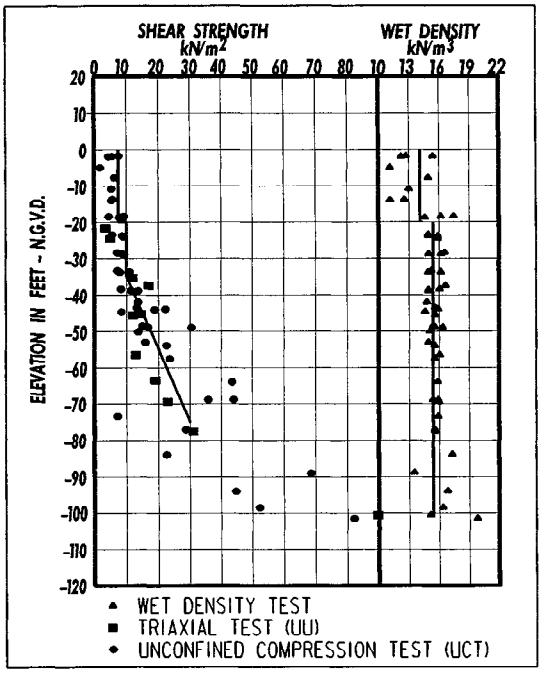

FIGURE 2. Shear Strength Profile

Test Section Analysis

Based upon the results from the previous test sections, the decision was made to design a test section that incorporated the predicted increase in soil strength as a result of consolidation during and immediately following construction. This section was to be constructed in approximately 0.75 meters of standing water and designed for a factor of safety of 1.0 using traditional design procedures. Two alternative sections were considered in the design phase: (1) reduce the size of the test section's cross section while utilizing the same geosynthetic tensile strength used in the mainline levee; or (2) keep the test section's cross section the same as the mainline embankment but reduce the required tensile strength of the reinforcement. The design of a levee section with a 1.0 factor of safety and geosynthetic having a 170 kN/m tensile strength did not prove to be feasible once the required wave berm and adequate clay cover for reinforcement pullout were considered. Furthermore, since this levee test section was going to be a part of a continuous hurricane protection levee system, it was advantageous for the test section to have the same geometry as the mainline levee. The stability analysis and resulting test section design are illustrated by Figure 3. This cross section would avoid any need for a transition section between the test section and the mainline levee system.

Cost estimates were established to determine the potential cost savings between an embankment with no reinforcement, the mainline levee design, and the test section alternative. This cost comparison is illustrated in Table 2. The total levee test section spans 274.5 meters of the mainline levee which is divided into three 91.5 meter reaches. The first reach contains a single layer of 85 kN/m geotextile, the middle reach uses a single layer of 85 kN/m uniaxial

geogrid, and the last is a double layer reach containing 57 kN/m uniaxial geogrid panels (top) and 17.5 kN/m biaxial geogrid panels (bottom). All tensile strength values mentioned above correspond to the wide width test values at 5% strain.

TABLE 2. DESIGN ALTERNATIVE COMPARISON

Design Analysis	Base Width (m)	Reinforcement	Cost	Savings
Preliminary	84	None	$4,397,646.80	-------
Mainline Levee	38	170 kN/m	$3,814,814.76	**$582,832 (13%)**
Test Section	38	85 kN/m	$3,573,039.40	**$824,607 (19%)**

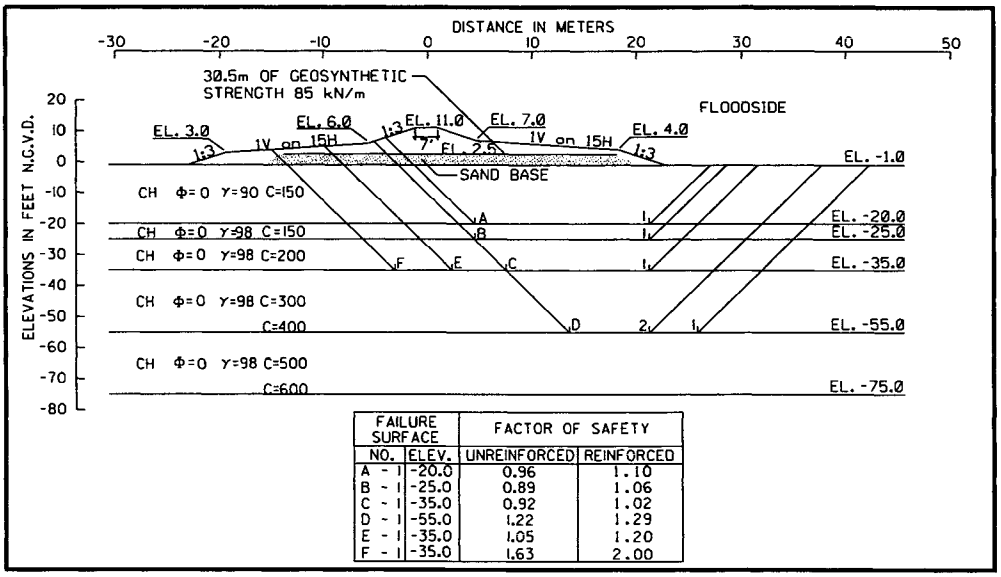

FAILURE SURFACE		FACTOR OF SAFETY	
NO.	ELEV.	UNREINFORCED	REINFORCED
A - 1	-20.0	0.96	1.10
B - 1	-25.0	0.89	1.06
C - 1	-35.0	0.92	1.02
D - 1	-55.0	1.22	1.29
E - 1	-35.0	1.05	1.20
F - 1	-35.0	1.63	2.00

FIGURE 3. Test Section Stability Analysis

FUNCTION OF INSTRUMENTATION

For the subject test section, five (5) types of instruments were chosen to determine the condition of the subsurface foundation and the geosynthetic reinforcement during and immediately following construction. These selected instruments included settlement plates (to determine actual settlement of the embankment and foundation), piezometers (to monitor changes in pore pressures), inclinometers (for measuring lateral movements in the foundation), and strain gages and extensometers (to keep track of the magnitude and location of the stresses in the geosynthetics). The layout of the instruments for this test section are illustrated in Figures 4 and 5. The results from the piezometers were used in conjunction with the settlement plates to determine when the foundation experienced consolidation. The inclinometer data was used to monitor potential failure surfaces and to determine the global strain present in the reinforcement. The strain gage and extensometer data were used to determine the localized strains in the

reinforcement due to the embankment loading. The combination of all of the instrumentation data, along with the information acquired from the previous test sections, would provide all of the information necessary to develop a new levee design methodology that would result in the smallest possible levee cross section while utilizing the geosynthetic reinforcement to its fullest potential.

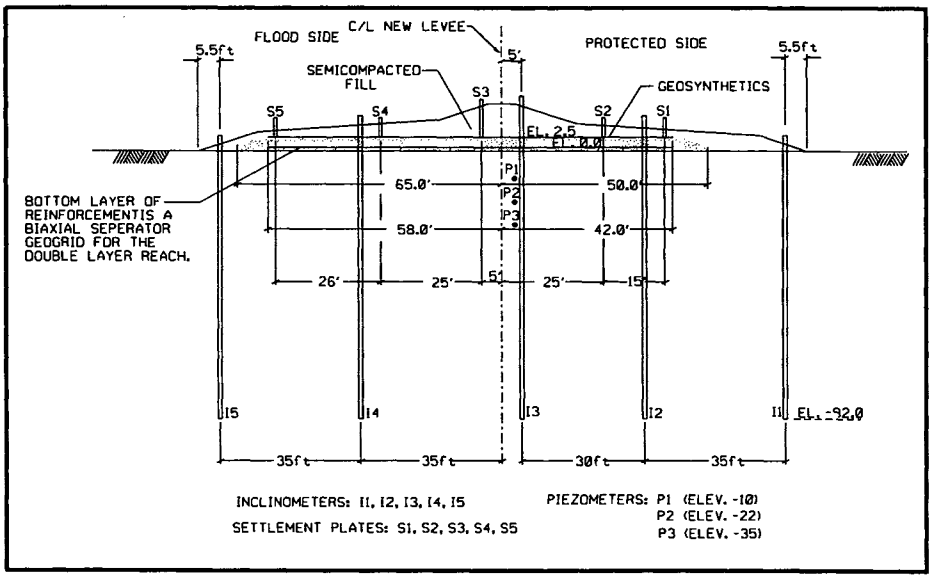

FIGURE 4. Location of Subsurface Instrumentation

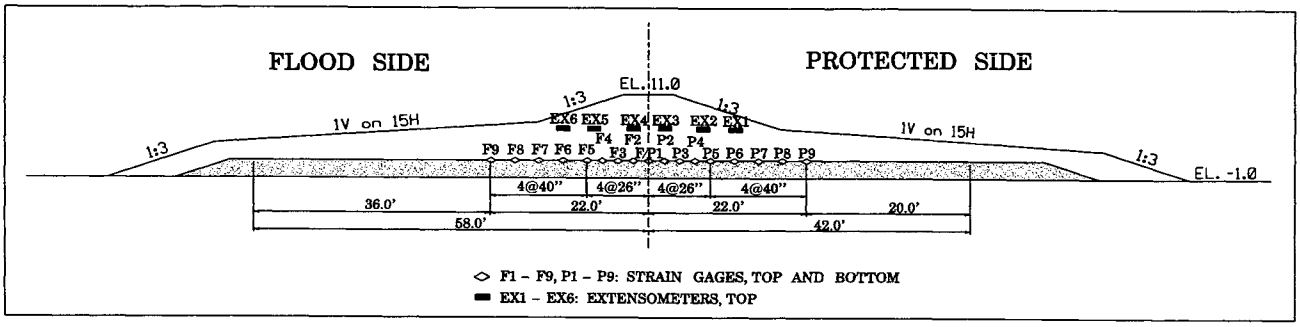

FIGURE 5. Location of Strain Gages and Extensometers

OBSERVED PERFORMANCE

Lateral Movement

The typical observed lateral displacements from the inclinometers for the three test section reaches are illustrated in Figure 6. The data plots illustrated in these figures reflect the lateral movements immediately following construction. Two important facts regarding embankment stability and performance can be established from these plots. First, it should be noted that the lateral movement of the foundation extended toward both the flood and protected sides of the

levee centerline. This confirms that the test section embankment is in a stable condition since gross movement in both directions is not indicative of an expected embankment failure mode. In addition, the magnitude of the observed horizontal movements did not exceed approximately 50 mm in either direction which is well within expected lateral movements beneath a hurricane protection levee on a soft foundation. This also indicates that a stable foundation condition exists beneath the test section embankment. Despite the fact that the test section was designed for a factor of safety of only 1.0, it is indeed stable and a reliable portion of the mainline levee system.

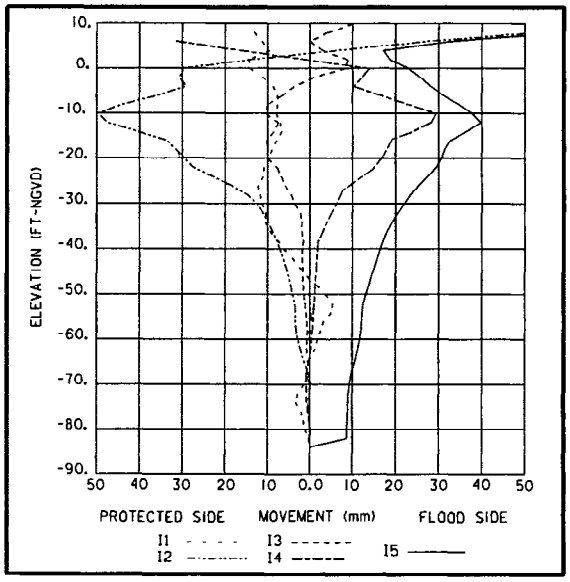

FIGURE 6. Typical Inclinometer Data

In addition to the condition of the levee's stability, the global strain present in the reinforcement may also be demonstrated by the inclinometer data. By taking the difference in horizontal movement measured from two inclinometers, with the greatest difference in horizontal movement at the elevation of the reinforcement, and dividing this value by the horizontal distance between the inclinometers, the global strain in the reinforcement is obtained. The global strain calculated for each of the three sections should be considerably lower than the local strains measured by the strain gages since the global strain takes into account the areas within the reinforcement which experience zero and/or negative strain. The following procedure was used for determining the global strain in the reinforcement (using inclinometers I2 and I5):

$$\epsilon_I = |(\Delta_{I2} - \Delta_{I5})|/D \qquad \text{(Eq. 1)}$$

where: ϵ_I = global strain

Δ_{I2} = the displacement read from inclinometer I2

Δ_{I5} = the displacement read from inclinometer I4

D = the horizontal distance between the inclinometers

Taking the appropriate values from Figure 6:

ϵ_I = [|(-53-42))|/32000]*100
= 0.30 % strain

The calculated global strain for each test section reach using this method of strain analysis can be found in Table 3:

TABLE 3. Global Strain Results from Inclinometer Data

Test Section Reach	Inclinometers Used	Global Strain (%)
Geotextile Section	GTI2 & GTI4	0.62
Single Layer Geogrid Section	G1I2 & G1I4	0.35
Double Layer Geogrid Section	G2I2 & G2I5	0.30

Pore Pressure

The information acquired from monitoring changes in excess pore water pressure in the 12 piezometers would be vital to comprehending the increases in shear strength that occurred in the foundation as well as the time and rate these increases occurred. As the height of the levee cross section increased during embankment construction, there were corresponding increases in pore pressure as indicated by the rising of the piezometric levels. This is illustrated by the typical Piezometric Level vs. Time graph, see Figure 7. Once the piezometric levels peak near day 50, and there is a subsequent time-dependent dissipation of pore pressures, these soft clayey layers undergo primary consolidation according to the Terzaghi theory of consolidation (Lambe & Whitman, 1969).

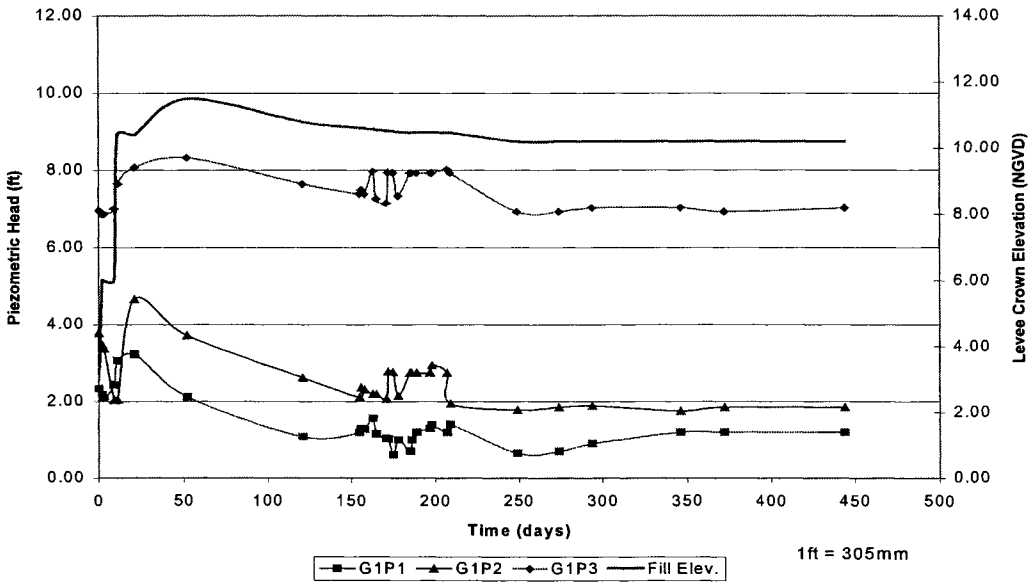

FIGURE 7. Typical Piezometer Data

Minor fluctuations did occur in the piezometric levels between days 160 and 210 that were not associated with increases in embankment fill. These subtle increases and almost immediate decreases in piezometric level were more than likely caused from numerous and intense rainfall weather patterns during that time. The rapid rise and fall of the piezometric levels during these periods indicates the presence of additional drainage paths other than vertical dissipation through the foundation. These paths could be associated with existing desecration cracks, large voids caused from biodegradation of organic materials, lenses and layers of silts and sands, etc., and therefore add to the rapid increase in shear strength found from classical consolidation.

Settlement

As various lifts of the embankment material were placed on the levee, there were corresponding increases in settlement at those times. This is what is expected to happen when constructing a levee embankment on a soft foundation. This is similar to the behavior of the piezometric levels mentioned earlier; and comparing Figure 8 to Figure 7, we see that the sudden increases in piezometric levels occurred at the same times as the increases in the settlement curves – both of which corresponded to significant increases in embankment material.

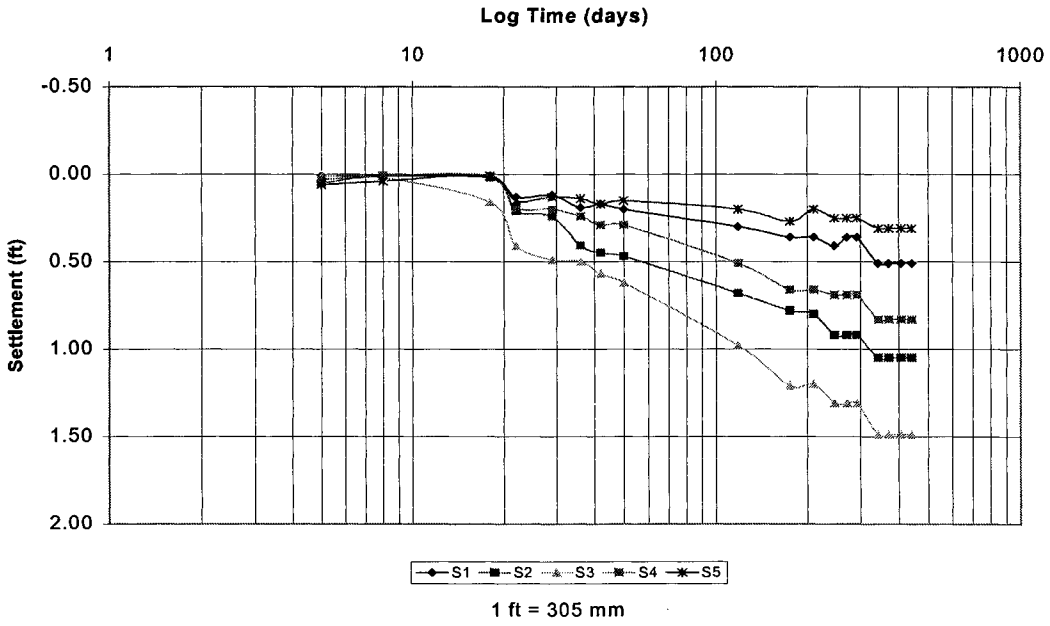

Figure 8. Typical Settlement Data

Further observing Figure 8, the amount of settlement experienced by the foundation after approximately 440 days ranged between 150 and 450 mm beneath the levee berm toe and centerline, respectively. This is well below the predicted total compression of 920 and 1830 mm derived from Boussinesq settlement analysis. This illustrates the additional benefit of lower overall settlement beneath an embankment constructed on a semi-rigid foundation created by the geosynthetic reinforcement. Since this is a multi-lift construction project, less material, effort, and overall cost will be required during second lift construction as a result of this reduced

settlement. In addition, there is an apparent decrease in the slope of the curves between days 40 and 50. This is evidently due to the upper strata completing primary consolidation, therefore causing the rate of settlement of the total foundation to decrease. It was anticipated during the design phase of this levee test section that the majority of the increases in shear strength would occur during primary consolidation and that this consolidation would occur rapidly during the construction of the levee. This has indeed been proven to be the case based upon the presented piezometer and settlement data and will be further shown by the ensuing discussion on the post-construction boring information.

Post Construction Borings

Approximately 6 months after the construction of the levee, four 5 inch undisturbed borings were taken through the centerline of the test section. In addition, one undisturbed boring was taken along the alignment of the nearby Westminster North-South Levee Test Section mentioned earlier. The logs for these five borings are illustrated in Figure 9. Visual classifications, water content, unit weight, and Atterberg liquid and plastic limits tests were performed on selected samples. Soil laboratory tests consisting of consolidation, unconsolidated-undrained triaxial (UU), and consolidated-undrained triaxial (CU) tests were performed on representative soil samples from all five post-construction borings. The results from the UU triaxial tests were plotted with depth and compared to the strength line derived from the pre-construction boring test data. The results are illustrated in Figure 10 and the magnitude of the soil strength increase is evident. In the upper stratum, from elevation 0.0 to –10.0 feet NGVD, there was a 135% increase in the cohesive strength of the soil (from 7.1 kN/m^2 to 16.8 kN/m^2). In the subsequent strata, the increases ranged from 50% to 67% gains in strength of the cohesive materials. Post-construction consolidated-undrained tests were also performed on samples from the more critical strata to determine how the foundation materials would react to consolidation conditions.

Strain Readings

During the design phase of this project, it was determined that the geosynthetic reinforcement should have been subjected to a stress of 85 kN/m in order to maintain stability. Based upon the specifications for this project, this stress should have correlated with a strain of approximately 5%. However, the highest recorded strains for the geotextile, the single layer geogrid, and the double layer geogrid reaches during the construction phase were 2.63, 2.15, and 1.97 percent, respectively. Figure 11 illustrates the typical strain rate over time. The strain in the reinforcement was established via 36 strain gages installed on each of the three reaches (18 gages on the top and 18 on the bottom) for a total of 108 gages over the entire test section. The results from the strain gages indicated that the general trend of the strain over time was very much as it was expected to be, i.e. a gradual increase in strain over time. There are a few possible reasons that the strain in the reinforcement did not reach the anticipated 5% during construction, the most probable reason being that the gains in shear strength which occurred due

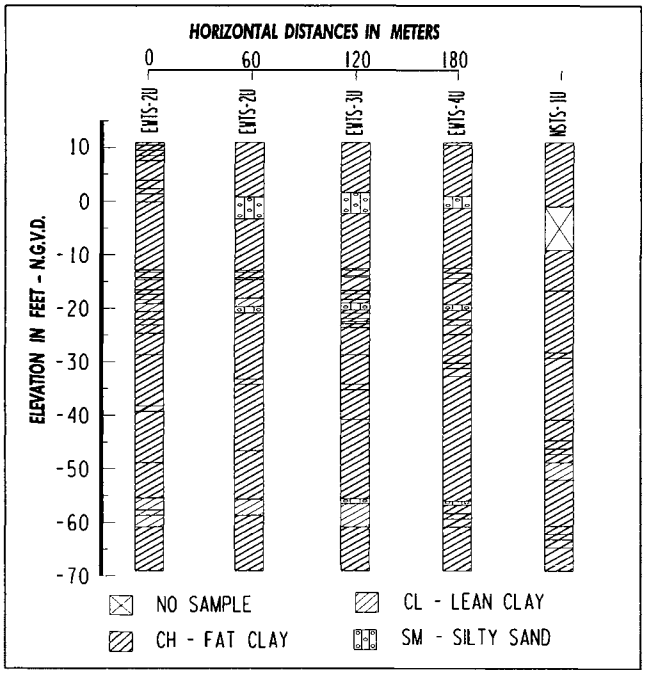

FIGURE 9. Post Construction Soil Boring Logs

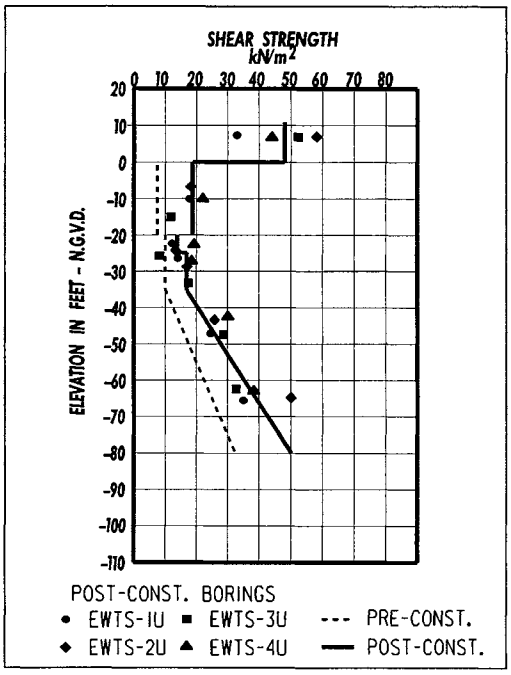

FIGURE 10. Shear Strength Profile

The strains with respect to location beneath the levee section were also plotted. It was found that the recorded strains in the top and bottom gages at the same location were quite different in many cases. This is an indication that reinforcement may not be lying flat in the ground which could be caused from potential rutting of the sand base by mechanical equipment, improper installation of the reinforcement, mud waves caused by fill placement, or variations in near surface settlement due to non-uniform sand base and embankment loading. This would affect

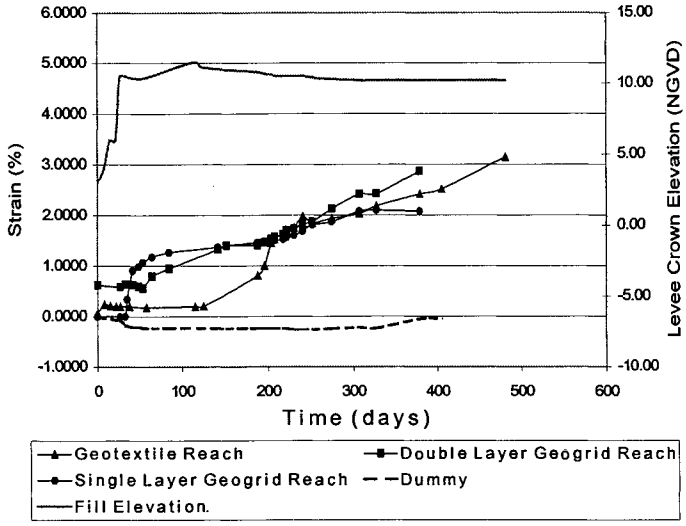

FIGURE 11. Strain vs. Time

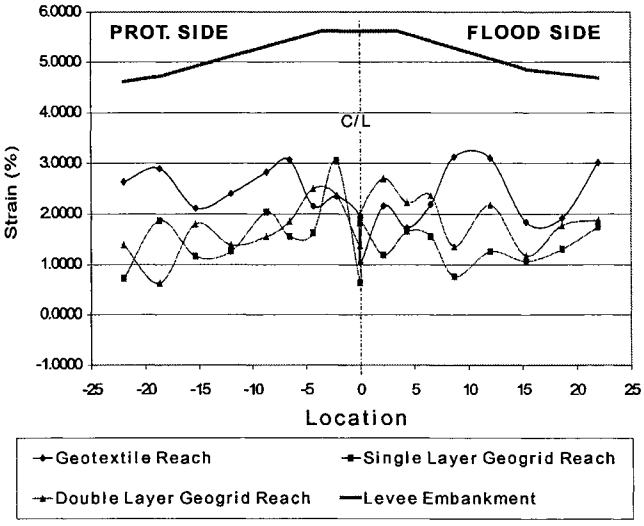

FIGURE 12. Strain vs. Location

the overall length of the reinforcement (L) affecting the strain ($\Delta L/L$) for each particular gage. To compensate for this condition, the average of the top and bottom strains were calculated for the three test section reaches. The maximum recorded average strains for the three reaches during the total monitoring period were 3.6, 2.6, and 3.0 percent and are illustrated in Figure 12.

During the installation of the strain gages to the geosynthetics, a rubber-type coating was placed over each gage to combat any potential effects that the ground water might have on the gage readings. To determine the performance of this coating (and therefore the reliability of the gage readings), a small section of reinforcement with a coated strain gage was placed outside of the loading area and at the same depth as the levee reinforcement for each test section reach. The strain readings for these gages was monitored over time to see if any notable change in strain reading occurred as a result of in situ ground conditions. No discernible change in strain reading was observed by these gages during the monitoring period as illustrated by the "Dummy" line in Figure 11.

The six extensometers that were installed on each the three test section reaches (a total of 18 extensometers) had the purpose of verifying the strains recorded from the strain gages. Observing these recorded strains, it was found that there were some problems with the readings from the 18 extensometers. The majority of the extensometers started to show strain in the first couple of months but then stopped recording strain after approximately day 25. This indicates that most of the extensometers were damaged during the construction of the levee; and therefore, the extensometer data is unfortunately of no real practical use for the purposes of this report.

Discussion of Results

The original boring data indicated that a substantial amount of very soft clayey and organic material existed in the upper strata of the foundation, particularly above elevation –20.0 ft-NGVD. The inclinometer data indicated that the largest lateral movements occurred within this stratum, just as expected for a soft sublayer beneath a stable earthen embankment. The embankment proved to be stable by virtue of the fact that the recorded displacements were minimal and showed logical horizontal movements away from the levee centerline.

The average strains measured in the geosynthetics correlate to stresses ranging from 22 kN/m for the geogrids to 41 kN/m for the geotextile. These values were less than what the reinforcement was designed to endure, despite the 1.00 factor of safety; however, these strains were quite a bit higher than those values recorded from the previous test sections.

The settlement data also indicated minimal movements partially due to the lateral spread of the upper soft strata indicated by the inclinometer data. These settlements correlated with observed increases and subsequent dissipation of pore water pressures after the levee embankment reached its designed cross section. This appears to have taken place within 160 days after construction began.

The shear strength increase due to the consolidation of the foundation, apparent from the foundation settlement and pore pressure dissipation, was further validated by the results from the post-construction UU triaxial test data. When compared to the original strength line, there were significant increases in shear strength (50 to 135 percent) throughout the embankment and the

subsurface foundation as a result of this consolidation. The data in Table 4 illustrates that it is reasonable to assume that the shear strength of the foundation material will act as defined by Equation 2 based upon the results from the triaxial test data illustrated in Table 4.

$$\tau = c + (\sigma - u)\tan\phi \qquad \text{(Eq. 2)}$$

where: τ = shear strength
c = cohesion
σ = effective stress (Boussinesq's Theory)
u = excess pore water pressure
ϕ = angle of internal friction

TABLE 4. TRIAXIAL TEST RESULTS

	Pre-Con. UU Test	Post-Con. UU Test	Post-Construction CU Test Data				Design Strength
Stratum	$\tau = c$ (kN/m^2)	$\tau = c$ (kN/m^2)	c_i (kN/m^2)	ϕ	$\Delta\sigma$ (kN/m^2)	$\tau_i = c_i + (\Delta\sigma)(\tan\phi)$ (kN/m^2)	$\tau_d = (\tau_i + c_i)/2$ (kN/m^2)
0.0 to -20.0	7.1	16.8	6.7	13	55	19.4	13.0
-25.0 to -35.0	9.5	14.4	8.6	11	48	17.9	13.3

A comparison of the shear strength values determined from the pre-construction UU tests with the cohesive intercepts obtained from the CU tests shows that the strength values proved to be approximately the same. It is evident then, that the CU test failure envelope closely approximates the relationship between the shear strength of the soil and the overburden pressure on the foundation. The CU test data also shows that the calculated shear strength which the foundation soil should feel due to the $\Delta\sigma$ stress after construction, τ_t, is higher than the value determined from the post-construction UU test, by about 25%. It can be concluded then, that the CU failure envelop over estimates the total shear strength of the foundation. Noting that the cohesive intercept is reasonable, this over estimation of shear strength likely results from assuming an excessive induced pressure, $\Delta\sigma$. The reduction of the estimation of $\Delta\sigma$ could be justified by considering the effects of lateral spread in the soft upper strata, excess pore pressures which potentially still exist in the foundation, and/or the geosynthetic's effect on the Bousinesq pressure bulbs, i.e. causing the embankment to act as one large, semi-rigid footing on the foundation. Realizing that the current methodology has proved to be too conservative and that assuming shear strengths based upon the CU failure envelope appears to be too unconservative, taking an average of these strength values, τ_d (Table 4), seems to be a reasonable approximation for the true shear strength. Of course, taking an average value of these strengths would only be legitimate if the pore pressures were allowed to dissipate and the foundation to consolidate during construction.

CONCLUSIONS

The results from the instrumentation showed that the test section embankment was stable with horizontal and vertical movements in the order of what would be expected of soft clayey soils in southern Louisiana. The pore pressure, settlement, and post construction boring test data indicated a very rapid and substantial increase in shear strength due to consolidation of the soft sublayers. These increases correlated very closely to values acquired from the post-construction CU triaxial tests performed on post construction boring samples. It is therefore the opinion of the authors that future reinforced levees, located on foundations similar to that discussed in this paper, could be designed by: (1) assuming the average strength value, τ_d, and varying this value along the levee cross section according to the appropriate $\Delta\sigma$, (2) analyzing the stability of the geosynthetic reinforced embankment for a factor of safety of 1.3 and (3) phasing the construction of the levee in stages such that pore pressures are allowed to dissipate and the foundation to consolidate as the embankment height increases. This new design methodology would significantly reduce the real estate, environmental and geosynthetic costs related to levee construction.

ACKNOWLEDGEMENTS

The authors would like to acknowledge the assistance of Barry Christopher, Ph.D., P.E., Geotechnical Engineering Consultant, and Khalid Farrag, Ph.D., P.E. of the Louisiana Transportation Research Center for providing their expertise during the design of the geosynthetic instrumentation and analysis of the test data.

REFERNCES

Bakeer, Hadj-Hamou, Duarte, and Satterlee, (1988) "Field Test of a Geotextile-Reinforced Levee", Journal of Geotechnical Engineering, pp 90-101.

Caver, William W. Jr., (1973) "Slope Stability in Soft Layered Soil Systems", Mississippi State University Graduate School, Master of Science Thesis, pp 23-34.

Chiu, Napolitano, & Duarte, (1988) "Bonnet Carre' Spillway Geotextile-Reinforced Test Section and Pullout Tests", USACE New Orleans District, pp 1-16.

Hadj-Hamou, Bakeer, and Gwyn, (1988) "Field Performance of a Geogrid-Reinforced Embankment", Journal of Geotechnical Engineering, p 80-89.

Lambe and Whitman, (1969) " Soil Mechanics", John Wiley and Sons, New York, pp 406-421.

Pinner, Richard, (1993) "St. Charles Parish Geotextile-Reinforced Levee Instrumented Section", USACE New Orleans District, p 2-14.

SOILS REINFORCED WITH DISCRETE SYNTHETIC FIBERS

Gunther Bauer, Professor, Faculty of Engineering, Carleton University, Ottawa, ON, Canada
Alexandru Oancea, Design Engineer, Windsor, ON, Canada

ABSTRACT

This paper discusses the technique of using discrete and randomly dispersed polypropylene fibers as reinforcement in granular soils. Two lengths of discrete fibers were tested in conjunction with four soils ranging from a uniform silica sand to a fine silt. Specimens of natural and reinforced soil were investigated in static triaxial compression. The compression behavior of these specimens was also used for comparison to the corresponding specimens of one-dimensional compression from oedometer tests. A constitutive model was employed to verify the experimental results.

The application of this technique of soil reinforcement was found to increase the strength properties of the four soils tested. This increase is more pronounced in fine silts than in medium or uniform sands. The strength increase is directly proportional to fiber concentration. The higher fiber concentration is, however, associated with larger strains to reach peak strength and corresponding greater volume changes.

INTRODUCTION

There are several studies reporting the results of triaxial testing on soil specimens reinforced with either continuous or randomly dispersed fibers. Leflaive (1982) used continuous filaments to improve the mechanical behavior of a uniform sand. Al-Refeai (1985) carried out triaxial tests on uniform sand specimens reinforced with discrete and randomly dispersed glass and reed fibers. Bouzaza (1994) tested dry sand enhanced with randomly dispersed polyamide fibers 20 mm in length. None of the previous researchers tested silty or well-graded soils to thr authors' knowledge. In these pervious studies there were also no volume change and pore pressure measurements reported.

The study consisted of testing triaxial specimens of uniform to well graded sand and silt specimens mixed with various concentrations of fibrillated polypropylene fibers. The pore pressures and volume changes were recorded under static compression. The results of these tests were compared to the corresponding behavior of the unreinforced soil specimens.

MATERIALS

Soils

Four types of soil were investigated: silty sand, sandy silt, medium sand and uniform sand. The grain size distribution of these soils is shown in Figure 1. The corresponding physical properties are given in Table 1. The maximum dry density and optimum moisture content for each natural soil was obtained from modified Proctor compaction tests. These four types of soil were chosen to cover a good range of granular materials. It should be noted however that the specimens tested were compacted by vibration using a surcharge weight to 85% of modified Proctor density. This compaction effort is somewhat lower as specified in the field but it assured a greater uniformity of soil density in the triaxial and oedometer tests as explained below.

Table 1. Physical properties of test soils

Soils	D_{50} (mm)	C_u	C_c	Max. Dry Density (kN/m^3)	Opt. Moisture (%)	φ^* (°)
Sandy silt	0.075	6.11	0.031	20.0	10.5	37
Silty sand	0.140	9.21	1.082	19.0	9.8	41
Medium sand	0.480	4.29	0.933	20.2	9.1	41
Uniform sand	1.500	1.68	1.112	16.0	3.5	39

* measured at peak stress

Fibers

A commercially available "heavy duty" polypropylene fiber was used to improve the physical properties of the test soils. These fibers are commonly used as twisted bundles in various lengths as secondary reinforcing elements in ready-mix concrete. These fibers are fibrillated (bundled), chemically inert and possess a high ultimate tensile strength (93 MPa). Due to the mixing action they become untwisted and disperse readily in the concrete mix. In this study they were used in their unbundled (separated) state. A special device was built (Oancea, 1996) to separate and untwist the "bundles". The resulting discrete fibers had two advantages, (1) the unbundled fibers increased the surface area in contact with the soil grains considerably compared to bundled fibers of the same weight and, (2) due to the curly or spirally shapes of the untwisted fibers it was assumed that they would disperse more uniformly in the soil matrix and would also provide better interlock. Two fiber lengths were investigated, 63 mm and 126 mm, in order to evaluate the effect of length on the mechanical properties of the composite. Four concentrations of fibers were used : 0.1, 0.2, 0.3 and 0.5 % of fiber weight to dry weight of soil.

TEST PROCEDURES AND RESULTS

Triaxial Tests

Compaction the triaxial specimens under similar conditions as in the Proctor test caused bunching of the fibers in the triaxial mold. In order to obtain a more uniform distribution of fibers within the soil, both

components were mixed in a dry state before water was added. This mixture was placed in a split mold mounted to a shaking table and vibrated under a surcharge weight to 85 % of modified Proctor density. It was realized that this density was lower than generally specified in the field but compaction (vibration) to a higher density caused the soil particles to segregate from the fibers. The cylindrical specimens, 100 mm in diameter and 200 mm in height, were then saturated in a triaxial compression cell under a specified back pressure. After consolidation they were sheared under drained conditions. The strain rate was kept sufficiently low in order to have fully drained conditions. The pore water pressure was monitored at the center of a specimen. The strain rate for a particular soil was adjusted accordingly in order not to generate any excess pore water pressures. The volume change during a test was also monitored. The confining pressure ranged from 100 to 700 kPa. The stress-strain relation for all four soils is shown in Figure 2 as a normalized plot where the deviator stress was divided by the corresponding confining pressures. The volume change with vertical strain for the four soils is given in Figure 3. The triaxial test results for the sandy silt specimens for various fiber contents are shown in Figure 4. From this figure it is quite evident that the peak deviator stress ratio increases with an increase in fiber content. For example, natural silty sand yielded a stress ratio of 8.1 at about 12.5% of vertical strain, whereas the composite having a fiber content of 0.5% yielded a peak stress ratio of 37 at 31% of strain. Therefore, it can be concluded that the increase in peak stress is associated with a corresponding increase in peak strain. But even at the same peak strain (12.5%) of the natural soils, the composites exhibited a pronounced increase in strength. Similar observations were made for the other three soils except the peak stress and corresponding strain increases were less pronounced than for the silty sand specimens.

Oedometer Tests

The one-dimensional compressive behavior of the soil specimens with various fiber concentrations was determined in a standard fixed-ring consolidometer (oedometer). The specimens, 100mm in diameter and 20mm in height, were prepared in the same fashion with corresponding dry densities and fiber contents as the triaxial specimens. In order to prevent a predominantly horizontal orientation of the fibers within the relatively thin specimen (i.e. 20mm) a collar was attached to the mold and the sample was compacted to double the height. It was then trimmed back. A series of 24 load increments were used in order to obtain a load-unload compression relationship. A total of ten oedometer tests were carried out. A typical test result is presented in Figure 5 for the silty sand specimens. One can observe from this figure that at any given load the corresponding compression or vertical strain increases with fiber content.

SHEAR STRENGTH

The shear strength of a fully drained soil is conveniently given by the Coulomb strength equation as

$$S = C' + \sigma' \tan \varphi' \qquad (1)$$

where c' and φ' are the effective parameters for cohesion and the angle of shearing resistance respectively and σ' is the effective normal stress. Several researchers (Fatani and Bauer, 1991; Gray and Ohashi, 1983 and Jewell and Wroth, 1987) have modified this equation to incorporate the effect of the reinforcing elements as follows:

$$S_R = C_R + \sigma' \tan \varphi_R \qquad (2)$$

where the subscript R refers to the strength parameters of the composite. Figure 6 gives the strength envelopes for the silty sand together with those of the composite having various fiber contents. As is apparent from this plot the increase in fiber content will only increase the cohesion intercept whereas the angle of shearing resistance remains unchanged from that of the natural soil. The term C_R is known as the " apparent cohesion " or "reinforcing effect " and will be treated analytically later. The other three soils exhibited similar parallel and linear failure envelopes over the range of confining pressures applied. Table 2 presents a summary of the shear strength parameters of the natural soil and reinforced specimens.

Table 2. Shear strength parameters of natural and fiber reinforced soils

Soil	Density (kN/m^3)	Fiber (%)	Strain (%)*	Volume change (%)*	Shear angle (φ or φ_R)*	Cohesion (kN/m^2)*
Sandy silt	19.1	0	13.2	3.2	37	80
	18.7	0.1	24.6	5.8	37	158
Silty sand	18.4	0	10.1	2.6	41	0
	17.9	0.1	22.8	3.1	41	180
	17.4	0.2	24.3	3.6	41	342
	17.0	0.3	27.4	5.8	41	492
	16.8	0.5	32.5	6.9	41	688
Medium sand	19.6	0	6.1	+0.9	41	0
	19.2	0.1	9.0	+0.7	40	80
Uniform sand	15.5	0	6.4	+3.4	39	0
	15.2	0.1	11.5	+3.0	39	44
	14.7	0.3	17.4	+2.0	38	142

* determined at peak stresses

SECANT MODULUS

The secant modulus is an indication of the "stiffness" or "compressibility" of a soil. This modulus is defined as the slope of a straight line between the origin of the deviator stress-vertical strain relation and a point on the curve at a given strain or stress level. Soils rarely behave elastically and, therefore, the secant modulus varies (i.e. decreases) with strain level. From the oedometer test results presented in Figure 5 it is clear that the secant modulus decreases with vertical strain (compression) and also seems to decrease with increasing fiber content. The latter observation seems to be contrary to expectations. But there are two possible reasons for this behavior. First, the unit weight of the composite decreases as the fiber content is increased as shown in Table 2. Second, the composite is deformed under one-dimensional compression and therefore the fibers will not be subjected to tensile strains in order to mobilize their tensile strength. Figure 7 shows the variation of the secant modulus with vertical strain for the silty sand specimens subjected to a confining stress of 100 kPa. The modulus decreases with continuing vertical strain for the natural soil whereas there is little change in modulus values for the composite beyond 2 % of vertical strain regardless of fiber

content. Table 3 gives a summary of secant moduli obtained from the triaxial tests. The values shown are for 2, 4 and 6 % of vertical strain. It seems that there is little improvement in values with the addition of fibers to the natural soils. This observation leads to several conclusions. The addition of fibers to soils is beneficial only if the tensile strength of the reinforcing elements is mobilized. In order for this to happen the composite must dilate when sheared. Figure 3 shows the volume change and the corresponding vertical strain under triaxial shear for the four soils. Both silty sand and sandy silt specimens contract under vertical strains. Only after large vertical strains (i.e. greater than 15 %) there seems to be sufficient tensile strains in the fibers in order to mobilize their strength as indicated in Figure 4. These large strains are usually not accepted under field conditions. Even the medium and uniform sand specimens start to dilate only after vertical strains of 5 and 3 % respectively. Higher initial dry densities would decrease the vertical strains needed to mobilize the tensile strains in the fibers.

Table 3. Summary of secant moduli (Mpa)

Soil	Fiber (%)	Confining stress (kN/m^2)	Modulus value at vertical strains of 2%	4%	6%
Sandy silt	0	300	19.1	16.4	14.8
	0.1	300	15.6	13.2	11.6
Silty sand	0	300	21.6	19.4	17.1
	0.1	300	20.4	19.3	17.6
	0.2	300	15.1	12.5	12.1
Medium sand	0	400	66.2	43.0	29.8
	0.1	400	59.7	42.6	32.1
Uniform sand	0	200	32.2	19.8	14.4
	0.1	200	33.5	20.7	15.0
	0.3	200	29.6	20.1	16.3

ANALYTICAL MODEL

The load transfer mechanism between granular soil and an inclusion such as a cylindrical fiber is quite complex. Finite and boundary element methods have been used to model the interaction between sand and reinforcement (Andrawes et al. 1984). Gray and Ohashi (1983) proposed a static model relating the increase in shear strength of a reinforced composite to the initial inclination of fibers, the tensile stress within the fibers and the soil properties as follows:

$$\Delta S_R = t_R [\sin(90-\beta) + \cos(90-\beta)\tan\varphi] \quad (4)$$

$$\text{and } \beta = \tan^{-1}\left[1 / [r + (\tan\alpha)^{-1}] \right]$$

where t_R is the tensile strength mobilized in the fibers, ϕ the soil friction angle, and β is the angle of the deformed fiber with shear plane which is a function of the initial fiber inclination angle, α, and the shear distortion ratio,r, to be determined experimentally. In equation (4) the mobilized tensile strength area per unit soil area (t_R) can be estimated from the following relationship:

$$t_R = \sigma_R [A_R / A_C] \quad (5)$$

where σ_R is the tensile stress in the fibers, A_R is the cross-sectional area of the fibers transgressing the shear surface and A_C is the sheared area. Gray - Ohashi's model is based on the assumptions that the fibers do not slip or pull out and the soil outside the shear zone is rigid. The thickness of the shear is known or has to be assumed is either dilating or there is sufficient shear displacement in order to create tensile strains in the fibers. In order to predict the strength increase in a triaxial specimen where the fibers transgress the failure plane at random orientation, a fiber count was carried out on several specimens. The silty sand and sandy silt specimens had sufficient inherent cohesion to support themselves especially after they were air-dried. The highly permeable sand specimens were "hardened" by permeating them with a hardening epoxy. All these specimens could easily be separated after testing at the shear plane for visual inspection and fiber count. It was found that the initial fiber orientation was in the order of 35 to 45° to the normal of the shear plane. Using these values and the angular distortion corresponding to the peak shear strain, the increase in shear strength could be estimated. The results based on equations (4) and (5) are given in Table 4 together with the experimental results for a fiber content of 1%. The agreement between experimental values and those obtained from the Gray-Ohashi's model is fairly good except for the medium sand.

Table 4. Increase in shear strength (kN/m^2) with 0.1% fiber content

Soil	Experimental #	Equations (4) and (5)		
		35° *	45°*	max**
Sandy silt	158	156	159	162
Silty sand	180	162	168	174
Medium sand	80	67	70	78
Uniform sand	44	62	67	72

values also given in last column of Table 2
* angle of initial fiber inclination
** angle to yield maximum shear strength increase

CONCLUSIONS

The addition of discrete and randomly dispersed polypropylene fibers to four granular soils increased the shear strength considerably. This increase was in direct relation to fiber content. The shear strength of the composites can conveniently be expressed by the linear relationship of equation (2) over a range of confining pressures varying from 100 to 700 kPa. The angle of shearing resistance remained unchanged from the natural soil regardless of fiber content.

The vertical strains necessary to achieve the increase in shear strength were large and would generally not be acceptable in field applications. Higher initial soil densities will probably overcome the large strain effect.

Doubling the fiber length from 63 mm to 126 mm had no observable effect on the shear strength or the compressibility of the composite for the fiber contents investigated. It seems that a larger specimen size would be more suitable to investigate the possible influence of fiber length on shear strength and compressibility.

An increase in fiber content resulted in a decrease of secant modulus. The secant modulus of the various composites is, therefore, not a function of the confining pressure only but also of fiber content. Regardless of fiber content and confining pressure, the secant modulus of the four composites remained fairly constant after a vertical strain of about 2%. In contrast, the modulus of the natural soil specimens continued to decrease with strain.

The strength increase due to fiber addition can be estimated by the Gray-Ohashi model (equations 4 and 5) provided the physical properties of the soil and reinforcing elements are known. In the case of randomly dispersed fibers, fiber density and the angle of fiber orientation had to be determined or assumed for each soil and fiber content. Therefore, the model can be used to estimate the expected strength increase for similar soils with polypropylene fiber concentrations equal to those used in this study.

REFERENCES

Al-Refeai, T.O. (1985), "Constitutive behavior of fabric vs. fiber reinforced sand", Ph.D. thesis, Civil Engineering Department, University of Michigan, Michigan.

Andrawes, K.Z., McGown,A., and Kabir,M.H. (1984), "Uniaxial stregth testing of woven and nonwoven geotextiles", Geotexties and Geomembranes, Vol.1, No.1, pp.41-56.

Bauer, G.E. and Zhao,Y.J. (1994), "Effect of soil dilatancy on shear strength of reinforced composites", Proceedings, 5th International Conference on Geotextiles, Geomembranes and Related Products, Singapore, Vol.1, pp.369-372.

Bouzaza, A., Amorkane, K. and Aberkane, T. (1994), "Granular soil reinforced with geotextile and randomly reinforced fibers: a comparison", Proceedings, 5th International Conference on Geotextiles, Geomembranes and Related Products, Singapore, Vol.1, pp. 391-394.

Fatani, M.N. and Bauer,G.E. (1991), "Reinforcing soil with aligned and randomly oriented metallic fibers", Geotechnical Testing Journal, Vol. 14, No. 1, March, pp.78-87.

Gray,D.H.and Ohashi, H. (1983), "Mechanics of fiber reinforcement in sand", Journal of Geotechnical Engineering, ASCE, Vol. 109, No. 3, pp.335-353.

Jewell, R.A. and Wroth, C.P. (1987), "Direct shear tests on reinforced sand", Geotechnique, Vol. 37, No. 1, pp. 53-68.

Leflaive, E. (1982), "The reinforcement of granular material with continuous fibers", Proceedings, 3rd International Conference on Geotextiles, Las Vegas, Nevada, Vol. 3, pp. 21-726.

Oancea, A. (1996), "Triaxial compression of soils reinforced with discrete synthetic fibers", M.Eng. thesis, Department of Civil and Environmental Engineering, Carleton University, Ottawa, Ontario.

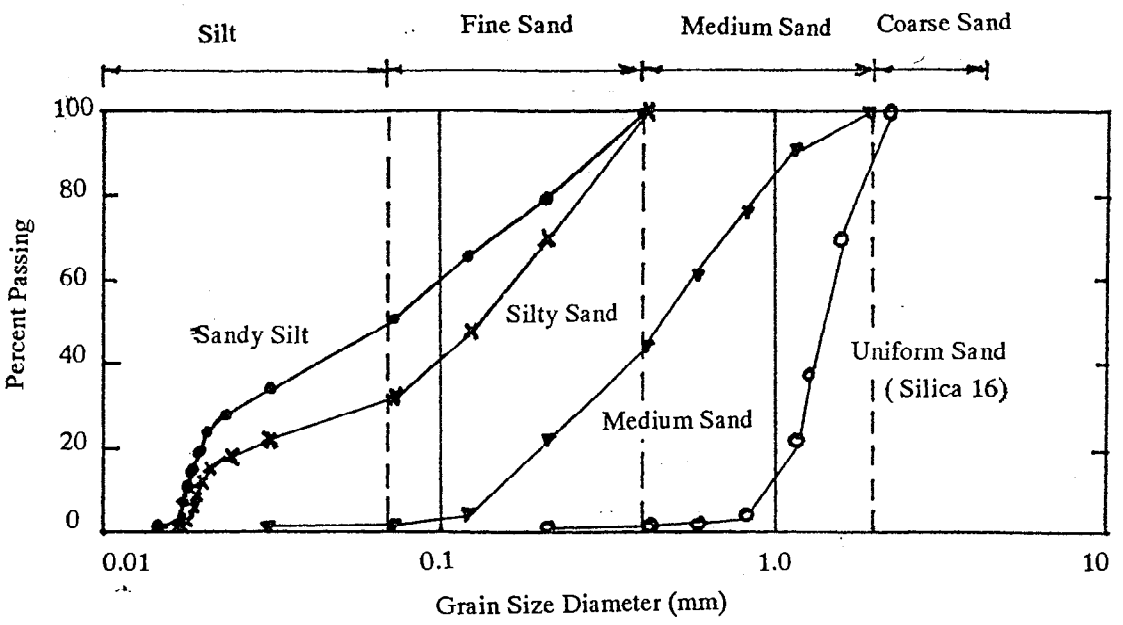

Figure 1. Grain Size Distribution of Test Soils

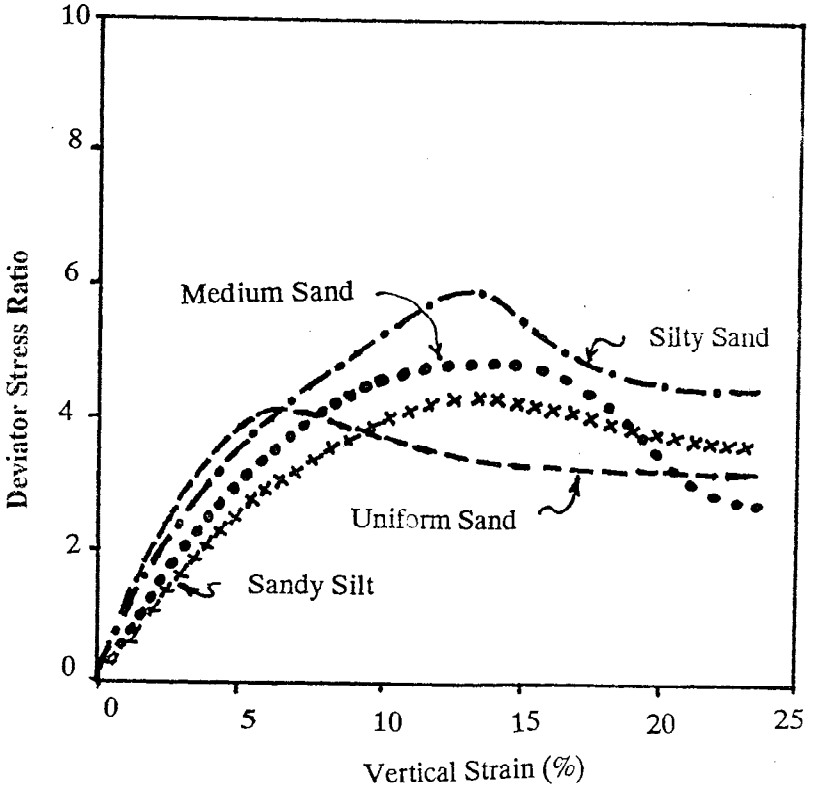

Figure 2. Deviator Stress Ratio vs. Axial Strain for Natural Soil Specimens

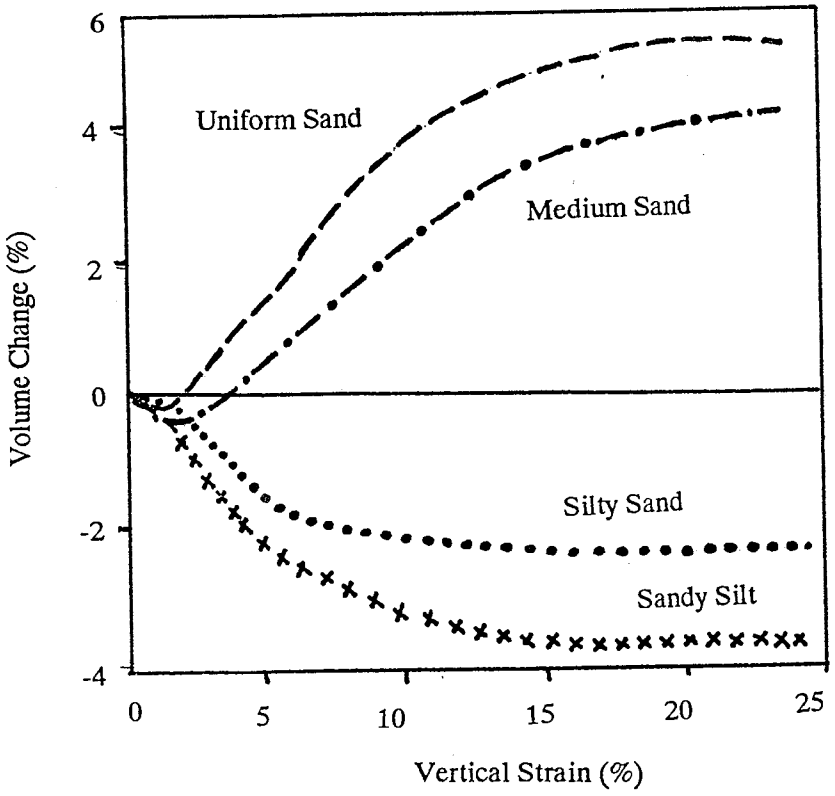

Figure 3. Volume Change vs. Axial Strain for Natural Soil Specimens

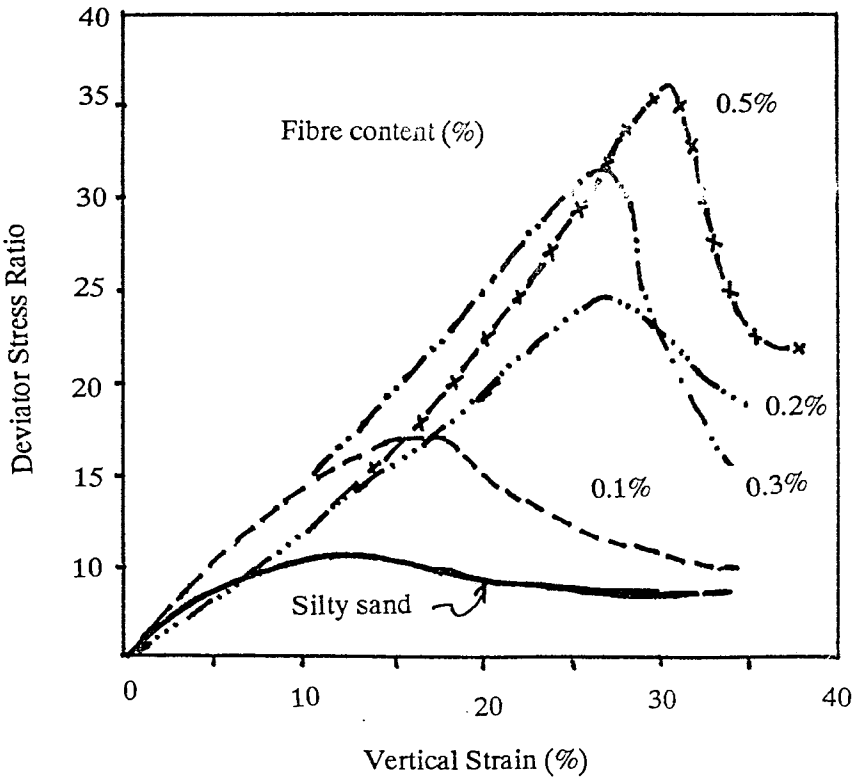

Figure 4. Deviator Stress Ratio vs. Axial Strain for Composites of different Fiber Content

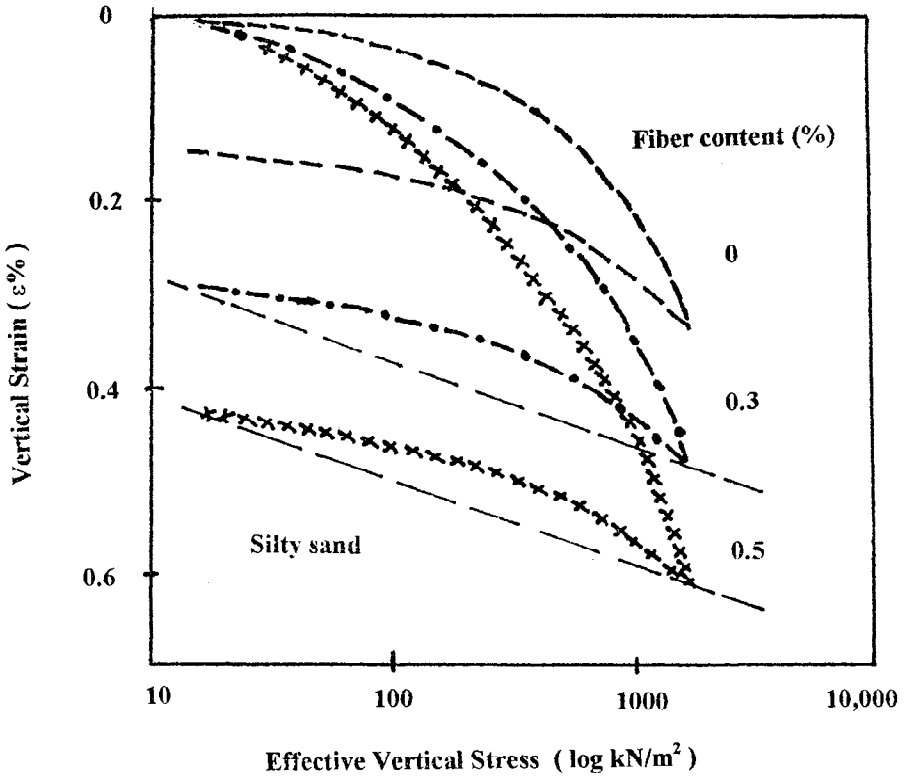

Figure 5. Compression of Silty Sand Specimens in Oedometer

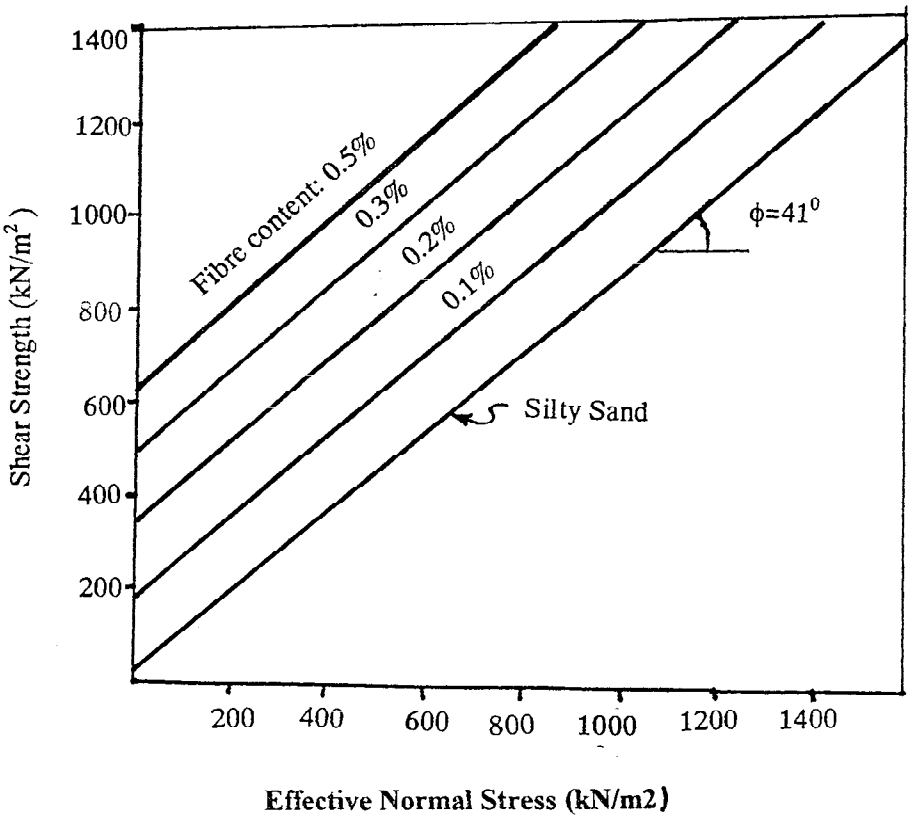

Figure 6. Coulomb Shear Strength Envelopes for Silty Sand Specimens

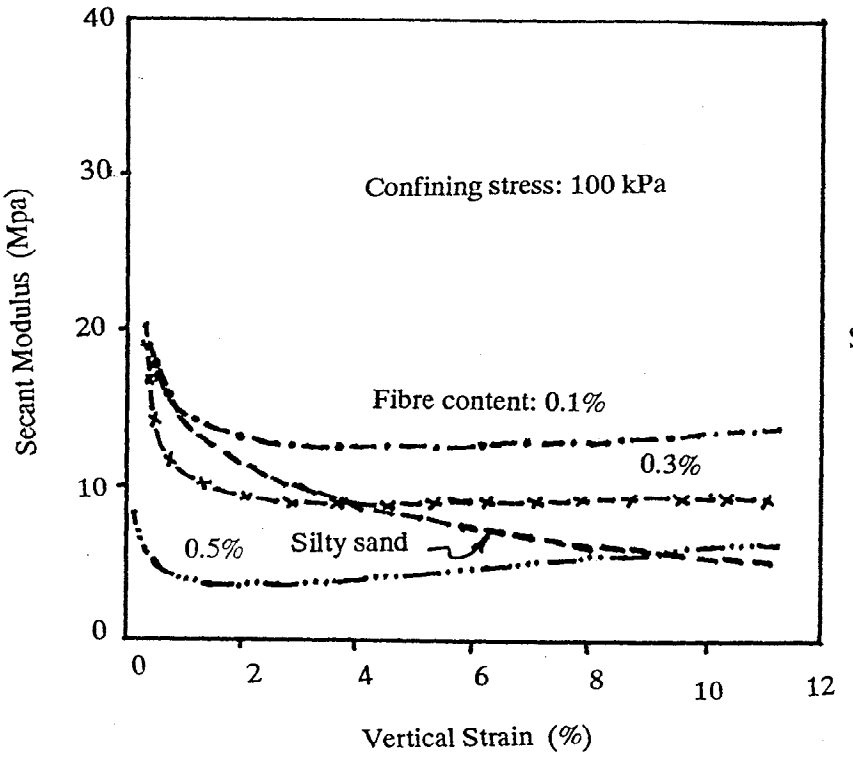

Figure 7. Secant Modulus vs. Axial Strain for Silty Sand and Composites

REINFORCED EMBANKMENTS AND THE EFFECT OF CONSOLIDATION ON SOFT COHESIVE SOIL DEPOSITS

ALLEN LUNZHU LI AND R. KERRY ROWE
THE UNIVERSITY OF WESTERN ONTARIO, LONDON, ONTARIO, CANADA

ABSTRACT

The behaviour of geosynthetic reinforced embankments constructed on a soft cohesive foundation is studied under undrained, partially drained and drained conditions using a finite element program based on an elliptical cap soil model coupled with Biot consolidation theory. Factors examined include reinforcement stiffness, consolidation of the foundation soil and stage construction. The strains in the geosynthetic reinforcement and the deformations of the foundation soil are evaluated at different stages of consolidation. It is shown that the effects of consolidation of the foundation are more pronounced and beneficial for reinforced embankments than unreinforced embankments. Used without enhancing drainage, a multi-stage construction sequence with relatively short consolidation periods is inefficient. Reinforcement can significantly reduce both the lateral deformations and foundation soil heave.

INTRODUCTION

Soft clay foundations are often unable to support the desired embankment fill thickness due to their low bearing capacity and high compressibility. The undrained behaviour of reinforced embankments constructed over soft clay foundations has been extensively investigated using the Mohr-Coulomb and Modified Cam-clay models to describe foundation soil behaviour (Rowe and Soderman 1987a, b; Hird et al. 1990). Several researchers (e.g. Chai and Bergado 1993, Litwinowicz et al. 1994 and Rowe et al. 1996) have used effective stress analysis method to model the behaviour of several case histories. However, the effect of reinforcement on the construction of embankments over foundations under partially drained

conditions and the effect of subsequent consolidation is still not fully addressed. The combined effect of construction method and reinforcement are investigated in this paper considering the time-dependent behaviour of the embankment due to consolidation of the foundation soils and the interaction between soil and reinforcement during this process.

SCOPE

The objective of the present study is to theoretically investigate the time-dependent behaviour of embankments during the undrained and partially drained construction followed by consolidation to identify and highlight the beneficial effect of geosynthetic reinforcement. Particular attention will be given to the use of geosynthetic reinforcement combined with stage construction to allow construction of substantially higher embankments in considerably shorter periods than unreinforced embankments without vertical drains. Although an important topic in and of itself, the use of prefabricated vertical drains is beyond the scope of the present paper and will be addressed in a subsequent paper.

NUMERICAL MODEL AND PROBLEM CONSIDERED

A modified version of a finite element program AFENA (Carter and Balaam 1990) implemented with an elliptical cap (Chen and Baladi 1985, Chen and Mizuno 1990) undrained/drained soil model and a transient model coupled with Biot consolidation theory is used in this study. The elliptical cap undrained model has been applied to describe the undrained behaviour of Boston blue clay under an MIT test embankment loading (McCarron and Chen 1987). Rowe and Hinchberger (1998) used an elasto-viscoplastic cap model to successfully predict the time-dependent behaviour of the reinforced Sackville test embankment and Hinchberger and Rowe (1988) applied the same model to the unreinforced Gloucester test embankment.

In this study, the construction of a four-lane highway embankment (see Fig. 1) with 27 m crest width and 2(horizontal):1(vertical) side slopes was examined. The soft foundation was taken to be 15 m deep and underlain by a relatively permeable layer. The water table was assumed to be at the ground level and initial pore pressure prior to embankment construction was taken to be hydrostatic. The centreline of the embankment (a line of symmetry) and the far field lateral boundary were taken to be smooth and rigid with the lateral boundary located 100 m from the centreline (see Fig. 1). The bottom of the finite element mesh was assumed to be rough and rigid. A total of 1694 linear strain triangular elements (3194 nodes) were used to discretize the embankment and foundation soils. Two noded bar elements were used for modeling the reinforcement and two noded joint elements were used for both the embankment fill/reinforcement interface and the embankment fill/foundation interface (Rowe and Soderman 1987a). Embankment construction was simulated as 0.75 m thick lifts in which body forces were applied using 200 to 600 incremental load steps depending on the stage of construction.

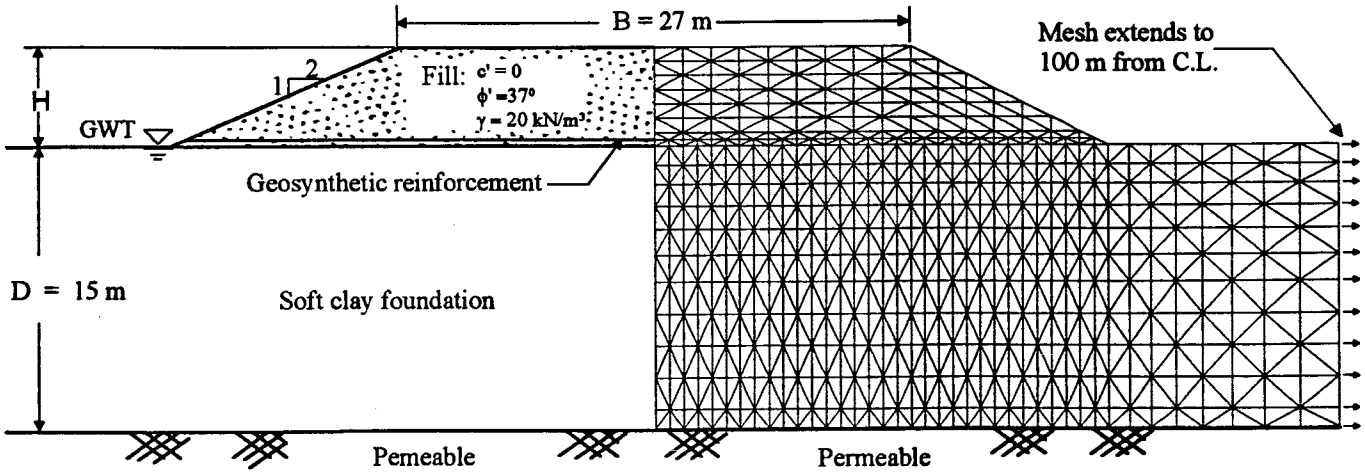

Figure 1. Reinforced Embankment and Foundation

MODEL PARAMETERS

Selection of Foundation Soil Properties

The foundation soil examined was a typical very soft clay with a liquid limit of 76%, a plasticity index of 40% and a preconsolidation pressure increased linearly with depth from 18.5 kPa at the surface at an average rate of 4.3 kPa/m. Thus the soil was slightly over-consolidated with an OCR of 1.1 to 2.6 except for the first two metres of soil where the OCR was much greater since the vertical effective stress approached zero. The average compression index, C_c, was assumed to be 0.69 (i.e. in the range of 0.54-0.72 for highly compressible clays based on Whitlow 1983). The recompression index, C_{cr}, was taken to be 10% of C_c (which falls within rages quoted by Holts and Kovacs 1981, Terzaghi et al. 1996). The initial void ratio and unit weight of this clay deposit at ground surface was assumed to be 2.5 and 14.7 kN/m^3 respectively. The variation in unit weight and void ratio with depth were taken to be consistent with the initial void ratio and unit weight at the ground surface, the preconsolidation pressure profile and the compression and the recompression indices. Thus the calculated saturated unit weight increased from 14.7 kN/m^3 to 15.6 kN/m^3, and the initial void ratio decreased from 2.5 to 1.94 over the 15 m deep deposit. A coefficient of earth pressure at rest $K_0' = 0.6$, and Poisson ratio $\nu' = 0.35$ were assumed. The normally consolidated strength characteristics were defined by an effective cohesion intercept $c' = 0$ and effective friction angle $\phi' = 27^0$. Based on the observation of the typical limit state curves for natural soft clays (Leroueil 1997), the elliptical cap was assumed to have an aspect ratio R = 0.7. Using these parameters, the calculated undrained shear strength s_{uo} at surface was 5 kPa and the rate of increase in undrained strength with depth, ρ_c, was 1.5

kPa/m. The undrained shear strength profile of this soil is similar to that of a soft clay in Queensland, Australia (Litwinowicz et al. 1994).

The initial hydraulic conductivity k_{vo} was taken to be $1x10^{-9}$ m/s at the reference void ratio e_o of 2.5 for the clay in its normally consolidated state. Consolidation of soft clays involves a decrease in void ratio and hydraulic conductivity and they can be related by:

$$k_v = Ak_{vo}\exp(e-e_o)/C_k \quad [1]$$

where C_k is the hydraulic conductivity change index ($C_k \cong 0.5e_o$ was assumed based on Tavenas et al. 1983); A is hydraulic conductivity factor for over-consolidated clay. A value of A=10 was adopted for this clay in the over-consolidated stage reducing to A=1 in the normally consolidated state to reflect the fact that in the over-consolidated portion of loading the hydraulic conductivity may be substantially higher than in the normally consolidated state (Tavenas and Leroueil 1980; Tavenas et al. 1983). Considering the anisotropy of hydraulic conductivity in a natural clay deposit, a ratio of horizontal to vertical hydraulic conductivity $k_h/k_v = 3$ was selected for the analyses.

Embankment Fill Parameters

The embankment fill was assumed to be a purely frictional granular soil with a friction angle $\phi' = 37^0$, dilatancy angle $\psi = 6^0$, and an unit weight $\gamma = 20$ kN/m^3. The non-linear elastic behaviour of the fill was modelled using Janbu's (1963) equation:

$$(E/P_a) = K(\sigma_3/P_a)^m \quad [2]$$

where E is the Young's modulus of the soil; P_a is the atmospheric pressure; σ_3 is the minor principal stress; and K and m are material constants selected to be 100 and 0.5 respectively based on tests on typical fill material (Rowe et al. 1984).

Interface Parameters and Reinforcement Stiffness

Elastoplastic joint elements (Rowe & Soderman 1987a) were used to model the fill/reinforcement interface and fill/foundation interface. The fill/reinforcement interface was fictional with $\phi' = 37^0$. The fill/foundation interface had the same shear strength as that of the foundation soil at the ground surface (i.e. $s_{uo} = 5$ kPa in undrained analyses and $c' = 0$, and $\phi' = 27^0$ in coupled analyses). Reinforcement with tensile stiffness, J, varying from 0 to 8000 kN/m was examined.

RESULTS AND DISCUSSION

Effect of Geosynthetic Reinforcement Under Undrained Conditions

The calculated variation of net embankment height above original ground surface with fill thickness for embankments reinforced using reinforcement of different stiffness is presented in Fig. 2. The unreinforced embankment failure height, H_f (i.e. the fill thickness H corresponding maximum net embankment height), was just over 2.1 m. A change of reinforcement stiffness from 250 kN/m to 8000 kN/m resulted in an increase in failure heights by between 21% to 73% relative to the unreinforced case (Fig. 3) while the maximum reinforcement strain reduced from 6.7 % to 1.5 %. The deformed foundation mesh for a 2 m high embankment with a reinforcement J = 500 kN/m is shown in Fig. 4. Figure 5 shows the calculated reduction in horizontal displacements and heave at the toe (Point A in Fig. 4), and vertical displacements below the crest (Point B in Fig. 4) due to the use of basal reinforcement at an embankment height of 2 m. Referring to Figure 3 and 5, it is noted that the effect of reinforcement tensile stiffness is significant up to J = 2000 kN/m, but there is only a small improvement in going from J = 2000 kN/m to J = 4000 kN/m, and negligible improvement for J > 4000 kN/m. These findings are consistent with earlier finding by Rowe and Soderman (1987b). What is now of interest is to see how these embankments behave when one considers the effect of consolidation.

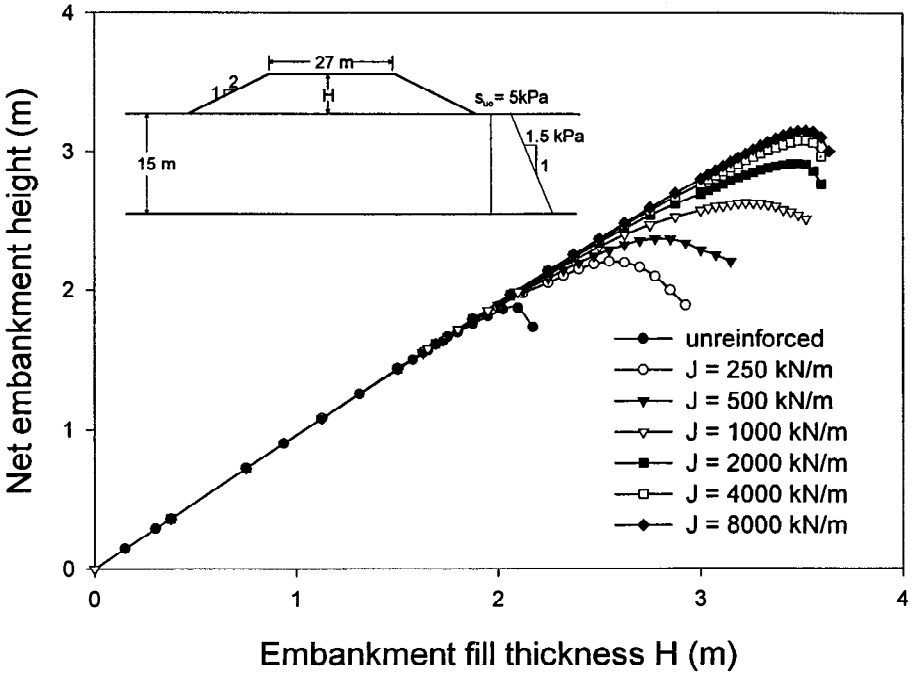

Fig. 2. Variation in Calculated Net Height vs Fill Thickness Under Undrained Conditions

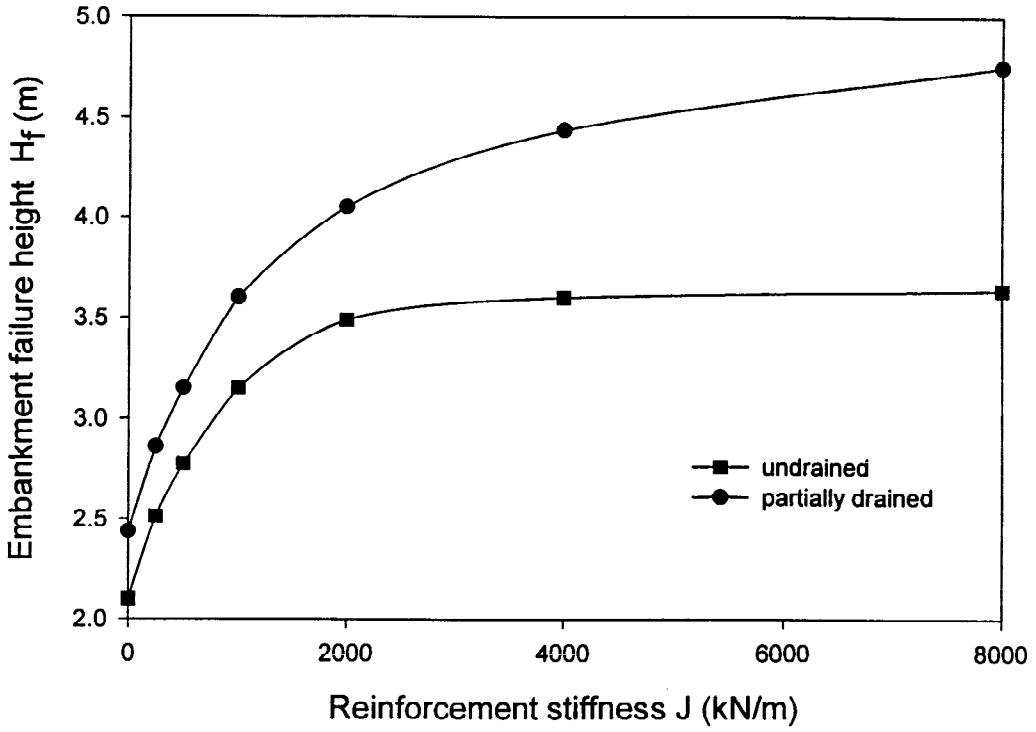

Figure 3. Effect of Reinforcement Stiffness on Embankment Failure Height for both Undrained and Partially Drained Conditions

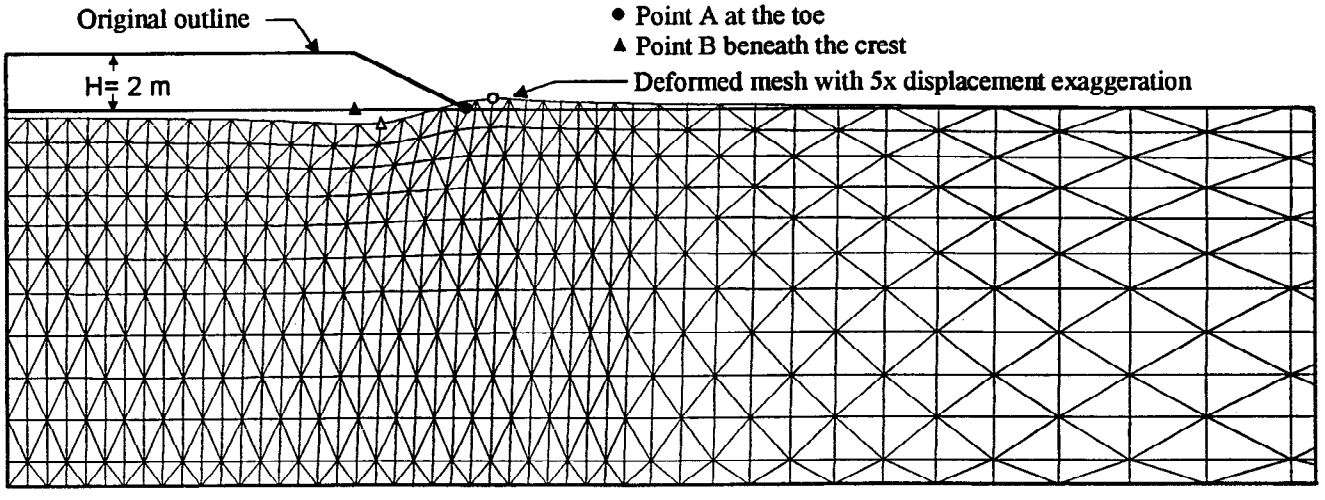

Figure 4. Deformed Foundation Mesh for the Embankment with J = 500 kN/m at H = 2 m

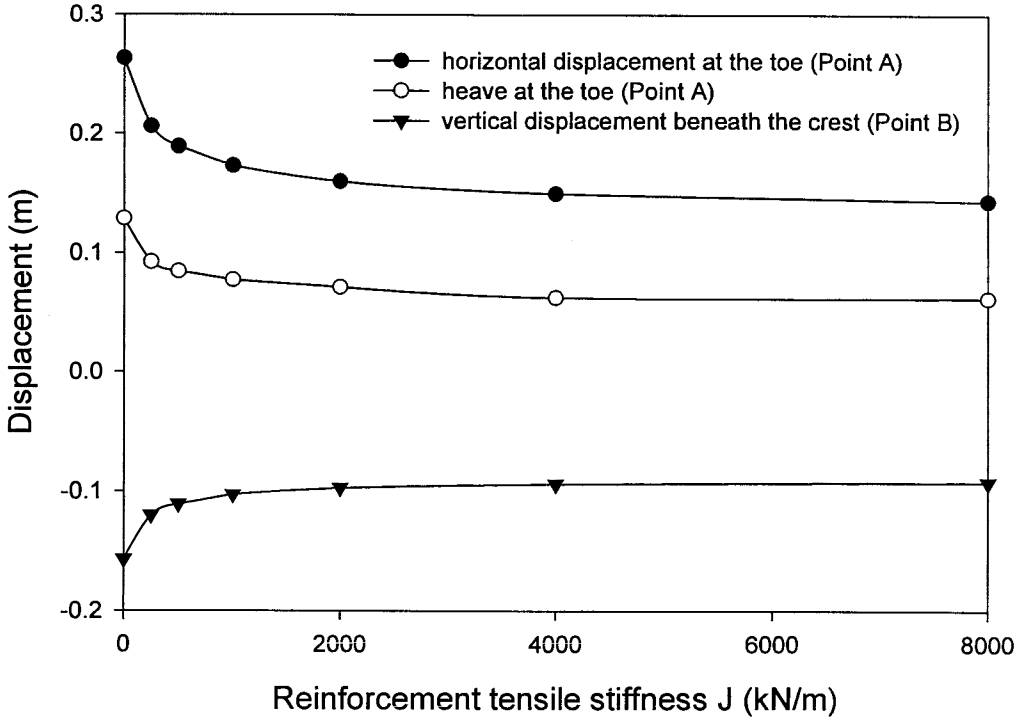

Figure 5. Variation in Undrained Foundation Displacement at a Fill Thickness H=2 m

Effect of Consolidation for Single Stage Construction

Recognizing that most real soils are initially over-consolidated and will experience some consolidation during embankment construction, the analyses reported in the previous section were repeated using a fully coupled analysis. A construction rate of 0.85 m/month was used. The partial consolidation that will occur during construction can be observed by examining the embankment settlement. For example, with J = 8000 kN/m and a fill thickness of 3.6 m, the calculated immediate undrained settlement is 9.3 cm while the total partially drained settlement is 21.8 cm at the end of construction. However more important is the effect that the increase in shear strength within the top layers of the foundation soil, due to the consolidation, has on the embankment failure height. Figure 3 shows a comparison of the calculated embankment failure heights under both undrained and partially drained conditions. It can be seen that partial consolidation during construction increased the height to which an unreinforced embankment could be constructed by about 0.3 m, but for reinforced embankment the improvement was far more substantial (e.g. the increase in failure height was 1.1 m for J = 8000 kN/m).

Effect of Multi-Stage Construction Method for Reinforced Embankments

Two stage, three stage and four stage construction sequences with 9 months of consolidation between stages will now be examined for an embankment assumed to be reinforced using geosynthetics with a tensile stiffness J = 2000 kN/m. Each embankment stage

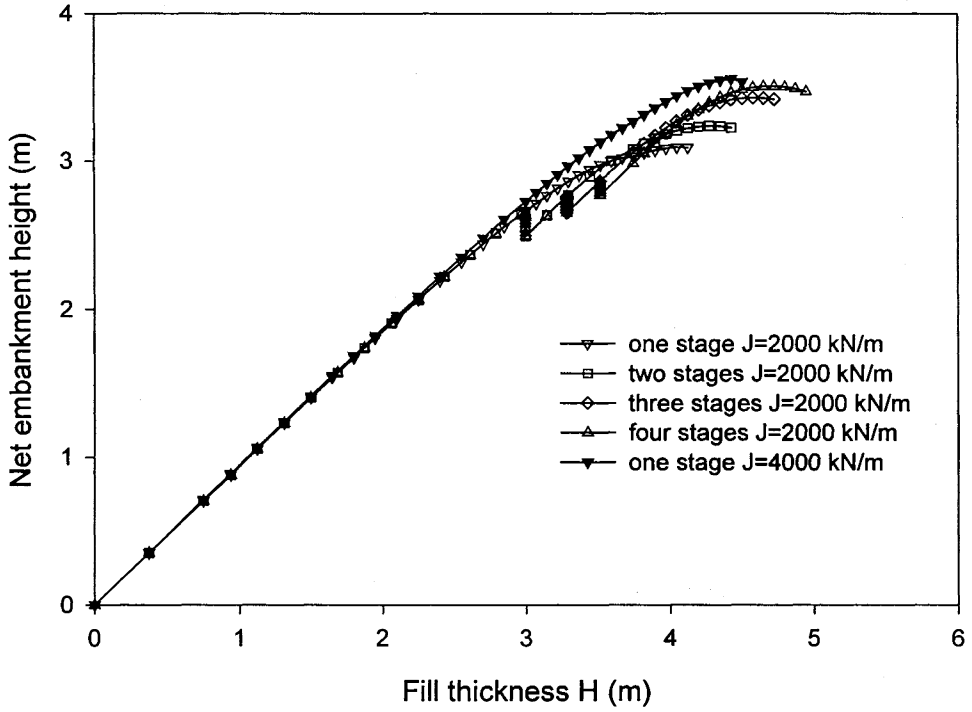

Figure 6. Effect of Multi-stage Construction on Embankment Height

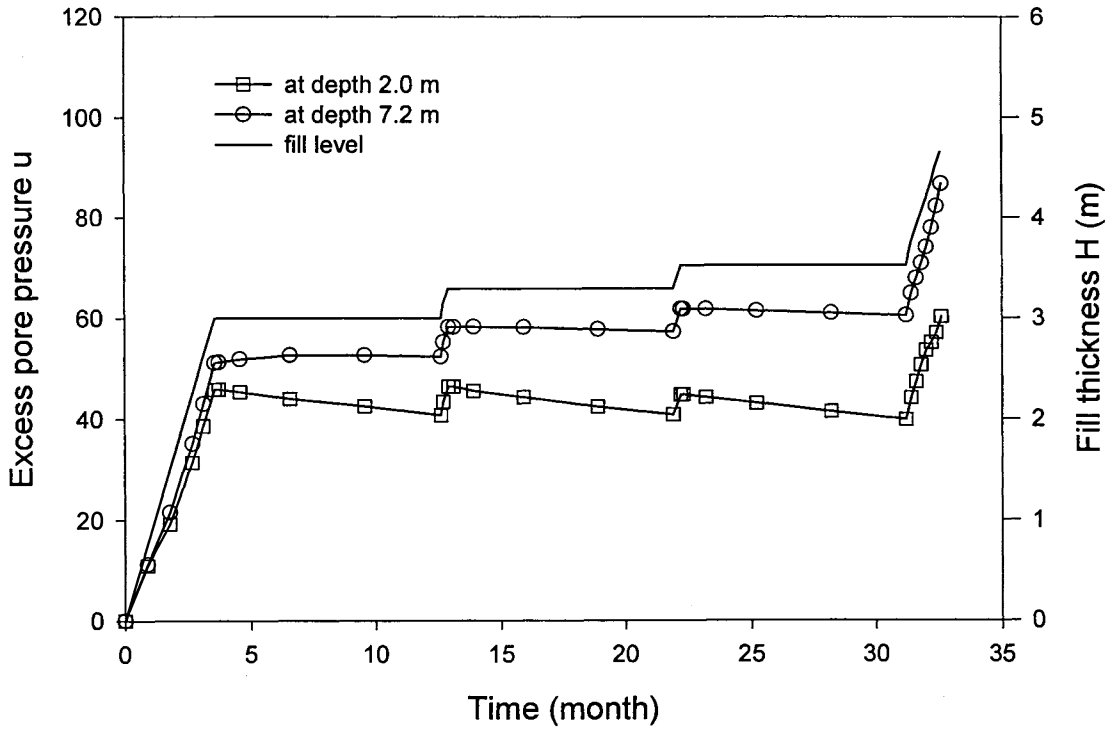

Figure 7. Excess Pore Pressure at the Centre Line Beneath the Embankment

was constructed to a height such that a factor of safety of 1.3 was maintained at the end of each stage except the last. The final stage was then constructed until the failure height was reached. The variation in the net embankment height with fill thickness for different stage construction methods is shown in Fig. 6. Each consolidation stage results in an increase of embankment failure height due to the shear strength gain of the foundation soil during consolidation, however, the increase of failure height was limited (0.3 m, 0.6 m and 0.8 m for two, three and four stage construction respectively). The reason for the limited gain in failure height due to multi-stage construction is that while there may be a significant dissipation of excess pore pressure during the early stage of loading (when the soil is initially over-consolidated), there is very little dissipation of excess pore pressure during the subsequent 9 months between construction stages due to the low hydraulic conductivity of clay once the soil becomes normally consolidated. This is shown in Fig. 7 where there is significant pore pressure dissipation during the first stage of construction, where $\Delta\sigma = 60$ kPa, $\Delta u = 40$ kPa at 2 m and $\Delta u = 52$ kPa at 7.2 m within the foundation. However, after the first stage the rate of excess pore pressure dissipation is small at 2.0 m depth and negligible at a depth of 7.2 m. After the first stage the increase in excess pore pressure mirrors the increase in total stress ($\Delta u = \Delta\sigma$). In order to gain a greater improvement due to consolidation, one would require either a longer waiting period between construction stages or alternatively vertical drains could be used to speed up the dissipation of excess pore pressures.

Also shown in Fig. 6 are the results for single stage construction with J = 4000 kN/m and it can be seen that the improvement by doubling the reinforcement stiffness and using one stage construction is comparable to the improvement by using the multi-stage construction technique for embankments with lower reinforcement stiffness. Obviously, it would take considerable shorter time to complete the construction for one stage method than for multi-stage method.

Effect of Consolidation Time on Embankment Stability

After the completion of embankment construction, the foundation soil will consolidate and the shear strength of the foundation soil will increase. Two series of analyses were performed to examine the influence of consolidation time and reinforcement on construction.

The first series of analyses considered one unreinforced and one reinforced (J = 2000 kN/m) embankment. The embankments were first constructed to a grade of 1.6 m and 2.7 m for the unreinforced and reinforced respectively to maintain the same factor of safety 1.3 against failure under undrained conditions for both cases. The embankments were then constructed to failure after allowing different periods for consolidation and the increase of failure height due to consolidation is presented in Fig. 8. The increase of failure height is defined as the difference between the failure height using two stage construction and the failure height using one stage construction. The time for an average of 95% consolidation was 25 years in both cases. The beneficial effect of consolidation is more pronounced for the reinforced embankment than the unreinforced. After 95% consolidation the increase of failure height of the reinforced

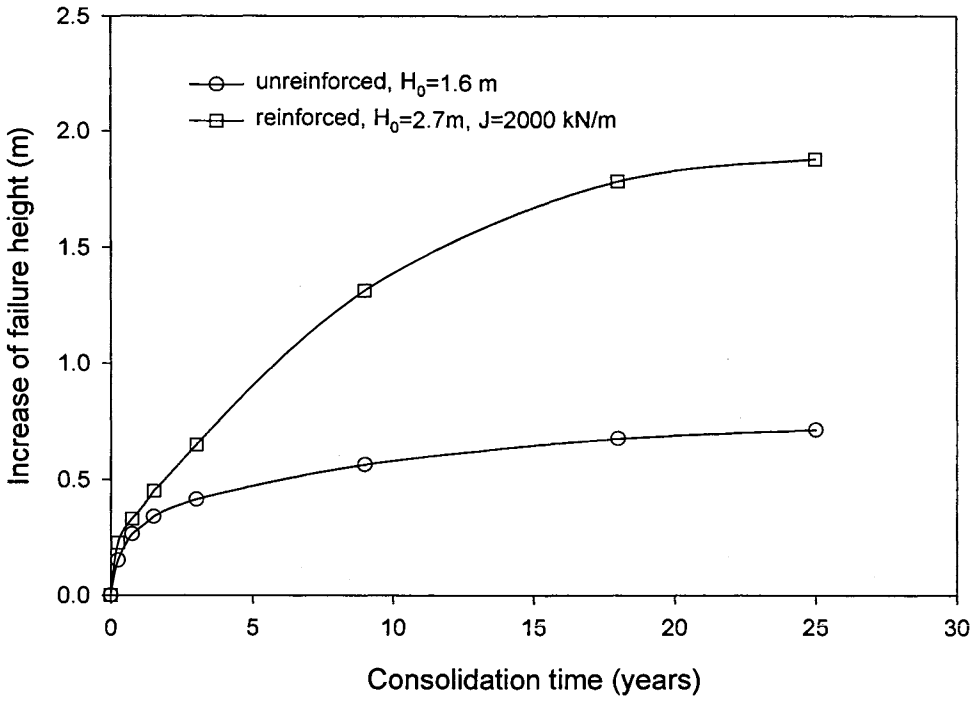

Figure 8. The Effect of Consolidation Time on Embankment Stability

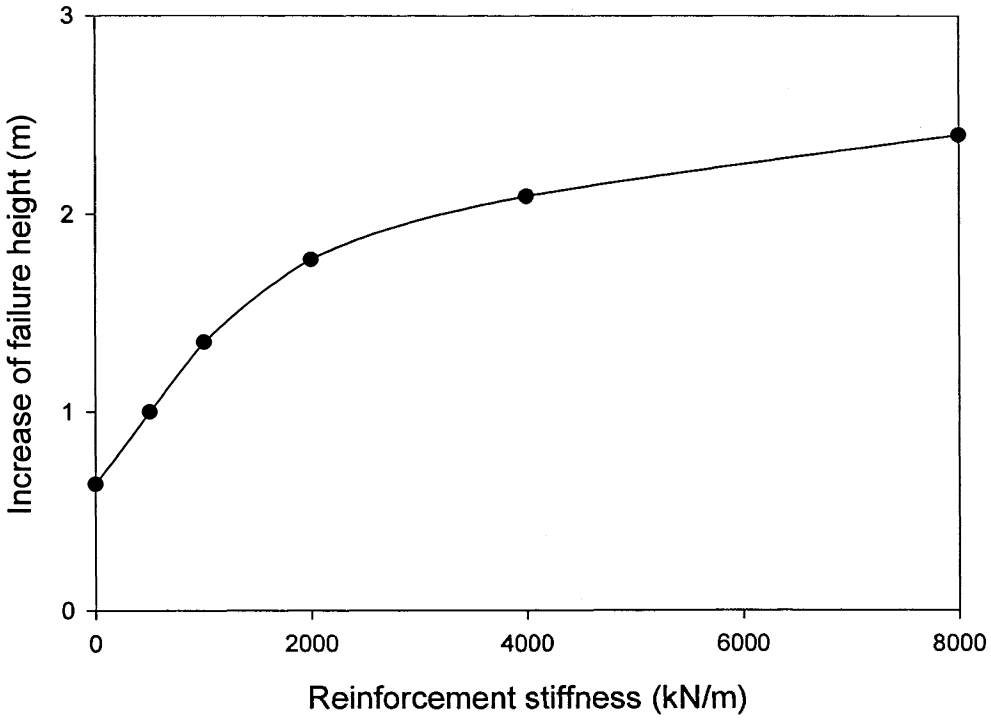

Figure 9. Increase of failure height after 95% consolidation

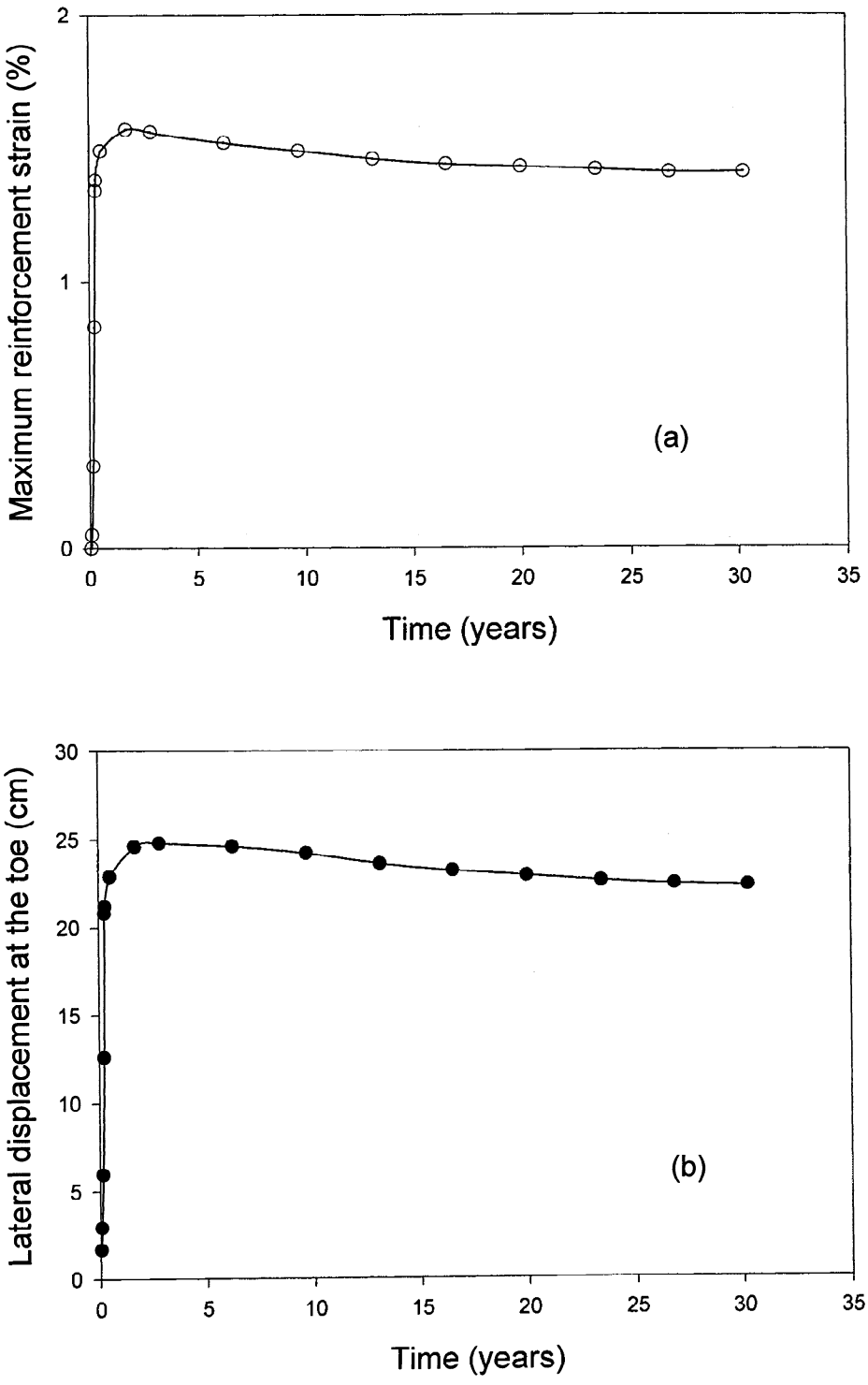

Figure 10. Variation of Maximum Reinforcement Strain and Lateral Displacement at the Embankment Toe withTime: (a) maximum reinforcement strain; (b) lateral displacement

embankment is 47% above the height of one stage construction compared to 29% for the unreinforced embankment. The failure height of the reinforced embankment is 1.8 times of unreinforced embankment height after 95% of consolidation.

The second series of analyses involves embankments with different stiffness reinforcement. All embankments were first constructed to a grade with factor of safety of 1.3 and then constructed to failure after an average of 95% consolidation of the foundation soil had been achieved. The increase of failure heights are shown in Fig. 9 and it can be seen the stiffer the reinforcement, the greater are the beneficial effects of foundation consolidation.

Effect of Consolidation on Calculated Reinforcement Strain and Lateral Deformation

An embankment reinforced with J = 2000 kN/m was constructed to a fill thickness of 2.7 m (i.e. to a height with a factor of safety of 1.3 against failure) over a 3 month period. Then the embankment fill thickness was held constant and the change in strain in the reinforcement was monitored with time until to the end of consolidation. The variation of maximum reinforcement strain and lateral displacement at the embankment toe with time is shown in Fig. 10. It can be seen that the reinforcement strain and lateral displacement increases during construction and a short period after construction, then slightly decreases during consolidation. The decrease of reinforcement strain during consolidation is consistent with earlier finding (Rowe et al. 1984).

CONCLUSIONS

The numerical study presented here has shown that:

1. Geosynthetic reinforcement can substantially increase the stability of embankments on the soft foundation soils both under undrained and partially drained conditions.

2. The initial consolidation of the foundation soil that may occur during the early stage of loading, when the soil is over-consolidated, can have a significant effect on embankment stability and this effect is enhanced by the use of soil reinforcement.

3. The multi-stage construction method with relatively short consolidation periods is not efficient. On the other hand, the two stage construction method is more effective if there is significant consolidation of foundation soil between the two stages. The effect of consolidation of the foundation soil is more pronounced for the reinforced embankments than for the unreinforced embankment. This suggest that the provision of additional drainage (e.g. prefabricated vertical drains) may have a more substantial benefit for reinforced embankments than for unreinforced embankments. This hypothesis warrants more investigation.

4. Reinforcement reduces the vertical and lateral shear deformations beneath the embankment crest and heave at the toe during embankment construction. The reinforcement strain and lateral deformation significantly increase with increasing fill thickness for a given soil profile. However their change is insignificant during consolidation of the foundation soil.

ACKNOWLEDGEMENT

The research reported in the paper was funded by the National Science and Engineering Research Council of Canada.

REFERENCE

Carter, J.P. and Balaam, N.P. (1990), "AFENA - A general finite element algorithm: users manual", School of Civil and Mining Engineering, University of Sydney, N.S.W. 2006, Australia.

Chai, J. and Bergado D.T. (1993), "Performance of reinforced embankment on Muar clay deposit", Soils and Foundations, Vol. 33, No. 4, pp. 1-17.

Chen, W.F. and Baladi, G.Y. (1985), "Soil plasticity: theory and implementation", Elsevier, Amsterdam.

Chen, W.F. and Mizuno, E. (1990), "Nonlinear analysis in soil mechanics - theory and implementation", Elsevier, New York.

Hinchberger, S.D. and Rowe, R.K. (1998), "Modelling the rate sensitive characteristics of the Gloucester foundation soil", Canadian Geotechnical Journal, Vol. 35 (In press).

Hird, C.C., Pyrah, I.C. and Russel, D. (1990), "Finite element analysis of the collapse of reinforced embankments on soft ground", Geotechnique, Vol. 40, No. 4, pp. 633-640.

Holtz, R.D. and Kovacs, W.D. (1981), "An introduction to geotechnical engineering", Prentice-Hall, New Jersey.

Janbu, N. (1963), "Soil compressibility as determined by oedometer and triaxial tests", Proceedings of the European Conference on Soil Mechanics and Foundation Engineering, Wiesbaden, Germany, Vol. 1, pp. 19-25.

Leroueil, S. (1997), "Critical state soil mechanics and the behaviour of real soils", Proceedings of the International Symposium on Recent Developments in Soil and Pavement Mechanics, Rio

de Janeiro, Brazil, June, in *Recent Developments in Soil and Pavement Mechanics*, A.A. Balkema/Rotterdam/Brookfield, pp. 41-80

Litwinowicz, A., Wijeyakulasuriya, C.V. and Brandon, A.N. (1994), "Performance of a reinforced embankment on a sensitive softy clay foundation", Fifth International Conference on Geotextiles, Geomembranes and Related Products, Singapore, September, Vol. 1, pp. 11-16.

McCarron, W.O. and Chen, W.F. (1987), "A capped plasticity model applied to Boston blue clay", Canadian Geotechnical Journal, Vol. 24, No. 4, pp. 630-644.

Rowe, R.K. Maclean, M.D. and Soderman, K.L. (1984), "Analysis of a geotextile reinforced embankment constructed on peat", Canadian Geotechnical Journal, Vol. 21, No.3, pp. 563-576.

Rowe, R.K. and Soderman, K.L. (1987a), "Very soft soil stabilization using high strength geotextiles: The role of finite element analysis," International Journal of Geotextiles and Geomembranes, Vol. 6, pp. 53-81.

Rowe, R.K. and Soderman, K.L. (1987b), "Reinforcement of embankments on soils whose strength increases with depth", Proceedings of Geosynthetics '87, New Orleans, pp. 266-277.

Rowe, R.K., Gnanendran, C.T., Landva, A.O. and Valsangkar, A.J. (1996), "Calculated and observed behaviour of a reinforced embankment over soft compressible soil", Canadian Geotechnical Journal, Vol. 33, No. 2, pp. 324-338.

Rowe, R.K. and Hinchberger, S.D. (1998), "The significance of rate effects in modelling the Sackville test embankment", Canadian Geotechnical Journal, Vol. 35, No. 3, pp. 500-516.

Tavenas, F. and Leroueil, S. (1980), "The behaviour of embankments on clay foundations", Canadian Geotechnical Journal, Vol. 17, No. 2, pp. 236-260.

Tavenas, F., Jean, P. Leblond, P., and Leroueil (1983), "The permeability of natural soft clays. Part II: Permeability characteristics", Canadian Geotechnical Journal, Vol. 20, No. 4, pp. 645-660.

Terzaghi, K., Peck, R.B. and Mesri, G. (1996), "Soil mechanics in engineering practice", Wiley, New York.

Whitlow, R. (1983), "Basic soil mechanics", Longman Scientific & Technical, New York.

DESIGN OF HIGH REINFORCED EMBANKMENTS CONSTRUCTED WITH POOR QUALITY SOIL AND DEGRADABLE SHALE

Jessee A. Scarborough, George M. Filz, James K. Mitchell, and Thomas L. Brandon
Virginia Polytechnic Institute and State University, USA
Edward J. Hoppe
Virginia Transportation Research Council, USA
Stanley L. Hite
Virginia Department of Transportation, USA

ABSTRACT

Relocation of US Highway 29 near Lynchburg, Virginia, will require new embankments up to 27.4 m (90 ft) high. The available backfill is a degradable and water-sensitive phyllite, as well as residual soil derived from this shale-like parent rock. Experience has shown that embankments constructed of these materials must have slopes at inclinations of about 2.5H:1V or flatter to exhibit good performance. Geosynthetic reinforcement of the borrow material to enable steeper slopes, up to 1.5H:1V, will result in very considerable savings in required right-of-way and embankment material. However, use of the available borrow materials requires special considerations in selection of suitable reinforcements, design, and construction. This study has shown that geosynthetics can be used to reinforce high embankments constructed of poor quality backfill. Successful completion of this project would help to open a broad market for such structures nationwide.

INTRODUCTION

The proposed US 29 bypass, located northeast of the City of Lynchburg, Virginia, includes earth embankments up to 27.4 m (90 ft) high. The locally available borrow soils are less than ideal. The Virginia Department of Transportation (VDOT) has found that embankments built of these materials must have slopes at an inclination of 2.5H:1V or flatter to exhibit good performance. If steeper side slopes could be provided, savings in right-of-way acquisition and fill placement costs would result. Consequently, VDOT is investigating the feasibility of reinforcing two of the US 29 bypass embankments with geosynthetics to allow steeper side slopes. To the authors' knowledge, these embankments would be the highest reinforced embankments yet constructed using poor quality fill. This paper describes field explorations, laboratory studies, and analyses that were performed to provide the data needed for design of stable, reinforced 1.5H:1V side slopes for the proposed embankments.

SITE DESCRIPTION

The proposed reinforced embankments are located northeast of Lynchburg, Virginia, in an area known as Madison Heights. The bypass alignment traverses broad ridges and valleys that have been eroded by small intermittent and perennial streams flowing south and east to the James River. The proposed embankments cross these valleys, and the borrow material will be obtained from cuts that are made through the ridges.

The site is underlain by residual soil and bedrock that consists primarily of phyllite with thin beds of quartz. Phyllite is a metamorphosed mudstone that is similar to shale. As part of this project, a review of literature concerning classification and use of shale-like materials in embankments was performed (Huber, 1998). Two characteristics, hardness and durability, are generally examined in shale classification systems. The relationships among hardness, durability, and field performance of shales in embankments are summarized in Table 1. Poor performance can result when hard, non-durable shales are used in embankments because large pieces of hard shale may be placed haphazardly with large voids between the pieces, which can later degrade and erode, causing settlement and stability problems in the embankment. When non-durable shales are used in embankments, satisfactory performance depends on breaking the material down to soil-size particles and compacting the processed material to reduce the size of interparticle voids.

Table 1. Use of Shales in Embankments

	Durable	Not Durable
Hard	Difficult to break down during excavation, placement, and compaction. Material not expected to degrade in the embankment. Treat as rockfill, and good performance is expected.	Difficult to break down during excavation, placement, and compaction. Material is likely to degrade in the embankment, possibly causing excessive settlement or instability. Additional effort is required during construction to break down and compact for good long-term performance.
Not Hard	Material can be broken down during excavation, placement, and compaction to a soil-like material that would be expected to exhibit good performance in a well-constructed embankment.	

At the borrow sites, the weathering decreases and hardness increases with depth. Based on analysis of data from auger borings and rock core, it is estimated that about 70 percent of the cut volume is residual soil, about 25 percent is a very soft weathered rock that can be broken down into a soil-like material with ordinary excavation, placement, and compaction equipment. About 5 percent would require either crushing or removal from the fill prior to compaction.

The designs presented in this paper are based on the results of laboratory tests performed using residual soils obtained from the borrow sites.

BORROW SOIL PROPERTIES

Two residual soils were identified in the borrow areas: a brown, silty sand and a red, sandy silt to sandy, elastic silt. The red soil is more plastic than the brown soil. The discussion here is limited to the red soil, upon which the embankment design was based. About 50 to 60 percent of the red soil passes the US No. 200 sieve. The average values of the liquid limit and plasticity index for the red soil are about 50 and 10, respectively.

Consolidated-undrained (CU) triaxial compression tests with pore water pressure measurements were performed on back-pressure saturated samples to obtain values of effective stress strength parameters. The measured values of effective stress friction angle, ϕ', and cohesion intercept, c', at 95 percent relative compaction (ATSM D698) were 30° and 13 kPa (270 psf), respectively. These values were not significantly affected by compaction water content. Values of $\phi' = 30°$ and $c' = 0$ were used for analyses of long-term stability.

Unconsolidated-undrained (UU) triaxial compression tests were performed to obtain values of the total stress strength parameters at several moisture-density compaction conditions. Partial results are shown in Table 2. As indicated in the table, the total stress friction angle decreases as the compaction water content increases, but the total stress cohesion intercept was not affected by compaction water content over a range from 3 to 5 percentage points wet of optimum. Standard VDOT specifications allow embankment fill to be compacted as wet as 1.2 times the optimum water content. Since the optimum water content for the red soil is about 25 percent, this means that the red soil could be compacted 5 percentage points wet of optimum, according to VDOT's standard specifications. Stability analyses described below demonstrate that significantly more reinforcement is required for embankment fill compacted 5 percentage points wet of optimum than for fill compacted 3 percentage points wet of optimum. Consequently, it is recommended that a special provision limiting the maximum water content to 3 percentage points wet of optimum be included in the specifications for this project.

Table 2. UU Test Results for the Red Soil at 95% Relative Compaction

Compaction Water Content	Friction Angle degrees	Cohesion Intercept kPa (psf)
3% wet of optimum	11	48 (1,000)
5% wet of optimum	7	48 (1,000)

Relying upon the relatively large cohesion intercept measured in the UU tests was judged to be potentially unconservative. Consequently, a bilinear total stress strength envelope was used for short-term analyses of stability: $\phi = 30°$ and $c = 0$ kPa for normal stress less than 125 kPa (2,600 psf), and $\phi = 11°$ and $c = 48$ kPa (1,000 psf) for normal stress greater than 125 kPa (2,600 psf).

Initially, it was anticipated that the embankment would consolidate fairly slowly. However, the average value of the coefficient of consolidation measured in the laboratory was 2.3×10^{-5} m^2/s (22 ft^2/day), which produces 90 percent consolidation in about 2½ months for a double-drained layer 27.4 m (90 ft) thick. Thus, it is expected that the embankment will consolidate almost as quickly as it is placed. Even though the consolidation rate is expected to be very rapid, short-term stability analyses of the reinforced embankments were performed using the total stress strength envelope described above, but the value of the factor of safety for this case was only required to be 1.1. The required reinforcement force for this condition is significantly less than was anticipated at the time the soil-geosynthetic interaction testing program was initiated.

SOIL-GEOSYNTHETIC INTERACTION TESTS

Based on preliminary analyses and an originally anticipated need for internal drainage, four geosynthetics were selected for soil-geosynthetic interaction testing: 2 different geogrids, a non-woven composite that combines high strength and in-plane drainage, and a non-woven geosynthetic. Wide-width tensile strength tests, interface shear strength tests, and pullout tests were done by GeoSyntec Consultants in their Atlanta, Georgia, and Boca Raton, Florida, offices. The wide-width tensile strength test results are listed in Table 3.

Table 3. Geosynthetic Tensile Strengths

Geosynthetic	T_{ult} kN/m (lb/ft)
Mirafi 20XT grid	152 (10400)
Strata PEC100 composite	117 (8030)
Tensar UX1700 grid	166 (11400)
Trevira 1155 non-woven	36 (2500)

Interface shear strength test results are listed in Tables 4 and 5. Specific provisions for drainage were not provided for the interface tests; however, based on the sample dimensions (300 mm x 300 mm shear box) and the displacement rate (1 mm/min), it is likely that the test results represent conditions approaching drained behavior. The following conclusions can be drawn from the data in Tables 4 and 5:

- The interface friction angles are largest for geosynthetics that incorporate a non-woven geotextile, such as the Strata PEC100 composite and the Trevira 1155 non-woven geotextile. The measured friction angles were smaller for the two grids (Mirafi 20XT and Tensar UX1700).
- When the soil is compacted on the dry side of optimum, the interface friction angles are higher than when compacted on the wet side of optimum, even when the soil is soaked after compaction.
- The increase in strength due to consolidation is not large.

Table 4. Interface Test Results for Red Soil Compacted 5 Percentage Points Wet of Optimum

Interface	Peak		Large Displacement[1]	
	Friction angle, δ Degrees	Intercept kPa (psf)	Friction angle, δ Degrees	Intercept kPa (psf)
Soil on soil	27°	24.66 (515)	26°	12.21 (255)
Mirafi 20XT Grid	20°	15.08 (315)	16°	11.25 (235)
Strata PEC100 Composite	26°	11.25 (235)	22°	4.31 (90)
Tensar UX1700 Grid	17°	18.19 (380)	15°	7.90 (165)
Trevira 1155 Non-woven	26°	14.12 (295)	24°	8.62 (180)
Trevira on Mirafi	17°	7.42 (155)	17°	4.79 (100)
1) The large-displacement strengths were evaluated at a displacement of at least 50 mm (2 inches).				

Table 5. Interface Test Results for Red Soil Compacted 5 Percentage Points Dry of Optimum

Interface	Peak		Large Displacement[1]	
	Friction Angle, δ Degrees	Intercept kPa (psf)	Friction Angle, δ Degrees	Intercept kPa (psf)
Strata PEC100 As compacted	33°	8.38 (175)	33°	1.92 (40)
Strata PEC100 Soaked 48 hr	29°	7.90 (165)	23°	7.90 (165)
Strata PEC100 Soaked 48 hr Consolidated 48 hr	31°	5.03 (105)	24°	3.11 (65)
1) The large displacement strengths were evaluated at a displacement of at least 50 mm (2 inches).				

Based on the test results in Tables 4 and 5, the values of interface friction angle listed in Table 6 were recommended for reinforced embankment design. An interface adhesion intercept value of zero was recommended.

Table 6. Values of Interface Friction Angle Recommended for Design

Geosynthetic	δ
Mirafi 20XT grid	20°
Tensar UX1700 grid	17°
Strata PEC100 composite	26°
Trevira 1155 non-woven	26°
Trevira & Mirafi, together	17°

The pullout test results shown in Figure 1 provided the data necessary to determine required embedments beyond deep failure surfaces and to analyze the stability of shallow surfaces near the slope face.

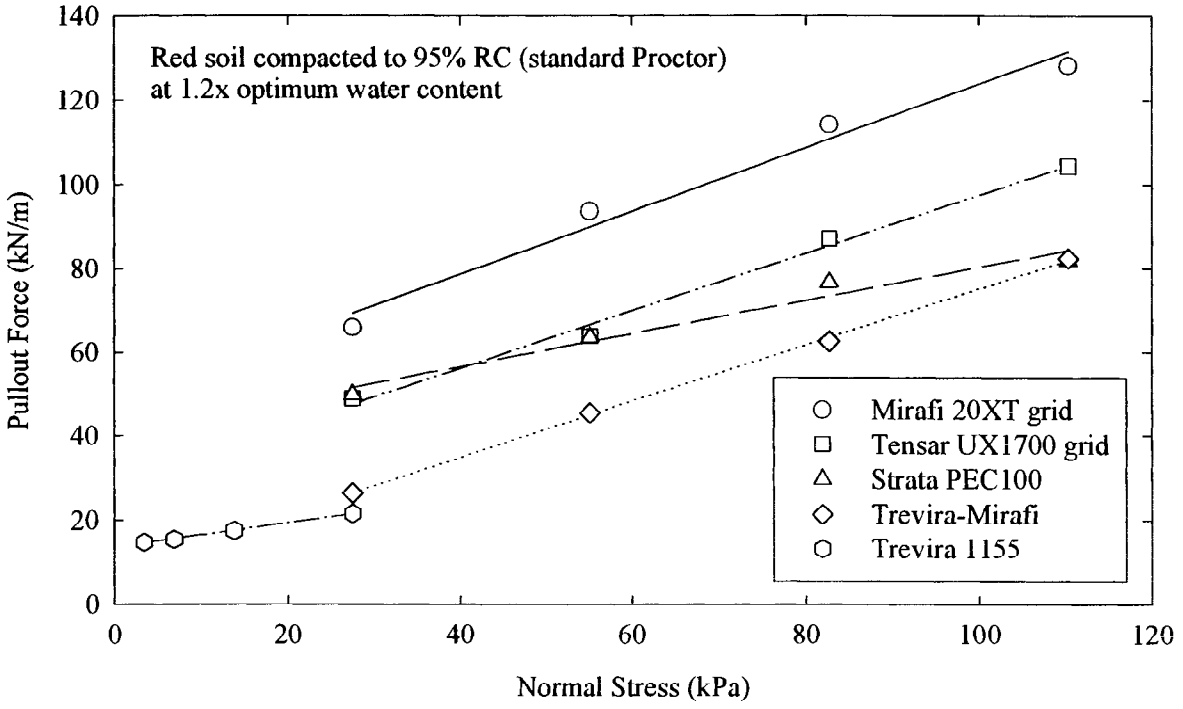

Figure 1. Pullout Test Results

REINFORCED EMBANKMENT DESIGN PROCEDURES

Design of reinforced embankments ordinarily makes use of limit equilibrium analyses of slope stability with tensile forces from the reinforcement taken into account. Many of the design procedures recommended by Elias and Christopher (1996) are incorporated in the computer program RSS by Marr and Werden (1997). In its design mode, RSS progresses through the three steps illustrated in Figure 2. In step 1, circular failure surfaces are analyzed using Bishop's modified method to determine the reinforcement tensile force necessary to provide a desired factor of safety and to establish initial reinforcement lengths. In step 2, sliding blocks at three levels are analyzed without tensile reinforcement, and the reinforcement is extended to the back of the active wedges for the unreinforced sliding blocks that produce the desired factor of safety. The strength parameter values along the base of these sliding blocks are those for the soil-geosynthetic interface. In step 3, "compound" circles are analyzed, and reinforcement lengths are increased if necessary to produce the desired factor of safety. Compound circles are circular surfaces that cut across some layers of reinforcement but extend beyond other layers of reinforcement in the upper part of the embankment. Lengths required to resist pullout are considered for the circular arcs in steps 1 and 3.

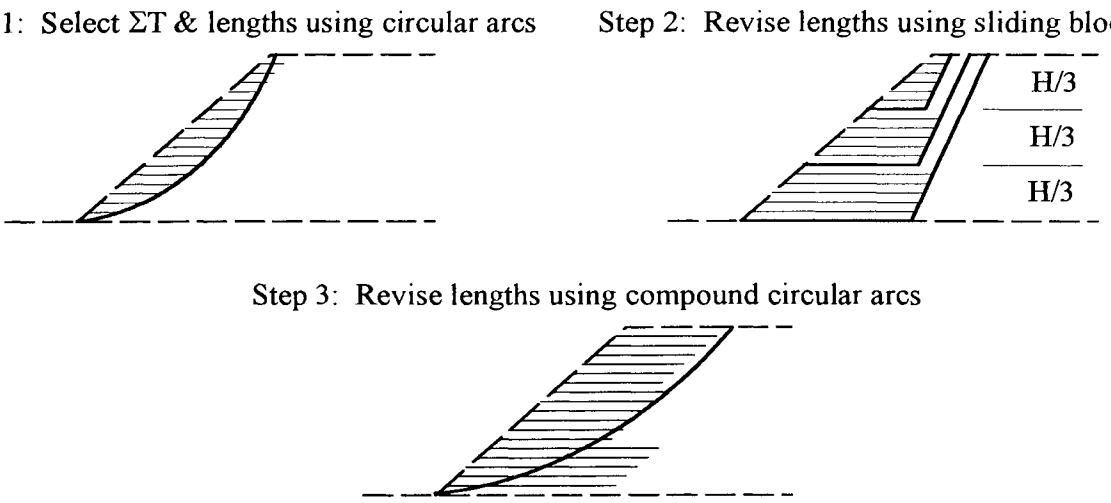

Figure 2. RSS Reinforced Embankment Design Procedure

RSS does not analyze the stability of sliding blocks with active wedges that cut across some or all layers of reinforcement.

As part of this study, the computer programs RSS and UTEXAS3 (Wright, 1991) were compared. These programs have important differences, which are described in detail in the project report (Scarborough et al., 1998) and are being summarized for publication elsewhere. One difference is that UTEXAS3 is capable of analyzing sliding blocks with active wedges that cut across layers of reinforcement. Such surfaces can produce larger required reinforcement forces than those based on circular failure surfaces for the same factor of safety. This may occur when the interface strength is significantly less than the soil strength.

The designs presented in the next section were developed using analyses performed with UTEXAS3 and procedures very similar to those incorporated in RSS, except that both circles and sliding blocks were analyzed to determine the required reinforcement force. The same values of safety factor were applied to both the soil and reinforcement strengths.

PRELIMINARY REINFORCED EMBANKMENT DESIGNS

Based on the recommendations in Elias and Christopher (1996) and considering the relatively rapid rate of consolidation expected for these embankments, the factors of safety listed in Table 7 were used for reinforced embankment design. If the expected consolidation rate had been slow, then geosynthetics with an in-plane drainage capacity may have provided significant benefits. An approach for considering such benefits in design is described in Christopher et al. (1998). Following the recommendation of Kramer (1996), pseudo-static seismic stability analyses were performed using a pseudo-static seismic coefficient, a, equal to one-half of the maximum ground acceleration. The maximum ground acceleration at this site is 0.1 gravity

from the NEHRP (1994) maps for a 90 percent probability of non-exceedance in a 50-year return period.

Table 7. Factors of Safety Required for Slope Stability Analyses

Case	Required Factor of Safety	Conditions
Long term stability	1.3	Drained shear strength
Pseudo-static seismic stability	1.1	Drained shear strength a = 0.05
Short term stability	1.1	Undrained shear strength Bilinear envelope

To provide a basis for comparison with the reinforced slopes, analyses of unreinforced slopes at inclinations of 1.5H:1V and 2.25H:1V were performed using UTEXAS3. The results listed in Table 8 are in agreement with analytic solutions for an infinite slope. The calculated factors of safety indicate that unreinforced slopes at an inclination of 1.5H:1V would not be stable and that a slope inclination of about 2.25H:1V is needed to satisfy the criteria in Table 7 for embankments without reinforcement.

Table 8. Factors of Safety for Unreinforced Embankments

Condition Analyzed	Factor of Safety	
	1.5H:1V	2.25H:1V
Long-term	0.87	1.31
Pseudo-static seismic	0.78	1.14
Short-term, Red Soil Bilinear Envelope 3% Wet of Optimum	0.87	1.31

According to Elias and Christopher (1996) the allowable geosynthetic strength, T_{al}, and the design geosynthetic strength, T_a, are defined by:

$$T_{al} = \frac{T_{ult}}{R_f} \tag{1}$$

$$T_a = \frac{T_{al}}{FS} = \frac{T_{ult}}{FS \cdot R_f} \tag{2}$$

where: T_{ult} is the ultimate tensile strength of a geosynthetic obtained from wide-width tensile tests; FS is the global factor of safety against slope instability, such as the design values in Table

7; and R_f is the reduction factor applied to account for losses in strength due to creep, degradation, and installation damage.

Care must be taken when using design (T_a), allowable (T_{al}), and ultimate (T_{ult}) strengths of reinforcements for analysis and design of reinforced slopes. For example, UTEXAS3 uses design strengths, whereas RSS generates allowable strengths necessary for a particular factor of safety. Further, comparisons between analysis cases with different factors of safety but the same R_f value can only be made on the basis of allowable or ultimate strengths, and comparisons between analysis cases with different factors or safety and different R_f values can only be made on the basis of ultimate strengths. This means, for example, that the design strengths used in UTEXAS3 analyses must be converted to allowable or ultimate strengths when comparing different analysis cases. Finally, a consistent expression of strength must be used when the required reinforcement force from stability analyses is compared with geosynthetic strength to determine the required number of layers of reinforcement.

For the purposes of this preliminary study, a value of R_f equal to 3.5 was applied to all the geosynthetics for all the analysis cases in this study. This value of R_f was selected based on information in Elias and Christopher (1996) and on conversations with Mr. Jerry DiMaggio, Senior Geotechnical Engineer, Federal Highway Administration. An important consideration in arriving at this value of R_f is the assumption that large, angular particles not be included in the embankment fill. If large, angular particles are included in the embankment fill, larger values of R_f would be appropriate. Values of R_f for final design would also vary from geosynthetic to geosynthetic.

The results of analyses to determine the total magnitude of allowable reinforcement force, T_{al}, necessary to satisfy the criteria in Table 7 for 27.4 m (90 ft) high embankments with 1.5H:1V slopes, a 12 kPa (250 psf) surcharge, and three different values of interface friction angle, δ, are presented in Table 9. It can be seen in the table that sliding blocks control the necessary reinforcement force when the interface friction angle is relatively low and circular surfaces control when the interface friction angle is relatively high. It can also be seen that the long-term static condition produces the largest required reinforcement forces provided that the embankment fill is compacted 3 percentage points wet of optimum, or drier. If the embankment fill is compacted 5 percentage points wet of optimum, the short-term condition produces the largest reinforcement force.

Table 10 provides a summary obtained from Table 9 of the required reinforcement forces for compaction at 3 and 5 percentage points wet of optimum. Because the required reinforcement forces are significantly greater for the wetter compaction condition for interface friction angles greater than 17°, it is recommended that compaction water contents be limited to 3 percentage points wet of optimum.

Table 9. Allowable Reinforcement Force, T_{al}, Necessary for Stability of Sliding Block and Circular Surfaces

Condition Analyzed	Interface Friction Angle, δ Degrees	Required Tensile Force kN/m (lb/ft)	Controlling Type of Sliding Surface
Long-term	17°	1,190 (81,400)	Block
$FS_{req} = 1.3$	20°	950 (65,100)	Block
$\phi = 30°$, c = 0	26°	770 (53,000)	Circle
Pseudo-static Seismic	17°	860 (58,700)	Block
$FS_{req} = 1.1$, a = 0.05	20°	640 (44,000)	Block
$\phi = 30°$, c = 0	26°	530 (36,200)	Circle
Short-term	17°	640 (44,000)	Block
$FS_{req} = 1.1$, Bilinear Envelope	20°	370 (25,100)	Circle
3% Wet of Optimum	26°	370 (25,100)	Circle
Short-term	17°	1,190 (81,400)	Circle
$FS_{req} = 1.1$, Bilinear Envelope	20°	1,190 (81,400)	Circle
5% Wet of Optimum	26°	1,190 (81,400)	Circle

Table 10. Summary of Allowable Tensile Forces, T_{al}, Necessary for Stability

Interface Friction Angle, δ Degrees	Required Tensile Force, T_{al} kN/m (lb/ft)	
	Compaction at 3% Wet of Optimum Water Content	Compaction at 5% Wet of Optimum Water Content
17°	1,190 (81,400)	1,190 (81,400)
20°	950 (65,100)	1,190 (81,400)
26°	770 (53,000)	1,190 (81,400)

Reinforcement designs were prepared using three reinforcement distributions: triangular, uniform, and trapezoidal. The trapezoidal distribution, which is based on the work of Zornberg et al. (1998), provides more reinforcement in the middle of the slope, where centrifugal model studies showed that rupture initiated. While attractive from the point of view of mechanics, the trapezoidal distribution may be difficult to implement in the field, particularly when the embankment height changes along the road alignment. Therefore, designs using triangular and uniform distributions are presented here. These designs are presented in Table 11.

The required reinforcement forces are smaller than were anticipated at the onset of the project for two reasons:

1. The borrow site soils consolidate more rapidly than was expected so that a relatively low value of factor of safety could be used for short-term analyses.

2. A decision was made to reduce the maximum compaction water content from 5 percentage points wet of optimum to 3 percentage points wet of optimum. This increased the allowable undrained shear strength used for design.

Table 11. Primary Reinforcement Designs

Reinforcement Type	Reinforcement Distribution	Distribution Details			Totals	
		Zone	Spacing m (ft)	Length m (ft)	T_{al} Provided kN/m (lb/ft)	Length Required m/m (ft/ft)
Mirafi 10XT $\delta = 20°$ $T_{ult} = 115$ kN/m	Triangular	Top	1.52 (5)	18.3 (60)	1,020 (70,000)	1804 (5,920)
		Middle	0.91 (3)	24.4 (80)		
		Bottom	0.61 (2)	36.6 (120)		
	Uniform	Top	0.91 (3)	21.3 (70)	990 (67,700)	1676 (5,500)
		Middle	0.91 (3)	25.9 (85)		
		Bottom	0.91 (3)	36.6 (120)		
Strata PEC100 $\delta = 26°$ $T_{ult} = 100$ kN/m	Triangular	Top	1.52 (5)	24.4 (80)	830 (56,700)	1553 (5,095)
		Middle	1.22 (4)	27.4 (90)		
		Bottom	0.61 (2)	27.4 (90)		
	Uniform	Top	0.91 (3)	24.4 (80)	860 (58,600)	1581 (5,190)
		Middle	0.91 (3)	27.4 (90)		
		Bottom	0.91 (3)	27.4 (90)		
Tensar UX1600 $\delta = 17°$ $T_{ult} = 131$ kN/m	Triangular	Top	1.22 (4)	22.9 (75)	1,240 (84,900)	2179 (7,150)
		Middle	0.91 (3)	29.0 (95)		
		Bottom	0.61 (2)	41.1 (135)		
	Uniform	Top	0.84 (2.75)	24.4 (80)	1,240 (84,900)	2106 (6,910)
		Middle	0.84 (2.75)	30.5 (100)		
		Bottom	0.84 (2.75)	41.1 (135)		

Because the required reinforcement forces are smaller than originally anticipated, more efficient designs are possible using lighter weight grids than the Mirafi 20XT and the Tensar UX1700 used in the soil-geosynthetic testing program. Designs using Mirafi 10XT and Tensar UX1600 grids are included in Table 11. These designs were based on the assumption that the interface friction angles and pullout resistance factors would be the same for different grade grids in the same product line. The actual interface friction angles and pullout resistance factors for the chosen geosynthetic will have to be determined by testing during final design. The manufacturer's values of T_{ult} were used to develop the designs in Table 11.

The designs in Table 11 suggest that a uniform distribution of reinforcement force may be slightly more efficient than a triangular distribution in terms of the required total length of geogrid per foot of embankment. However, considerations of changing embankment height should also be taken into account when establishing the final reinforcement layout.

Illustrations of the reinforced embankment designs are presented in Figure 3 for a uniform reinforcement distribution for the Mirafi 10XT, Strata PEC100, and Tensar UX1600 grids.

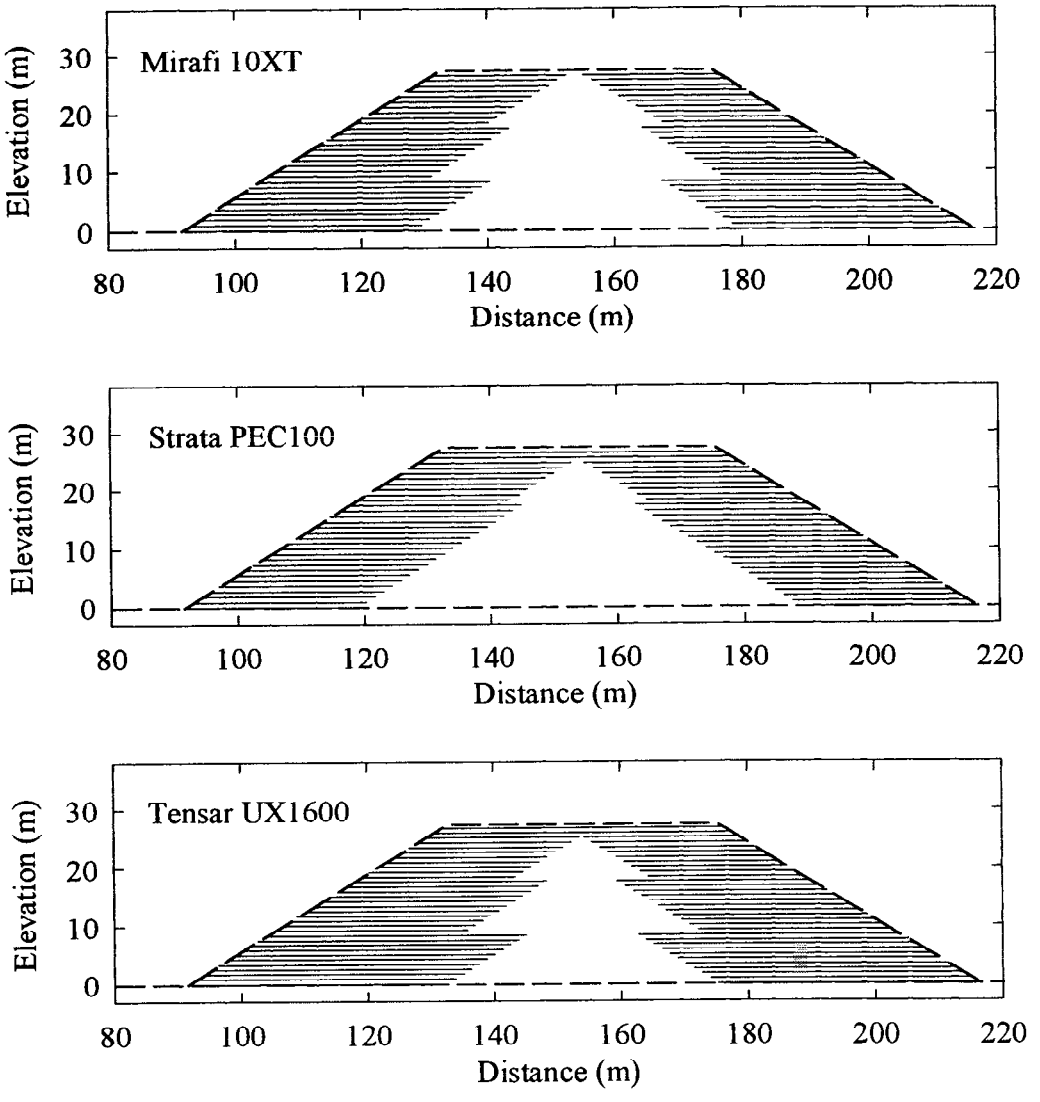

Figure 3. Reinforced Embankment Designs with Uniform Reinforcement Distribution

OTHER DESIGN AND CONSTRUCTION ISSUES

Several other features are important for good embankment performance, including secondary reinforcement, drainage, and erosion protection. Guidelines are provided by Elias and Christopher (1996) and others.

SUMMARY AND CONCLUSION

The feasibility of constructing 27.4 m (90 ft) high geosynthetically reinforced embankments with 1.5H:1V side slopes using poor quality embankment fill for the US 29 Bypass near Lynchburg, Virginia was investigated. The investigation included field explorations, laboratory tests, and slope stability analyses. It was found that the borrow sites consist of residual soil and weathered phyllite. The weathered phyllite is non-durable. Unless the weathered phyllite is broken down to soil-sized particles, it is expected to degrade and erode in the embankment with the potential to cause settlement and stability problems. Most of the weathered phyllite in the borrow area is soft enough that it can be broken down with ordinary excavation, placement, and compaction equipment.

Reductions in the required reinforcement force can be obtained if the embankment fill is compacted within ±3 percentage points of the optimum water content instead of the wider range usually allowed in VDOT's standard specifications.

Laboratory tests indicate that the borrow soils consolidate much more quickly than had been originally anticipated. Because of this, geosynthetics with very high strengths are not required, nor is internal drainage required.

Important differences were found between the slope stability analysis programs RSS and UTEXAS3. One of these differences is that RSS determines the required reinforcement force without analyzing sliding blocks. When the soil-geosynthetic interface friction angle is relatively low, the required reinforcement force to prevent sliding block failure can exceed that from circular sliding surfaces.

As discussed in the paper, care must be taken to ensure compatibility among the reinforcement strength values, e.g., design, allowable, and ultimate strengths, that are used for stability analyses and design of reinforced slopes. Consistency can be ensured by basing comparisons on ultimate strengths.

Analyses have shown that stable embankment slopes at an inclination of 1.5H:1V can be designed using three geosynthetics: a polyvinal chloride (PVC) coated polyester (PET) geogrid, a high density polyethylene (HDPE) geogrid, and a composite, non-woven polypropylene (PP) geotextile with polyester (PET) yarn as reinforcement. A final design selection of a geosynthetic for primary reinforcement should also consider factors such as cost and allowable deformations. In addition, other design features such as secondary reinforcement, drainage, and erosion protection must be taken into account to assure good embankment performance.

ACKNOWLEDGMENTS

The Virginia Transportation Research Council provided financial support for this work. Important contributions were made by Mr. Ken Huber of Langan Associates, Mr. Greg Alber of the University of Virginia, Mr. Rob Swan and Mr. Zehong Yaun of GeoSyntec, Mr. Jerry DiMaggio and Mr. Chris Dumas of the FHWA, and Mr. Don French of VDOT.

REFERENCES

Christopher, B.R., Zornberg, J.G., and Mitchell, J.K. (1998). "Design Guidance for Reinforced Soil Structures with Marginal Backfills, *Proceedings of the Sixth International Conference on Geosynthetics*, Atlanta, GA, pp. 797-804.

Elias, V., and Christopher, B.R. (1996). *Mechanically Stabilized Earth Walls and Reinforced Soil Slopes, Design and Construction Guidelines*, Report No. FHWA-SA-96-071, US Department of Transportation, Washington, DC., 367 pg.

Huber, K.A. (1998). *Design of Shale Embankments*, Geotechnical Engineering Report, Virginia Tech, Blacksburg, Virginia, 91 pg.

Kramer, S.L. (1996). *Geotechnical Earthquake Engineering*, Prentice Hall, Upper Saddle River, NJ, 653 pg.

Marr, A., and Werden, S. (1997). *RSS Reinforced Slope Stability, A Microcomputer Program User's Manual*, Report No. FHWA-SA-96-039, US Department of Transportation, Washington DC, 92 pg.

NEHRP (1994). *NEHRP Recommended Provisions for Seismic Regulations for New Buildings*, Federal Emergency Management Agency, Washington, DC.

Scarborough, J.A., Filz, G.M., Mitchell, J.K., and Brandon, T.L. (1998). *Geosynthetic Reinforcement of the US 29 Bypass Embankments, Madison Heights, near Lynchburg, Virginia*, Geotechnical Engineering Report, Virginia Tech, Blacksburg, Virginia, Vol. 1, 96 pg.

Wright, S.G. (1991). *UTEXAS3, A Computer Program for Slope Stability Calculations*, Shinoak Software, Austin, Texas, 158 pg.

Zornberg, J.G., Sitar, N., and Mitchell, J.K. (1998). "Performance of Geosynthetic Reinforced Slopes at Failure," *Journal of Geotechnical and Geoenvironmental Engineering,*, ASCE, Vol. 124/8, pp. 670-683.

SHEAR STRENGTH OF TEXTURED GEOMEMBRANE AND NONWOVEN GEOTEXTILE INTERFACES

MING-HAN LI
ENVIRONMENTAL MANAGEMENT PROGRAM
TEXAS TRANSPORTATION INSTITUTE, USA

ROBERT B. GILBERT, Ph.D, PE
DEPARTMENT OF CIVIL ENGINEERING
THE UNIVERSITY OF TEXAS AT AUSTIN, USA

ABSTRACT

This paper presents results from small-scale direct shear and double-interface shear tests on interfaces comprised of high-density polyethylene textured geomembranes and nonwoven geotextiles. Two geomembranes with different texturing techniques as well as two nonwoven geotextiles with different fiber types were used. The effects of normal stress, shear rate, texturing type, fiber type, specimen size, and displacement on interface shear strengths were investigated. Test results indicate that approximately 35-40% post-peak interfacial strength loss with displacement occur for all geomembrane and geotextile materials tested. These post-peak strength losses are apparently due primarily to polishing of the texturing on the geomembrane versus reorientation or breakage of nonwoven geotextile fibers. Other findings include that the failure envelopes are nonlinear and that shear rates do not have a noticeable effect on the shear strength for the interfaces tested.

INTRODUCTION

Municipal and hazardous waste landfills in the United States are required to have liner and cover systems. These systems usually incorporate geomembrane (GM) and geotextile (GT) components. The frictional characteristic of the interface between a geomembrane and a geotextile (GM/GT interface) is a concern for stability (e.g., Seed et al., 1988; Byrne et al., 1992; Stark and Poeppel, 1994). Due to the need for high shear strength when using lining systems with GM/GT interfaces, manufacturers have developed textured geomembranes (GMXs). Stark et al. (1996) investigated the frictional characteristics of the textured geomembrane/nonwoven geotextile interface (GMX/GTNW interface) using a torsional ring shear apparatus. They reported a substantial increase in shear strength over smooth GMs and a

significant post-peak strength loss with displacement that was primarily attributed to the pulling out and parallel re-orientation of fibers from GTNWs.

This study further analyzes the shear strength of GMX/GTNW interfaces in dry conditions using a small-scale direct shear apparatus and a double-interface shear device. The objectives of this study are (1) to evaluate the effects of normal stress, shear rate, material type, specimen size, and displacement on interface strengths, and (2) to evaluate the mechanism of post-peak strength reduction.

MATERIALS AND SPECIMEN PREPARATION

Geosynthetics. The geosynthetics tested in this paper were received from the manufacturers in 1995 and are described as follows:

(1) Textured geomembrane – Gundline HDT (GMXG). 1.5 mm (60 mils) thick, coextruded textured high-density polyethylene (HDPE) geomembrane manufactured by Gundle Lining System, Inc.

(2) Textured geomembrane – Friction Seal HD (GMXN). 1.5 mm (60 mils) thick, laminated textured HDPE geomembrane manufactured by National Seal Company.

(3) Nonwoven geotextile – Trevira 1145 (GTNWH). Polyester nonwoven continuous filament needle-punched geotextile manufactured by Hoechst Celanese Corp. The mass per unit area of GTNWH is 440 g/m^2 (13 oz/yd^2).

(4) Nonwoven geotextile – TS 800 (GTNWP). Polypropylene nonwoven continuous filament needle-punched geotextile manufactured by Polyfelt Americas Inc. The mass per unit area of GTNWP is 407 g/m^2 (12 oz/yd^2).

Specimen Preparation. Specimens were cut from the geosynthetic products to fit the testing devices. The GTNW specimen was clamped to the traveling shear box of the testing device and the GMX specimen was fixed to the stationary shear box. To avoid slippage of the GTNW specimen at the surface of the traveling shear box, a sand paper of #36 grit was fixed on the traveling shear box using epoxy. To reduce edge effects from cutting the GTNW specimen, the GTNW specimen was larger than the GMX specimen.

Specimen Sizes. The GMX specimen was cut into circles of 60 mm (2.35 inches) in diameter to fit the direct shear apparatus. The dimensions of the GTNW specimen for the direct shear test were 240 mm × 240 mm (9.4 inches × 9.4 inches). For double-interface tests, the GMX specimen was 102 mm × 102 mm (4 inches × 4 inches), and the GTNW specimen was 152 mm × 330 mm (6 inches × 13 inches).

TEST DEVICES, TEST TYPES AND NUMBER OF TESTS

Small-Scale Direct Shear Apparatus. A small-scale direct shear apparatus manufactured by CETec Inc. was used. The CETec machine provided displacement rates between 3.3×10^{-4} mm/min (1.3×10^{-5} inch/min) and 0.66 mm/min (0.026 inch/min). To avoid an area correction during shear and to increase the maximum shear displacement up to 23 mm (0.9 inch), the lower part of the shear box was replaced with a wooden substrate for this testing program. A cross-section through the modified shear box is shown in Figure 1. Three types of tests using the small-scale direct shear apparatus are described below:

(1) Baseline Tests: Three normal stresses of 16 kPa, 345 kPa and 690 kPa (2.26 psi, 50 psi and 100 psi), and a shear rate of 0.66 mm (0.026 inch) per minute were used to shear samples up to a displacement of 23 mm (0.9 inch).

(2) Slow Tests: A shear rate of 0.066 mm (0.0026 inch) per minute was used in the slow tests.

(3) Accumulated Displacement Tests: A single accumulated displacement test comprised a series of six repeated baseline tests (termed "cycles" herein). One "cycle" consisted of five steps: (i) performing a baseline test until the shear displacement reached 23 mm (0.9 inch), (ii) removing the normal stress, (iii) replacing one of the specimens with a fresh one, (iv) lifting and moving the shear box to its initial location, and (v) re-applying the same normal stress and then resuming the test. Six sets of the accumulated displacement tests in which the GTNW specimens were replaced with fresh ones were performed. One set was at a normal stress of 16 kPa (2.26 psi); four sets at a normal stress of 345 kPa (50 psi), and one set at a normal stress of 690 kPa (100 psi). In contrast with the above sets, one accumulated displacement test in which the GMX specimens were replaced with fresh ones was performed. Only three shear "cycles" were conducted for this set and the normal stress was 690 kPa (100 psi). The total accumulated displacement was about 69 mm after three "cycles" and 137 mm (5.4 inches) after six "cycles."

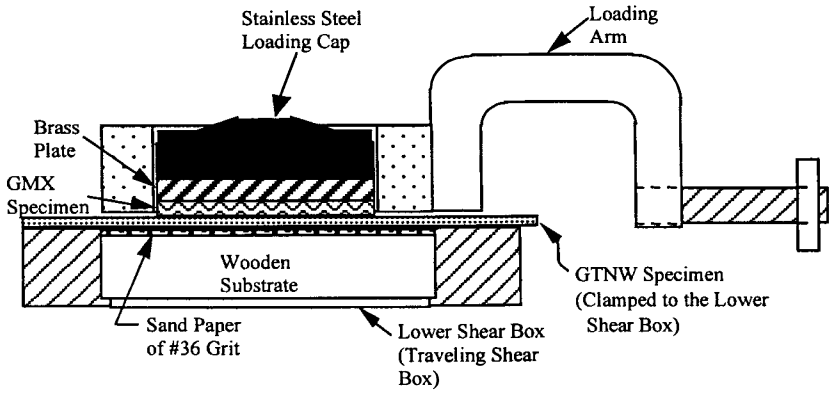

Figure 1. Assembly Drawing of Modified Direct Shear Box (Side View)

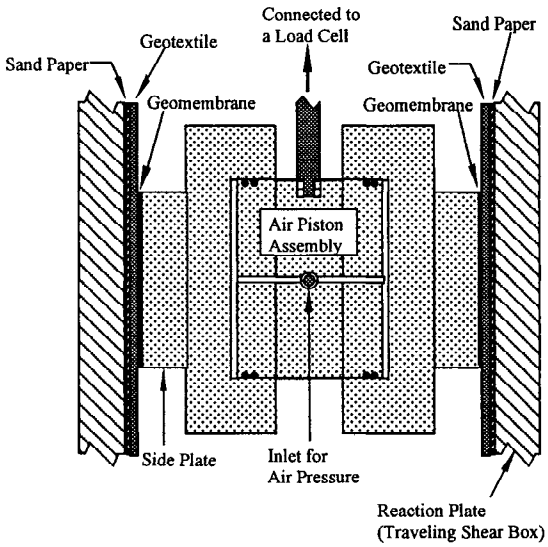

Figure 2. Schematic Drawing of Texas Double Interface Shear Device (Side View)

Texas Double Interface Shear Device. The Texas Double Interface Shear Device (TDISD) was described for measuring the shear strength of geosynthetics by Gilbert et al. (1995). The primary advantage of TDISD is the elimination of machine friction to shear. In addition, the specimen sizes (100 mm × 100 mm on both sides) and shear displacements (125 mm) are larger in comparison to the conventional direct shear apparatus. The schematic drawing of TDISD is shown in Figure 2. Other controlled variables associated with the TDISD test were a normal stress of 345 kPa (50 psi), and a shear rate of 0.64 mm (0.025 inch) per minute.

The number of tests for each test type is summarized in Table 1.

Table 1. Test Types And Number of Tests

Interface Tested GMX / GTNW	Small-Scale Direct Shear Apparatus			Texas Double Interface Shear Device
	Baseline / Slow / Accumulated Displacement [1]			
	σ_n=2.26 psi [2]	σ_n=50 psi	σ_n=100 psi	σ_n=50 psi
Gundline HDT / Trevira 1145	5 / 3 / 1	10 / 3 / 1	5 / 3 / 1 (1)	4
Gundline HDT / TS 800	NT [3]	5 / NT / 1	NT	3
Friction Seal HD / Trevira 1145	NT	5 / NT / 1	NT	4
Friction Seal HD / TS 800	NT	6 / NT / 1	NT	3

[1] Accumulated displacement tests performed by replacing the GTNW specimen, except for one test, where the GMX specimen was replaced (indicated by parenthesis).

[2] 1 psi = 6.903 kPa.

[3] Not tested.

TEST RESULTS

The shear stresses and secant friction angles (the inverse tangent of the ratio of shear stress to normal stress) presented in this paper are the averages for each interface. Large-displacement shear strength denotes the shear strength at a displacement of 23 mm (0.9 inch) for the direct shear apparatus and at a shear displacement of 125 mm (5 inches) for TDISD.

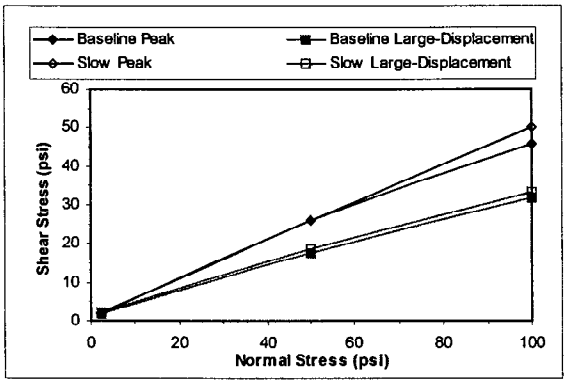

Figure 3. Failure Envelopes of Gundline HDT/Trevira 1145 Interfaces From Baseline and Slow Tests

Effect of Normal Stress. The baseline and slow test results for GMXG/GTNWH interfaces are shown in Figure 3. The failure envelopes of both peak and large-displacement

Table 2. Baseline and TDISD Test Results

Gundline HDT / Trevira 1145 Interface								
	Small-Scale Direct Shear Test						TDISD Test	
Test No.	Peak Shear Strength[1], psi			Shear Strength @ 0.9" Displacement, psi			Peak Shear Strength, psi	Large-Displacement Shear Strength [2], psi
	σ_n=2.26 psi	σ_n=50 psi	σ_n=100 psi	σ_n=2.26 psi	σ_n=50 psi	σ_n=100 psi	σ_n=50 psi	σ_n=50 psi
1	1.54	26.08	47.29	1.48	17.96	30.93	22.38	14.57
2	1.60	25.40	46.00	1.29	17.28	30.56	23.67	15.29
3	1.91	25.46	44.65	1.72	17.90	30.81	22.81	14.47
4	2.09	25.40	45.08	2.03	17.10	31.67	22.06	14.42
5	2.15	24.72	46.62	2.03	17.53	33.21		
6		25.34			17.34			
7		25.28			17.96			
8		25.71			16.60			
9		28.72			18.02			
10		26.38			17.22			
Average Values, psi:								
	1.87	25.9	45.9	1.71	17.5	31.8	22.80	14.70
Standard Deviations, psi:								
	0.265	1.104	1.064	0.329	0.477	0.988	0.695	0.370
Coefficients of Variation, %:								
	14.2	4.3	2.3	19	2.7	3.1	3.1	2.5

Table 2. Baseline and TDISD Test Results (*continued*)

Gundline HDT / TS 800 Interface								
	Small-Scale Direct Shear Test						TDISD Test	
Test No.	Peak Shear Strength[1], psi			Shear Strength @ 0.9" Displacement, psi			Peak Shear Strength, psi	Large-Displacement Shear Strength[2], psi
	σ_n=2.26 psi	σ_n=50 psi	σ_n=100 psi	σ_n=2.26 psi	σ_n=50 psi	σ_n=100 psi	σ_n=50 psi	σ_n=50 psi
1	28.29			18.57			24.33	14.20
2	26.01			18.02			23.69	14.38
3	28.04			18.76			23.77	14.26
4	25.77			17.90				
5	26.20			18.39				
Average Values, psi:	26.90			18.30			23.77	14.28
Standard Deviations, psi:	1.202			0.360			0.349	0.092
Coefficients of Variation, %:	4.5			2.0			1.5	0.6
Friction Seal HD / Trevira 1145 Interface								
	Small-Scale Direct Shear Test						TDISD Test	
Test No.	Peak Shear Strength, psi			Shear Strength @ 0.9" Displacement, psi			Peak Shear Strength, psi	Large-Displacement Shear Strength, psi
	σ_n=2.26 psi	σ_n=50 psi	σ_n=100 psi	σ_n=2.26 psi	σ_n=50 psi	σ_n=100 psi	σ_n=50 psi	σ_n=50 psi
1	24.85			17.04			24.99	15.14
2	25.83			17.47			24.12	14.24
3	26.94			19.19			23.59	15.50
4	28.41			19.37			24.96	15.99
5	27.31			18.88				
Average Values, psi:	26.70			18.40			24.42	15.22
Standard Deviations, psi:	1.372			1.079			0.695	0.751
Coefficients of Variation, %:	5.1			5.9			2.8	4.9
Friction Seal HD / TS 800 Interface								
	Small-Scale Direct Shear Test						TDISD Test	
Test No.	Peak Shear Strength, psi			Shear Strength @ 0.9" Displacement, psi			Peak Shear Strength, psi	Large-Displacement Shear Strength, psi
	σ_n=2.26 psi	σ_n=50 psi	σ_n=100 psi	σ_n=2.26 psi	σ_n=50 psi	σ_n=100 psi	σ_n=50 psi	σ_n=50 psi
1	28.97			20.91			25.83	14.02
2	26.63			21.03			26.49	15.19
3	27.43			21.28			25.85	14.85
4	27.55			21.52				
5	28.84			22.45				
6	28.23			19.68				
Average Values, psi:	27.94			21.15			26.06	14.69
Standard Deviations, psi:	0.904			0.903			0.375	0.602
Coefficients of Variation, %:	3.2			4.3			1.4	4.1

[1] 1 psi = 6.903 kPa.

[2] The total displacement is 127 mm (5 inches).

shear strengths are nonlinear; the average secant friction angles, which are summarized in Table 3, decrease with increasing normal stress. This significant change in the secant friction angle from low to high normal stress conditions suggests that the entire failure envelope be considered in stability analyses. Other researchers (Stark et al. 1996) also reported nonlinear failure envelopes for this interface.

Table 3. Average Secant Friction Angles of Gundline HDT/Trevira 1145 Interfaces From Baseline and Slow Tests

Test Type	Peak Secant Friction Angle (degree)			Large-Displacement Secant Friction Angle (degree)		
	σ_n			σ_n		
	2.26 psi [1]	50 psi	100 psi	2.26 psi	50 psi	100 psi
Baseline Test	40	27	25	37	19	18
Slow Test	46	27	27	42	20	18

[1] 1 psi = 6.903 kPa

Effect of Shear Rate. The "lower" and "higher" shear rates here denote 0.066 mm/min (0.0026 inch/min) in slow tests and 0.66 mm/min (0.026 inch/min) in baseline tests, respectively. As presented in Table 3, the average secant friction angles from the lower shear rate are generally equal to or slightly larger than those from the higher shear rate. To explore whether the small differences in the average results between the two tests are simply an artifact of variability in test results, the hypothesis that shear strength was not affected by shear rate was tested using a statistical test, the Student's t-Test (Ang and Tang, 1975). The null hypothesis, H_o, is "the average shear strength from the higher rate is equal to that from the lower rate." The results of this analysis are presented in Table 4 using p-values. A p-value larger than 0.05 or 0.10 generally indicates that the null hypothesis can be accepted with significant confidence. Since most of the p-values are larger than 0.10, it is concluded that the shear rate does not have a significant effect on the shear strength for this GMX/GTNW interface. This result is consistent with the conclusion reached by Stark et al. (1996).

Table 4. Results of Hypothesis Testing

	Baseline Test			Slow Test				
Peak σ_n	Mean $\bar{X}_I$	Standard Deviation σ_I	Sample Size n_I	Mean $\bar{X}_{II}$	Standard Deviation σ_{II}	Sample Size n_{II}	t	p-value
2.26 psi [1]	1.86	0.278	5	2.31	0.478	3	-1.73	0.134
50 psi	25.8	1.106	10	25.8	1.193	3	0.02	0.983
100 psi	45.9	1.083	5	50.2	2.250	3	-3.75	0.009
Large-Disp. σ_n	$\bar{X}_I$	σ_I	n_I	$\bar{X}_{II}$	σ_{II}	n_{II}	t	
2.26 psi	1.71	0.329	5	2.06	0.555	3	-1.16	0.292
50 psi	17.5	0.469	10	18.0	1.021	3	-1.36	0.202
100 psi	31.4	1.074	5	33.1	0.153	3	-2.64	0.039

[1] 1 psi = 6.903 kPa

Mechanism of Post-Peak Strength Reduction. The Accumulated Displacement Tests in which the GTNW specimens were replaced with fresh ones were conducted to investigate the mechanism of post-peak shear strength loss. Each cycle in this test corresponded to approximately 23 mm of displacement. Figure 4 shows that the peak shear strength of each interface in every test series decreases from the first to sixth shear "cycle." After the third shear "cycle," the peak shear strengths of almost every series are below 70% of the first shear "cycle" peak shear strength, and reach approximately 65% at the sixth shear "cycle." Also, no significant peak shear strength can be observed after two shear "cycles" (see Figure 5).

To further investigate the major cause of shear strength loss, another series of the Accumulated Displacement Tests replacing the GMX specimen were conducted. As plotted in Figure 6, the peak shear strength was 91% of the first "cycle" peak shear strength after three shear "cycles." Also, noticeable peak shear stresses were mobilized in each shear "cycle" in comparison with the tests in which the GTNW specimens were replaced (see Figure 6). Hence, the post-peak strength loss for the interface is likely due to polishing of the GMXs.

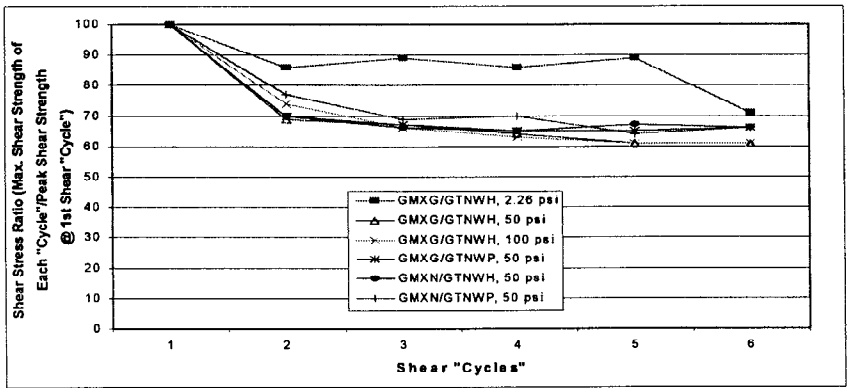

Figure 4. Peak Shear Stress Ratio of The Accumulated Displacement Tests (Replacing GTNW Specimen)

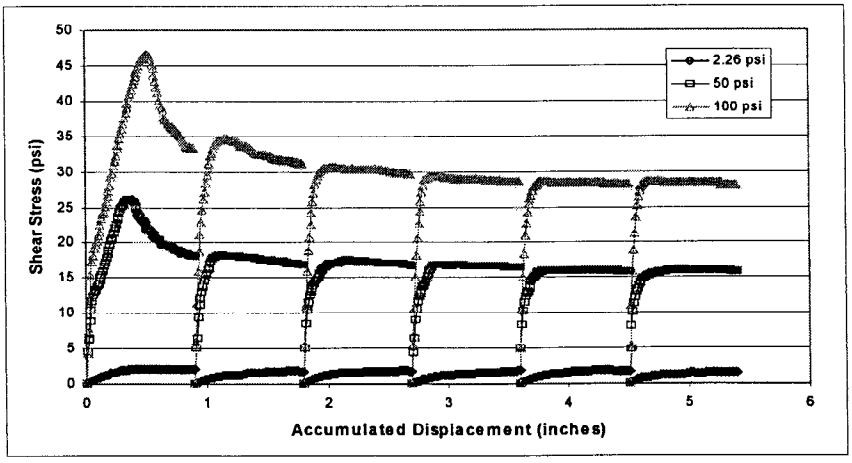

Figure 5. Examples of The Accumulated Displacement Test Results (GMXG/GTNWH Interface)

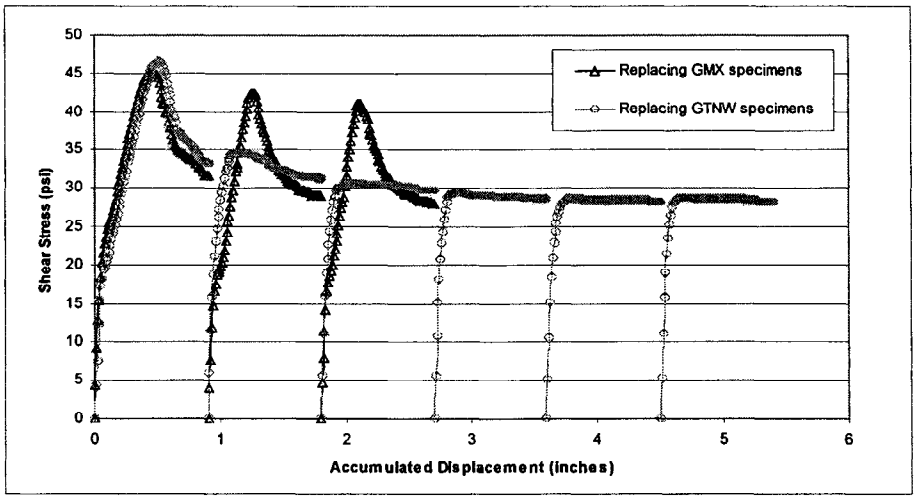

Figure 6. Accumulated Displacement Test Results of GMXG/GTNWH Interface at A Normal Stress of 100 psi

The effect of material types was also compared. As presented in Figure 7, similar strength loss behaviors from different interfaces appear regardless of the type of geomembrane or geotextile. It should be noted that in all of these tests in Figure 7, the GTNW specimens were replaced with fresh ones.

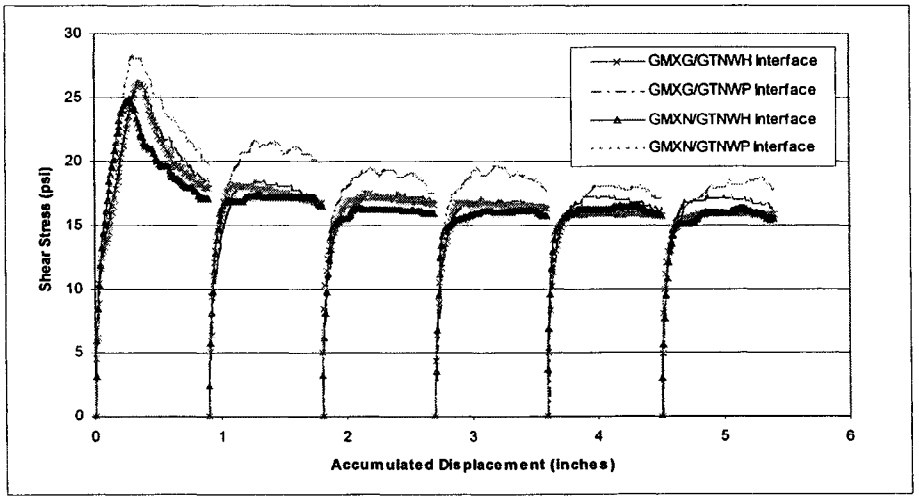

Figure 7. Accumulated Displacement Test Results of Four Types of Interfaces at A Normal Stress of 50 psi

From the above evidence, the shear strength loss of the GMX/GTNW interface apparently results mainly from the polishing of the GMX. This polishing was not visible with the naked eye, even after several cycles of displacement. However, it is clear from the data

shown on Figure 6, where the peak strength is nearly recovered when the textured geomembrane specimen is replaced but not when the nonwoven geotextile specimen is replaced after each cycle. It is important to point out that this conclusion is different from that in Stark et al. (1996). They used the torsional ring shear apparatus to investigate the GMX/GTNW interface and found a significant post-peak shear strength reduction. They attributed the post-peak strength loss primarily to failure of the fibers in the GTNWs. They observed that the textured geomembrane combed the fibers from the geotextile, leaving strands of fibers between the asperities on the textured geomembrane. In this study, when the GTNW specimen was replaced after each cycle in the Accumulated Displacement Tests, the loose fibers in the textured geomembrane were removed. However, the same reduction in strength that Stark et al. (1996) observed occurred. Therefore, the post-peak strength loss is apparently not caused by fiber failure but by subtle polishing of the textured geomembrane surface.

Comparison of Small-Scale Direct Shear Apparatus and TDISD Tests. Test results at the normal stress of 345 kPa (50 psi) from both test devices are presented in Table 5. The shear strengths measured from both devices are similar even though the specimen sizes were different. A possible reason for the slightly lower shear strengths measured with the TDISD is that friction within the air piston slightly reduced the applied normal stress compared to that measured (Gilbert et al., 1995).

Table 5. Comparison of Test Results Between Small-Scale Direct Shear Apparatus and Texas Double Interface Shear Device

Interface Tested GMX/GTNW	Small-Scale Direct Shear Apparatus Accumulated Displacement [1]		Texas Double Interface Shear Device	
	Peak Secant Friction Angle (°)	Large-Displacement [2] Secant Friction Angle (°)	Peak Secant Friction Angle (°)	Large-Displacement [3] Secant Friction Angle (°)
	σ_n=50 psi	σ_n=50 psi	σ_n=50 psi	σ_n=50 psi
Gundline HDT / Trevira 1145	28	18	24	16
Gundline HDT / TS 800	28	18	25	16
Friction Seal HD / Trevira 1145	26	17	26	17
Friction Seal HD / TS 800	29	19	28	16

[1] Peak secant friction angles represent the peak values of the first shear "cycle."
Large-displacement secant friction angles represent the values from the sixth shear "cycle."
[2] The total displacement is 137.2 mm (5.4 inches).
[3] The total displacement is 127 mm (5 inches).

To further understand the peak-strength displacement and large-displacement strength from both devices, results from the Accumulated Displacement and TDISD tests are compared. As shown in Figure 8, the stress-strain curves from both devices have similar patterns with respect to the peak-strength displacement, level of post-peak strength reduction, and large-displacement strength. These similar outcomes from two different test procedures are encouraging.

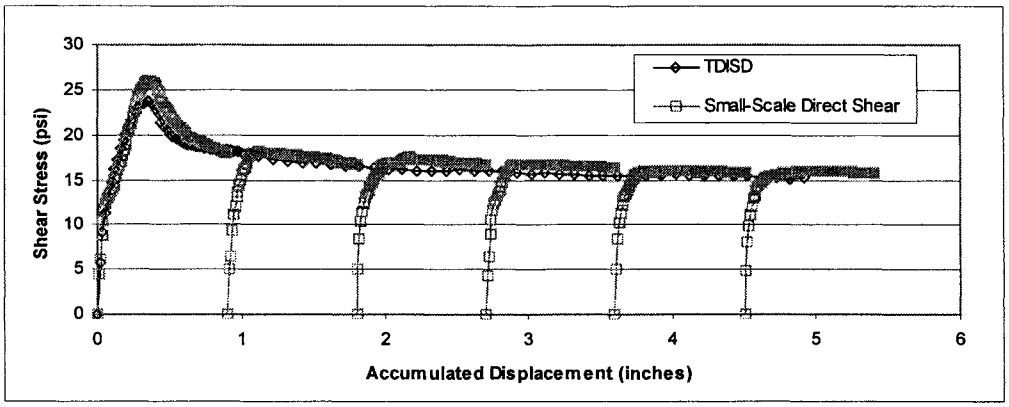

Figure 8. Stress-Strain Curves of The Accumulated Displacement And TDISD Tests (GMXG/GTNWH Interface at The Normal Stress of 50 psi)

CONCLUSIONS

The shear strengths of four textured geomembrane/nonwoven geotextile (GMX/GTNW) interfaces were measured using both the small-scale direct shear apparatus and Texas Double Interface Shear Device (TDISD). The conclusions of this paper are:

(1) All four GMX/GTNW interfaces exhibit post-peak reductions in shear strength and have similar stress-strain curve patterns regardless of the type of materials. The large-displacement shear strength of this interface is about 61 to 64% of the peak shear strength. From the Accumulated Displacement Tests, that is, performing repeated shear "cycles" in which the GMX or GTNW specimens were replaced with fresh ones, the shear strength reduction is apparently caused primarily by the polishing of the GMX surface. The reorientation or breakage of GTNW fibers is a minor factor resulting in post-peak strength reductions.

(2) The failure envelopes for the GMX/GTNW interfaces are nonlinear. The secant friction angle decreases approximately from 40 degrees to 25 degrees with increasing normal stress from 16 kPa (2.26 psi) to 690 kPa (100 psi). Therefore, adequate secant friction angles need to be carefully determined for design under different normal stress conditions.

(3) The shear rate shows no significant effects on the shear strength of the GMX/GTNW interfaces. Due to the limitation of the devices used in this paper, the fastest shear rate performed was only 0.66 mm (0.026 inch) per minute, which may not sufficiently represent a "high" shear rate. However, this insignificant effect of the shear rate on the shear strength is consistent with the conclusion in Stark et al. (1996).

(4) Two test procedures using the small-scale direct shear apparatus and TDISD yield similar and consistent results. Both devices produce similar peak strengths. In addition, it was possible to measure shear stress versus displacement behavior beyond the peak strength using

accumulated displacements with the small-scale direct shear apparatus. These results compared favorably with those obtained from continuous displacements with the TDISD.

ACKNOWLEDGEMENTS

The authors wish to thank Gundle Lining Systems, Inc., National Seal Company, Hoechst Celanese Corp., and Polyfelt Americas, Inc. for providing geosynthetic samples used in this paper.

REFEFENCES

Ang, A. H. S., and Tan, W. H. (1975) Probability Concepts in Engineering Planning and Design. John Wiley & Sons, Inc., New York.

Byrne, R. J., Kendall, J., and Brown, S. (1992) "Cause and mechanism of failure, Kettleman Hills Landfill B-19, unit IA." Proc., ASCE Spec. Conf. on Perf. and Stability of Slopes and Embankments-II, ASCE, Vol. 2, pp.1188-1215.

Gilbert, R. B., Liu, C. N., Wright, S. G., and Trautwein, S. J. (1995) "A double shear test method for measuring interface strength." Proc. Geosynthetics '95 Conf., IFAI, Vol.3, pp.1017-1029.

Seed, R. B., Mitchell, J. K., and Seed, H. B. (1988) "Slope stability failure investigation: landfill unit B-19, phase I-A, Kettleman Hills, California." Res. Rep. No. UCB/GT/88-01, Univ. of California, Berkeley, Calif.

Stark, T. D., and Poeppel, A. R. (1994) "Landfill liner interface strengths from torsional ring shear tests." Journal of Geotechnical Engineering, ASCE, Vol.120, No.3, pp.597-615.

Stark, T. D., Williamson, T. A., and Eid, H. T. (1996) "HDPE geomembrane/geotextile interface shear strength", Journal of Geotechnical Engineering, ASCE, Vol.122, pp. 197-203.

INFLUENCE OF HIGH LOAD DEFORMATIONS ON GEOMEMBRANE LINER INTERFACE STRENGTHS

MR. ALLAN J. BREITENBACH
AGRA EARTH & ENVIRONMENTAL, INC. COLORADO, U.S.A

MR. ROBERT H. SWAN, JR.
GEOSYNTEC CONSULTANTS, GEORGIA, U.S.A

ABSTRACT

The engineering design of geomembrane-lined fill structures, such as solid waste landfills, tailings impoundments, and heap leach pads, typically involves the use of one or more low permeability composite liner systems. A composite liner system generally includes a low permeability subgrade soil material in direct contact with a flexible geomembrane liner. These lined fill structures may also include an overlying geosynthetic drainage layer or natural drain fill cover to minimize hydraulic heads on the liner system and protect the geomembrane liner surface from punctures or tears during subsequent fill placement operations.

This paper presents measured direct shear interface strengths of composite liner systems with respect to the time-dependent deformation of the geomembrane liner surface under simulated fill loads at high confining stresses. The effects of a change in moisture content versus measured interface strengths have been incorporated into this study at a moisture range of minus 2 percentage points to plus 4 percentage points of optimum moisture content (OMC). Pre-test load consolidation times varied for 0 to 12, 24 and 48 hours. The test results show a significant increase in the interface strength with time in all of the test series due to soil consolidation and apparent micro scale load deformations on the geomembrane liner surface.

KEY WORDS

Composite liner, direct shear strengths, pre-test load consolidation, high load liner deformations.

INTRODUCTION

Past slope failures on geomembrane-lined fill structures such as solid waste landfills, heap leach pads, and reclamation cover fill caps have shown that liner induced slides generally occur by wedge failure at the planar geomembrane liner interface contact with fine grained soils or geotextiles. Most of the engineering community first became aware of the potential for low planar interface strengths in geomembrane liner systems following the Kettleman Hills landfill slope failure in Northern California in 1988 (Mitchell et al. 1990). The lesser known leach pad slope failures, occurring between 1985 and 1993 at several mine sites in North America, South America, and Australia, have also shown the importance of stabilizing the downhill pad toe limits to prevent

wedge slip failures on the geomembrane lined pad surfaces (Breitenbach 1997). The Northridge earthquake in Southern California in 1994 was a reminder that relatively thin liner cover fills on slopes have a high seismic risk of slope movement at the liner interface (Matasovic et al. 1995). These slope failures on lined fill structures, although relatively rare in occurrence, demonstrate the need for special liner design, testing, and operational considerations to prevent fill slope instability and movement on the geomembrane liner system.

There are several interrelated laboratory test parameters that influence the composite liner interface direct shear strength including the following list in no particular order of importance:

- Test equipment size (small versus large shear box)
- Normal confining stress loading (low versus high loads)
- Load consolidation time (quick versus delayed testing)
- Rate of applied shear force (slow versus fast)
- Geomembrane liner thickness (40-mil to 80-mil typical)
- Geomembrane interface contact (underliner soil, overliner soil or geotextile)
- Geomembrane liner anchorage (fixed (restricted) versus free (unrestricted))
- Geomembrane liner flexibility (more versus less flexible)
- Geomembrane liner surface (smooth versus textured)
- Geomembrane liner texture type (sprayed, colaminated, coextruded, or calendared)
- Underliner/overliner soil classification (gradation and plasticity)
- Underliner/overliner maximum rock size (distribution at the interface contact)
- Underliner/overliner rock particle shape (rounded versus angular)
- Underliner/overliner moisture content (dry versus wet of optimum moisture)
- Underliner/overliner compaction (low versus high density)
- Strength condition (effective versus total stress)
- Strength selection (peak versus residual shear strength)

This paper focuses on the measured increase in large-scale laboratory direct shear test shear strengths with respect to changing soil moisture contents due to apparent time-dependent high fill load deformations on the geomembrane liner interface contact with composite liner soils. Allowing as little as 12 to 24 hours of load consolidation time before testing appears to significantly increase both the peak and residual interface friction and apparent cohesion strengths for relatively high simulated test loads on moistened underliner soils. A schematic presentation of a simplified composite geomembrane liner system for a non-hazardous waste fill is shown in Figure 1.

INTERFACE DIRECT SHEAR TESTS

General Background

In the late 1980's and early 1990's, large scale direct shear box tests were performed for several mining leach pad liner projects. The test results showed a consistent difference in measured shear strengths for various types of geomembrane liners with the more flexible geomembranes achieving higher interface frictional strengths. Tests were conducted on smooth sheet geomembrane liners by the authors starting in 1990 to study the relative strength difference between a more rigid planar liner surface versus a more flexible or "dimpled" non-planar liner surface in a composite liner design.

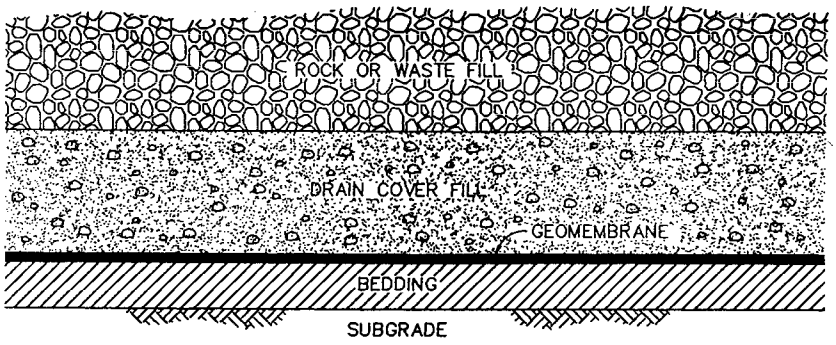

Figure 1. Schematic Diagram of Simple Composite Geomembrane Liner System

Initial testing was performed to determine the most conservative and consistent planar surface strength by conducting testing using wood blocks glued to the bottom of smooth sheet geomembrane liner surfaces with the upper liner surfaces in contact with a fine grained "underliner" soil material compacted at optimum moisture content. Additional testing was performed to develop a strength comparison by replacing the wood blocks with the same fine grained soil underliner material, in addition to placing a fine to medium grained free draining gravel above the smooth sheet geomembrane liner as the overliner material. The removal of the wood blocks allowed granular rock particle deformations to occur in the flexible geomembrane liner surface for an increase in interface frictional strength, independent of the pre-test load consolidation time discussed later in this paper. The relative difference in liner interface friction angles for these tests with instantaneous loading ranged between 2 to 6 degrees in peak frictional strength values depending on the type of geomembrane liner tested.

These early tests indicated that a micro scale dimpling or uneven geomembrane liner surface under high fill loads apparently causes the test failure surface to shear through a portion of the underlying or overlying soil materials for an overall increase in shear strength along the geomembrane interface contact. Schematic presentations of the planar (wood block) and non-planar (dimpling) shear tests are shown in Figures 2 and 3.

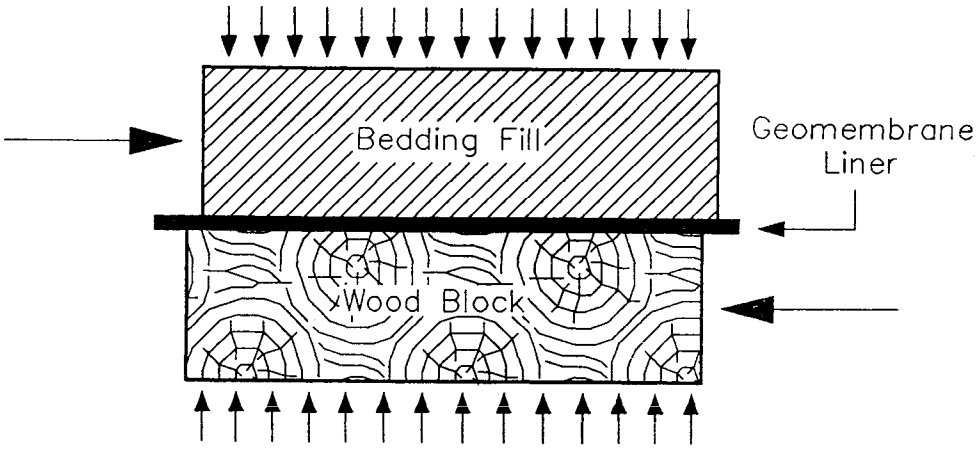

Figure 2. Schematic Diagram of Planar (Wood Block) Direct Shear Test Setup

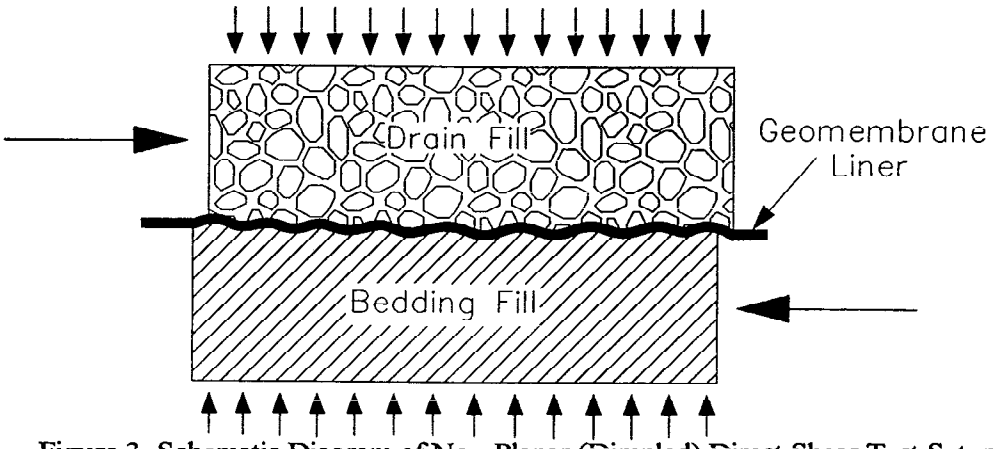

Figure 3. Schematic Diagram of Non-Planar (Dimpled) Direct Shear Test Setup

Based on these experimental test results, further tests were conducted in through 1990's on several mine projects to estimate the long-term field strength of each leach pad composite liner system subjected to multiple ore lift loads over an operational mine period of several years. The pre-test load consolidation times varied from 0 to 24 hours prior to shear testing and consistently showed a significant increase in both the peak and residual friction strengths with respect to the longer load consolidation time factor.

A recent series of direct shear tests were conducted by the authors in 1998 for this paper to further define this phenomena of high load liner deformations versus interface strength values by eliminating all test variables except for the pre-test consolidation time and soil moisture content. The recent tests were conducted with the same large scale direct shear test equipment using identical compacted underliner and loose lift overliner soil materials and geomembrane liner sheet at the same high confining stress loads and shear rates. These test series and test results are discussed herein and listed in Tables 1 and 2.

Direct Shear Test Series

A total of 26 direct shear test points were performed for the 4 test series listed as Tests 1 through 4 in Tables 1 and 2. The Test 1 series established the baseline interface shear strengths for a range of composite underliner moisture contents ranging from -2, 0, +2, and +4 percentage points of OMC at 0 hours of pre-test load consolidation time. The Test 2, 3, and 4 series fixed the underliner moisture contents at -2, 0, and +4 percentage points of OMC for each series, respectively, with the pre-test load consolidation time varied at 0, 12, 24, and 48 hours. Each large scale direct shear test was performed according to established American Society for Testing and Materials test procedures (ASTM D-5321) on the composite clayey soil (underliner), geomembrane liner (60-mil (1.5-mm) smooth high density polyethylene (HDPE) geomembrane), and drain gravel (overliner) using a direct shear device that consists of an upper and lower shear box. The upper box measures 300-mm square in plan by 75-mm high. The lower box measures 300-mm by 360-mm in plan by 75-mm high. Shearing in all of the tests occurred at the compacted clayey soil to geomembrane liner interface at a shear rate of 0.04-in/min (1.0-mm/min).

For simplification purposes, the test series discussions will generally address peak strength test results at the geomembrane liner interface, since the residual strength test results generally show a similar trend in pre-test load consolidation strength changes with respect to time. Underliner and overliner material properties are summarized in Table 1. Test conditions and interface direct shear test results are summarized in Table 2.

Table 1. Underliner and Overliner Materials Properties

Test Number	Underliner Characteristics								Overliner Characteristics							
	Max. Rock	% G	% S	% F	% PI	USCS	Compaction	Moisture	Max. Rock	% G	% S	% F	% PI	USCS	Compaction	Moisture
Test 1	2"	6	40	54	15	CL	90% D-698	-2.0%	1"	81	13	6	NP	GP-SM	Loose Lift	Wetted
	2"	6	40	54	15	CL	90% D-698	Optimum	1"	81	13	6	NP	GP-SM	Loose Lift	Wetted
	2"	6	40	54	15	CL	90% D-698	2.0%	1"	81	13	6	NP	GP-SM	Loose Lift	Wetted
	2"	6	40	54	15	CL	90% D-698	4.0%	1"	81	13	6	NP	GP-SM	Loose Lift	Wetted
Test 2	2"	6	40	54	15	CL	90% D-698	-2.0%	1"	81	13	6	NP	GP-SM	Loose Lift	Wetted
	2"	6	40	54	15	CL	90% D-698	-2.0%	1"	81	13	6	NP	GP-SM	Loose Lift	Wetted
	2"	6	40	54	15	CL	90% D-698	-2.0%	1"	81	13	6	NP	GP-SM	Loose Lift	Wetted
	2"	6	40	54	15	CL	90% D-698	-2.0%	1"	81	13	6	NP	GP-SM	Loose Lift	Wetted
Test 3	2"	6	40	54	15	CL	90% D-698	Optimum	1"	81	13	6	NP	GP-SM	Loose Lift	Wetted
	2"	6	40	54	15	CL	90% D-698	Optimum	1"	81	13	6	NP	GP-SM	Loose Lift	Wetted
	2"	6	40	54	15	CL	90% D-698	Optimum	1"	81	13	6	NP	GP-SM	Loose Lift	Wetted
	2"	6	40	54	15	CL	90% D-698	Optimum	1"	81	13	6	NP	GP-SM	Loose Lift	Wetted
Test 4	2"	6	40	54	15	CL	90% D-698	4.0%	1"	81	13	6	NP	GP-SM	Loose Lift	Wetted
	2"	6	40	54	15	CL	90% D-698	4.0%	1"	81	13	6	NP	GP-SM	Loose Lift	Wetted
	2"	6	40	54	15	CL	90% D-698	4.0%	1"	81	13	6	NP	GP-SM	Loose Lift	Wetted
	2"	6	40	54	15	CL	90% D-698	4.0%	1"	81	13	6	NP	GP-SM	Loose Lift	Wetted

Table 2. Direct Shear Strength Test Results

Test Number	Geomembrane Liner Type	Consolidation Time (hours)	Peak Strengths		Residual Strengths		Normal Load Confining Stress	Shear Box Size
			c (psf)	phi (deg.)	c (psf)	phi (deg.)		
Test 1	60 mil HDPE-Smooth	0	70	22	95	19	2 pts: 50 & 100 psi	12" x 12"
	60 mil HDPE-Smooth	0	65	18	90	14	2 pts: 50 & 100 psi	12" x 12"
	60 mil HDPE-Smooth	0	95	12	10	10	2 pts: 50 & 100 psi	12" x 12"
	60 mil HDPE-Smooth	0	100	4	120	4	2 pts: 50 & 100 psi	12" x 12"
Test 2	60 mil HDPE-Smooth	0	70	22	95	19	2 pts: 50 & 100 psi	12" x 12"
	60 mil HDPE-Smooth	12	455	22	220	19	2 pts: 50 & 100 psi	12" x 12"
	60 mil HDPE-Smooth	24	710	22	245	19	2 pts: 50 & 100 psi	12" x 12"
	60 mil HDPE-Smooth	48	720	23	260	19	2 pts: 50 & 100 psi	12" x 12"
Test 3	60 mil HDPE-Smooth	0	65	18	90	14	2 pts: 50 & 100 psi	12" x 12"
	60 mil HDPE-Smooth	12	410	20	0	17	2 pts: 50 & 100 psi	12" x 12"
	60 mil HDPE-Smooth	24	630	22	50	19	2 pts: 50 & 100 psi	12" x 12"
	60 mil HDPE-Smooth	48	660	23	215	20	2 pts: 50 & 100 psi	12" x 12"
Test 4	60 mil HDPE-Smooth	0	100	4	120	4	2 pts: 50 & 100 psi	12" x 12"
	60 mil HDPE-Smooth	12	140	9	105	9	2 pts: 50 & 100 psi	12" x 12"
	60 mil HDPE-Smooth	24	300	13	130	12	2 pts: 50 & 100 psi	12" x 12"
	60 mil HDPE-Smooth	48	570	18	285	14	2 pts: 50 & 100 psi	12" x 12"

Test 1 Series

The Test 1 series listed in Tables 1 and 2 were performed under the following controlled test parameters: (i) the underliner soil moisture content varied at -2, 0, +2, and +4 percentage points of OMC; (ii) the pre-test load consolidation time fixed at 0 hours; (iii) a smooth geomembrane liner sheet was not anchored to the test shear box (unrestrained); (iv) an underliner soil compacted to 90 percent of standard maximum dry density (ASTM D-698); and (v) confining stress loads applied at 50 and 100 psi (345 and 690 kPa) equivalent to about 72-feet (22-meters) and 144 feet (44-meters) of vertical fill height. The moisture control shear testing established a basis for comparing changes in the underliner soil moisture content to subsequent pre-test load consolidation liner strengths for the same test equipment, procedures and sample materials.

The changes in soil moisture content have a significant influence on both the composite liner interface shear strength and the underliner soil strength and permeability, and therefore the moisture factor has been included in this test study. Laboratory permeability tests on fine grained soils have shown a significant drop in permeability by increasing the moisture content to several percentage points wet of OMC (Hermann and Elsbury 1987) and (Estornell and Daniel 1992). However, there is a tradeoff with wetter soils having lower permeability for a given dry unit weight in the laboratory compared to having lower shear strengths and associated dessication cracks in the field (Swan et al. 1991) and (Daniel and Wu 1993).

The Test 1 series demonstrates the reduction in liner interface friction strength with increasing moisture content, independent of the influence of load consolidation time which will be discussed in Tests 2, 3, and 4. As the moisture content increased above optimum moisture content, excess pore water pressure conditions may have developed during shear testing. The maximum interface friction strength occurred on the dry side of optimum moisture at 22 degrees peak frictional strength. The interface strengths rapidly decreased on the wet side of optimum moisture to 4 degrees for both the peak and residual frictional strength. The peak and residual apparent cohesion values were similar, however these values showed a trend of a gradual increase in apparent cohesion strength with increases in moisture content. A summary of the Test 1 peak shear strengths versus moisture content with no pre-test load consolidation time is shown in Figure 4.

Test 2 Series

The Test 2 series listed in Tables 1 and 2 were performed on the same geomembrane and soil materials as for Test 1 with the pre-test load consolidation times added at 0 to 12, 24, and 48 hours and with underliner soils tested at only 2 percentage points dry of OMC. The drier underliner soils provide a more firm and less yielding (planar) surface, which would be less likely to develop pore water pressures and show less of an increase in relative strength during load consolidation.

The Test 2 series test results show high peak and residual frictional strengths independent of the time consolidation factor, however the peak apparent cohesion strengths increased dramatically in the first 12 to 24 hours indicating some deformation or change in the liner to soil contact may have occurred on the planar liner surface under the pre-test load conditions. A summary of the Test 2 peak shear strengths versus pre-test load consolidation time at minus 2 percentage points of the underliner OMC for the smooth HDPE geomembrane is shown in Figure 5.

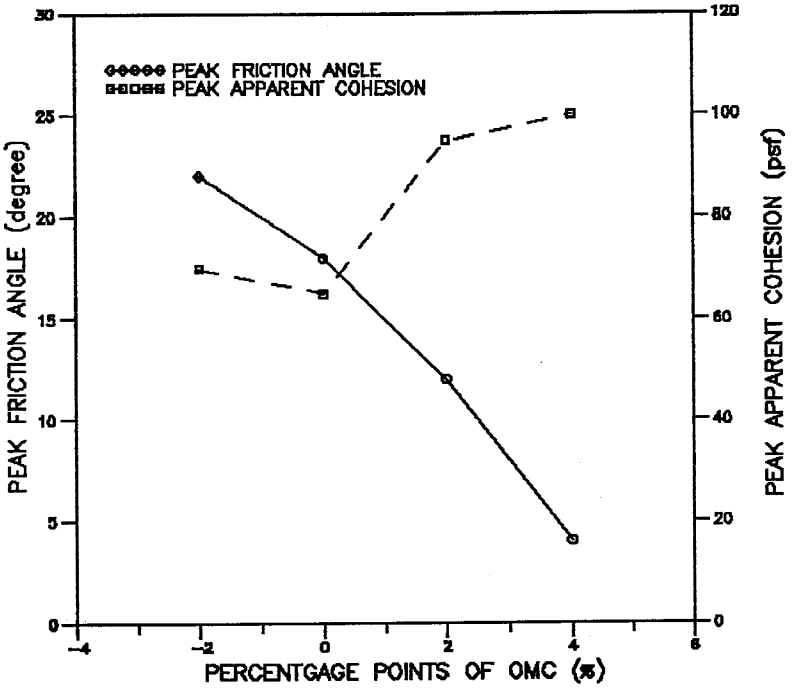

Figure 4. Plot of Test 1 Peak Shear Strengths Versus Percentage Points Wet or Dry of Optimum Moisture Content of Underliner Soil

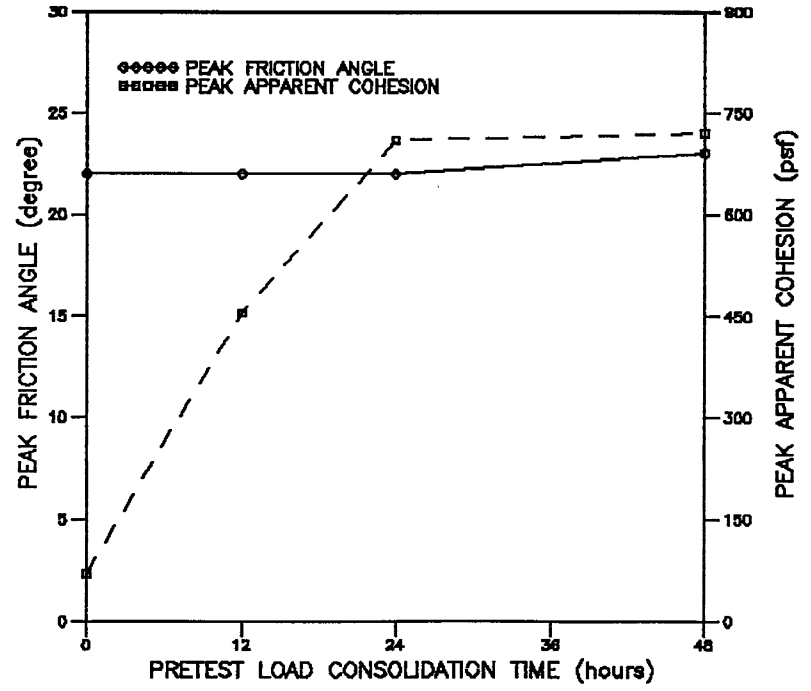

Figure 5. Plot of Test 2 Peak Shear Strengths Versus Pre-Test Load Consolidation Time at Minus 2 Percentage Points of Underliner Soil OMC

Test 3 Series

The Test 3 series listed in Tables 1 and 2 were performed on the same geomembrane and soil materials as for Test 1 with the pre-test load consolidation times added at 0 to 12, 24, and 48 hours and with underliner soils tested at only OMC. The increase in underliner moisture content increases the risk of developing pore water pressures, but should allow the liner load deformations or micro scale dimples to increase with consolidation and become less planar. A reduced interface shear strength from an increase in pore water pressures versus an offsetting increased interface shear strength from a non-planar moistened surface are beyond the scope of this paper, since the pore water pressures are difficult to measure with accuracy in a direct shear test.

The Test 3 series test results show lesser initial peak and residual frictional strengths compared to the Test 2 series, however the Test 3 friction strengths increased and exceeded the Test 2 friction strengths after pre-test load consolidation times longer than 24 hours. The peak apparent cohesion strengths increased dramatically in Test 3, similar to Test 2, in the first 24 hours of pre-test load consolidation time, while the residual apparent cohesion strengths showed a dramatic increase after 24 hours of pre-test load consolidation time. A summary of the Test 3 peak shear strengths versus pre-test load consolidation time at the underliner OMC for the smooth HDPE geomembrane is shown in Figure 6.

Test 4 Series

The Test 4 series listed in Tables 1 and 2 were performed on the same geomembrane and soil materials as for Test 1 with the pre-test load consolidation times added at 0 to 12, 24, and 48 hours and with underliner soils tested at only plus 4 percentage points of OMC. The increase in the Test 4 series underliner moisture content to plus 4 percentage points would be more likely to develop pore water pressures and allow larger liner load deformations or dimples to occur with load consolidation compared to the Test 3 series. However the potential for excess pore pressures to develop during shear testing of overly wet underliner soils will likely offset any increases in shear strength for the non-planar dimpled liner interface contact.

The Test 4 series test results (wet of OMC) show significantly reduced peak and residual frictional strengths compared to Test 2 (dry of OMC) and Test 3 (at OMC). In addition, the Test 4 peak frictional strengths are similar to the Test 4 residual frictional strengths in the pre-test load consolidation times of less than 12 hours indicating excess pore pressures developed during the loading and shearing phase. After 48 hours of pre-test load consolidation time, the Test 4 peak frictional strengths are similar to the initial optimum moisture strength of Test 3 at 0 hours of pre-test load consolidation time. The peak apparent cohesion strengths increased with pre-test load consolidation time, similar to Tests 2 and 3, but at a reduced rate. A summary of the Test 4 peak shear strengths versus pre-test load consolidation time at the plus 4 percentage points of the underliner OMC for the smooth HDPE geomembrane is shown in Figure 7.

SUMMARY OF TEST RESULTS

A series of 4 large scale direct shear tests involving 26 direct shear test points were presented to show the influence of the pre-test load consolidation time factor on the liner interface shear strengths at various underliner moisture contents. These test series were based on earlier test studies conducted in the early to mid 1990's by the authors for several heap leach pad projects in which the test results indicated the more dimpled or

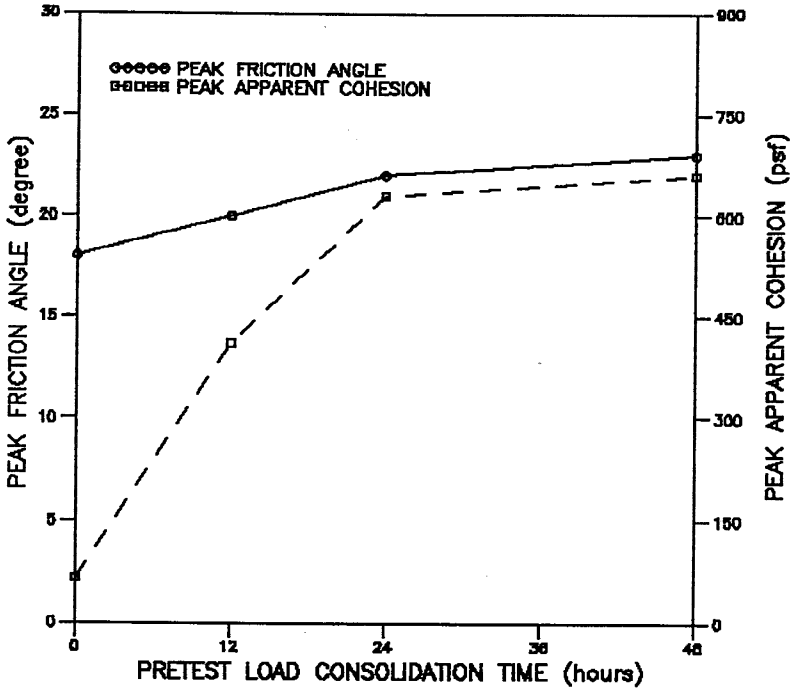

Figure 6. Plot of Test 3 Peak Shear Strengths Versus Pre-Test Load Consolidation Time at Underliner Soil OMC

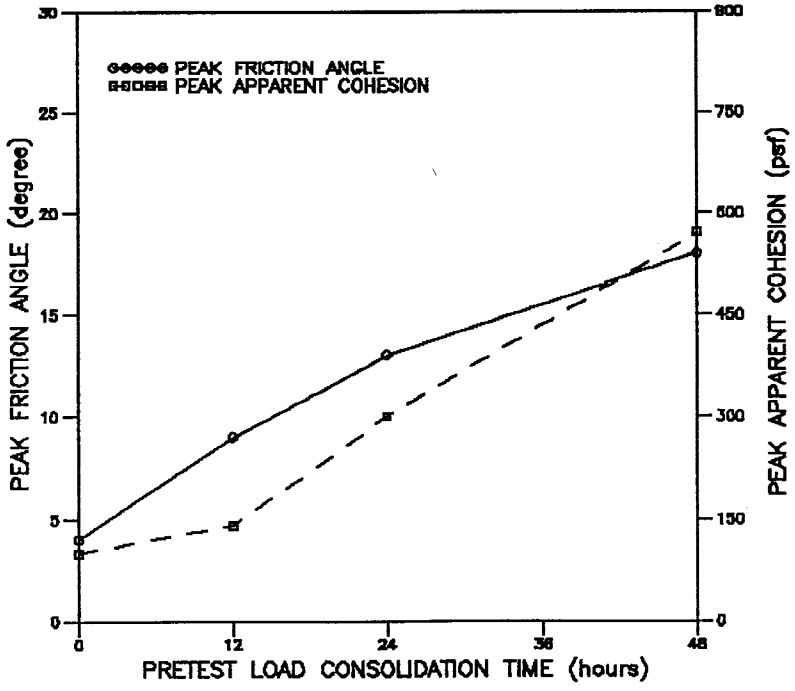

Figure 7. Plot of Test 4 Peak Shear Strengths Versus Pre-Test Load Consolidation Time at Plus 4 Percentage Points of Underliner Soil OMC

less planar liner interface surfaces increased in strength under high fill load conditions. Other factors influencing liner strengths such as test equipment, test procedures, and test sample materials were kept the same for performing Tests 1 to 4 in order to focus primarily on changes in pre-test load consolidation time versus underliner soil moisture content. A summary of each series of test results has been shown in Figures 4 to 7. An overall plot of peak shear stresses and pre-test load consolidation time versus moisture content is shown in Figure 8. An overall plot of the improvement in peak shear stresses with load consolidation time versus changes in underliner soil moisture content is shown in Figure 9. A discussion of the laboratory direct shear test results is listed as follow:

- The Test 1 series in Figure 4 show the effects of changes in the underliner soil moisture content relative to interface strengths at 0 hours of pre-test load consolidation time to establish a basis for comparing subsequent changes in load consolidation time for Tests 2, 3, and 4. Test results show a significant decrease in interface frictional strengths and a general increase in apparent cohesion strengths for underliner soils tested above optimum moisture content (OMC).

- The Test 2 series in Figure 5 show high interface frictional strengths for underliner soils at minus 2 percentage points of OMC, independent of the pre-test load consolidation time. Pre-test consolidation times from 0 to 48 hours show no significant increases in the friction strength with consolidation time likely due to the dry and firm underliner surface restricting the liner interface from developing micro scale dimples or undulations for improved strengths. However, the apparent cohesion strengths increased dramatically for the first 24 hours of pre-test load consolidation time.

- The Test 3 series in Figure 6 show lower interface frictional strengths for underliner soils at OMC and no pre-test load consolidation time compared to Test 2. However, the Test 3 interface frictional strengths were higher than the Test 2 strengths after 24 hours of pre-test load consolidation time. The apparent cohesion strengths increased dramatically for the first 24 hours of pre-test load consolidation time similar to Test 2.

- The Test 4 series in Figure 7 show a significant decrease in interface frictional strengths and apparent cohesion strengths for underliner soils at plus 4 percentage points of OMC with apparent excess pore water pressure conditions in the first 24 hours of pre-test consolidation loading or shearing phase. The Test 4 interface strengths continued to significantly increase with pre-test load consolidations to 48 hours. However, the test strengths remained below the Test 2 and 3 interface frictional strengths relative to consolidation time. The wetter underliner soils apparently provide a more flexible and yielding (less planar) surface, however, the interface strength gained from the micro scale dimpling may be reduced within the above OMC soils due to the potential for the development of excess pore water pressure conditions during shearing.

- The summary plot of peak shear stress versus underliner moisture content in Figure 8 show a decrease in shear strength with an increase in moisture content and an increase in shear strength with an increase in pre-test load consolidation time. The summary plot also shows a greater incremental change in strength at the higher confining stress load conditions with an increasing underliner moisture content. The summary plot indicates that the initial fill lift loads on a geomembrane liner system with minimal consolidation time and high underliner moisture content are the most critical for liner instability.

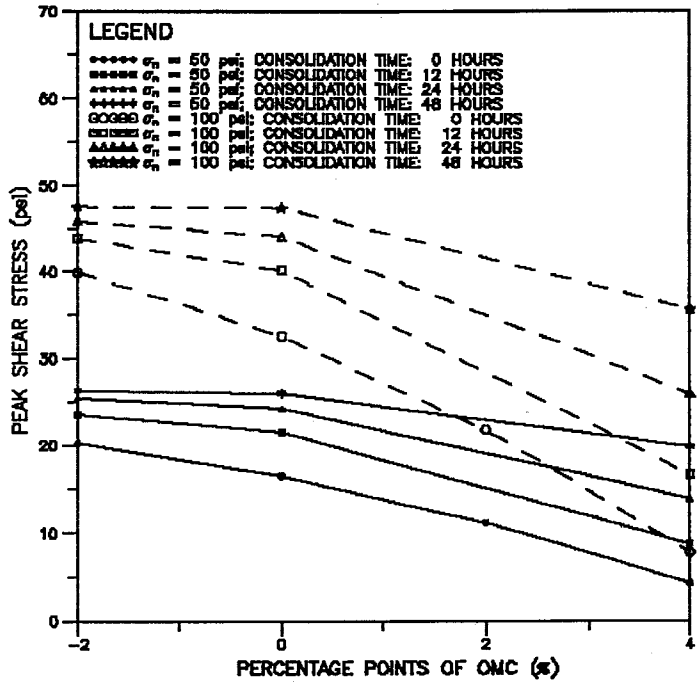

Figure 8. Plot of Tests 1, 2, 3, and 4 Peak Shear Strengths Versus Percentage Points Wet or Dry of Underliner Soil OMC as a Function of Normal Confining Stress and Pre-Test Load Consolidation Time

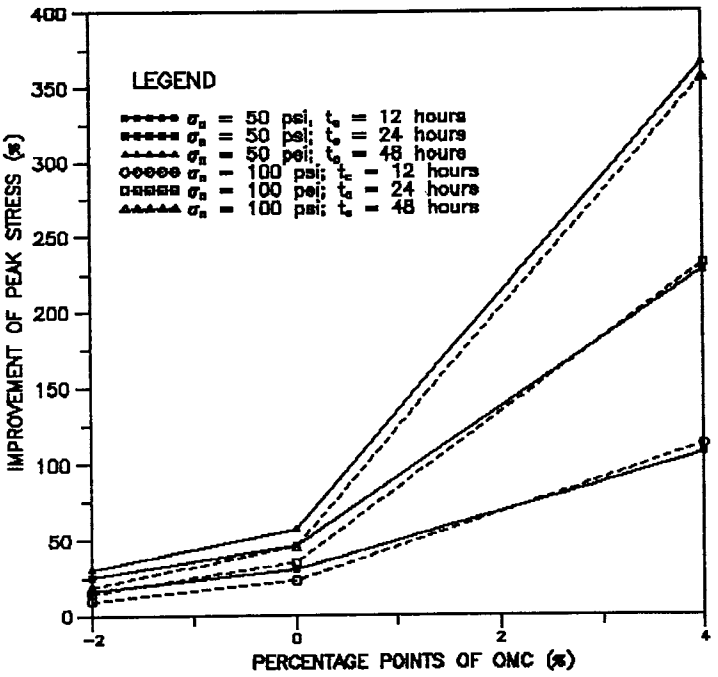

Figure 9. Plot of Test 1, 2, 3, and 4 Improvement in Peak Shear Strength Versus Percentage Points Wet or Dry of Underliner Soil OMC as a Function of Normal Confining Stress and Pre-Test Load Consolidation Time

- The summary plot of an incremental improvement in peak shear stress strengths versus underliner moisture content in Figure 9 show a significant increase in shear strength for wet of OMC underliner soils with respect to an increase in pre-test load consolidation time. Conversely the dry of OMC underliner soils show a minimal increase in shear strength with respect to an increase in pre-test load consolidation time. The summary plot indicates that there is a tradeoff in designing and constructing a dry and firm liner surface (no pore pressure and planar) versus a wet and dimpled or undulating liner surface (some development of pore water pressure and non-planar).

- Excess pore water conditions are difficult to measure in the direct shear box and are beyond the scope of this paper. However the trend toward an "optimum interface shear strength" versus underliner moisture content can be inferred in the Test 1 series (quick test) and the Test 2 to 4 series (longer term load consolidation time).

CONCLUSIONS

The engineering design of geomembrane-lined fill structures such as solid waste landfills, tailings impoundments, and heap leach facilities typically involves the use of a low permeability composite liner system. Composite liner systems generally are comprised of fine-grained silty and clayey soils overlain by a flexible geomembrane liner and overliner drain material. Although the intimate contact between the various components of these composite liner systems provides a highly effective seepage barrier with respect to the vertical migration of leachate or process solutions, they also create a relatively low shear strength interface plane that may be susceptible to instability. The accurate laboratory simulation of field conditions and testing of interface strengths is critical to the successful performance of the lined fill structures.

There are several interrelated factors that influence the liner interface test strength. This paper focused on the changes in moisture content and pre-test load consolidation time versus high load liner interface strengths. The laboratory test results presented in Figures 4 to 9 show a significant increase in the interface strengths with respect to load consolidation time in all of the test series due to apparent micro scale load deformations or "dimpling" of the geomembrane liner surface. This effect is likely to occur in the field as well.

The maximum dimpling effect for any given liner under high load consolidation occurs when large rock sizes are allowed in the granular overliner fill in combination with soft fine-grained silt and clay underliner materials placed at a low density and wet of optimum moisture content. The higher load consolidation strengths gained from the enhanced micro scale dimpling effect on the liner surface may be lost by the lower underliner wet soil shear strengths in addition to increasing the risk of liner rock puncture from liner system elongations and rutting during overliner fill placement. Therefore the selection of an "optimum liner interface strength" for a composite liner system requires some engineering judgment in determining the most appropriate liner type, overliner/underliner soil materials and placement requirements (lift thickness, gradation, plasticity, dry unit weight, moisture content, rock size, rock shape, etc.) to achieve an acceptable balance in the interface shear strength versus a protected low permeability composite liner system.

Engineering experience and judgment are required for selecting the most appropriate test parameters to simulate the site specific existing or planned construction and operation conditions. The measured changes in the interface shear strengths relative to underliner soil moisture content and load consolidation time presented in this paper may help to explain why several liner slope failures occurred early in fill placement operations.

Further test studies of micro scale liner deformation strengths are suggested under both low and high confining stress test loads to determine the range of "optimum interface shear strengths" for the most critical fill loading conditions.

ACKNOWLEDGMENTS

A special thanks to Dr. Zehong Yuan of GeoSyntec Consultants for oversight during the large scale laboratory direct shear testing in accordance with ASTM standards, sometimes pushing the limit of the test equipment to simulate the high design loads, and finding the right kind of glue in earlier tests to keep the geomembrane liners from sliding on the wood blocks.

REFERENCES

Breitenbach, A. J. (1997); "Geomembrane Pad Liner Failures Under High Heap Fill Loads", Geosynthetics '97 Conference, Industrial Fabrics Association International (IFAI), Long Beach, California, Mining Session, Volume 2, pp. 1045 to 1062.

Daniel, D. E. and Wu, Y. (1993); "Compacted Clay Liners and Covers for Arid Sites", Geotechnical Engineering Journal, ASCE, 119(2), pp. 223 to 237.

Estornell, P. and Daniel, D. E. (1992); "Hydraulic Conductivity of Three Geosynthetic Clay Liners", Geotechnical Engineering Journal, ASCE, 118(10), pp. 1592 to 1606.

Hermann, J. G. and Elsbury, B. R. (1987); "Influential Factors in Soil Liner Construction for Waste Disposal Facilities", Geotechnical Practice for Waste Disposal '87, R. Woods, ed., ASCE, pp. 522 to 536.

Matasovic, N., Kavazanjian Jr., E., Augello, A. J., Bray, J. D., and Seed, R. B. (1995); "Soil Waste Landfill Damage Caused by 17 January 1994 Northridge Earthquake", Woods and Seiple, eds., California Department of Conservation, Division of Mines and Geology.

Mitchell, J. K., Seed, R. B., and Seed, H. B. (1990); "Kettleman Hills Waste Landfill Slope Failure, Volume I: Linear Systems Properties", Geotechnical Engineering Journal,
ASCE, 116(4), pp. 647 to 668.

Swan, R. H., Jr., Bonaparte, R., Bachus, R. C., Rivette, C. A., and Spikula, D. R. (1991); "Effect of Soil Conditions on Geomembrane-Soil Interface Strength", Geotextiles and Geomembranes, Vol. 10, pp. 523 to 529.

THE DESIGN OF A REDUCED STRENGTH LANDFILL LINER INTERFACE FOR SEISMIC LOADING CONDITIONS

J. R. LUELLEN
URS GREINER WOODWARD-CLYDE, USA
J. E. DOVE
GEORGIA INSTITUTE OF TECHNOLOGY, USA
R. H. SWAN
GEOSYNTEC CONSULTANTS, USA
M. L. JOHNSON, JR.
GEORGIA INSTITUTE OF TECHNOLOGY, USA

ABSTRACT

The design of Subtitle D containment systems for landfills located in seismically active areas can be complicated by factors such as potential earthquake-induced deformations and the inherent strength limitations of many liner system types. This paper reports results of laboratory investigations to develop an engineered reduced peak strength interface for design of a solid waste landfill containment liner system. A reduced peak strength interface forces any potential seismically-induced deformation to occur above, rather than within, the liner system. Residual strength of this interface must also be great enough to limit deformation of slopes. The design approach consisted of testing combinations of materials to achieve an optimum combination of relatively low peak and high residual shear strengths. Results show that: 1) sand/smooth geomembrane and textured geomembrane/woven geotextile interfaces represent suitable material combinations for a reduced peak strength interface; 2) sand particle shape greatly influences strength behavior; and, 3) contact conditions control shear behavior of sand/geomembrane interfaces.

INTRODUCTION

The potential for damage to a landfill liner system subjected to large deformations by earthquake shaking is significant. Tensile stresses imposed on components of the liner could cause tearing or severe straining of the geosynthetics. Post-earthquake repair of a damaged liner is expensive and disrupts filling operations. As described by Richardson et al. (1998), design of an engineered low strength interface above the composite-geosynthetic landfill liner can minimize the potential for damage from seismically-induced displacements. A reduced peak strength (RPS) interface is placed above the composite liner system to be protected. This "sacrificial" interface has lower peak strength than other interfaces and fails first as deformation-induced shear stresses increase. This interface must also have a relatively small degree of post-peak strain softening to prevent excessive deformation of refuse slopes.

This paper reports results of laboratory investigations to design the RPS interface for a landfill cell in California that will protect the composite liner system from forces induced by horizontal acceleration of an interim unbuttressed fill slope of up to 0.46g from a magnitude 7.2 earthquake. The fill slope will be unbuttressed for a period of four to five years. At the critical design section the cell has 3H:1V slopes, and a 35 m long by 67 m wide floor. The final refuse-fill height over the lined cell will be approximately 27 m.

DESIGN CRITERIA/INTERFACE ALTERNATIVES

The design concept developed for this landfill containment system is based on incorporating a RPS interface above the composite geosynthetic liner system. The composite liner system to be protected consisted of a double nonwoven, needle-punch reinforced GCL placed on prepared native subgrade, overlain by a 1.5 mm high density polyethylene (HDPE) geomembrane. The internal and interfacial shear strengths of the composite liner are designed sufficiently strong to withstand expected shear forces, as discussed below.

To provide for adequate internal shear strength of the GCL, it was required that the GCL exhibit a minimum peel strength of 111 N (25 pounds). The peak internal shear strength GCL used was 30 degrees. Fox et al. (1998) showed that needle-punched GCLs with high peel strengths also possess high peak internal shear strengths. Gilbert et al. (1996) and Fox et al. (1998) demonstrated that GCL peak shear strength failure envelopes are non-linear. However, Richardson (1997) found peak internal shear strength failure envelopes for a needle-punched, reinforced GCL can remain approximately linear over stress ranges up to and exceeding about 478 kPa (10,000 psf).

The GCL was also selected to optimize the value of peak interface shear strength between the GCL and the overlying geomembrane. Project specifications required that the bottom side of the overlying HDPE geomembrane be textured. Studies by Hewitt et al. (1997), Daniel et al. (1998) and Eid and Stark (1997) suggest that peak interface friction angles of non-woven needle punched reinforced GCLs are higher than woven needle punch reinforced or a stitch-bonded woven/nonwoven GCLs when tested against a textured geomembrane

Preliminary static stability analyses of the new cell configuration indicated that a peak shear strength of at least 18 degrees would be required for the RPS interface within the containment system. This analysis was based on use of the GCL and assumed geomembrane texturing characteristics. In order to limit potential seismically-induced displacements of an unbuttressed refuse slope, a post-peak interface friction angle of greater than 14 degrees was required for the RPS interface. This post-peak friction angle is higher than the range of residual interface friction angles typically reported for more conventional geosynthetic interfaces used as "sacrificial" interfaces above liners.

Two interface systems were evaluated for their suitability as the RPS interface. Each system incorporates a layer of sand as the leachate collection/drainage layer beneath the waste. The leachate collection layer is located either as part of, or immediately above interface. The trial interface systems consisted of:

- A 0.3 m thick drainage layer composed of subrounded to rounded sand placed directly on a HDPE geomembrane (smooth upper surface); and,

- A woven geotextile placed above the HDPE geomembrane (textured upper surface). The sand-drainage layer to be placed on top of the geotextile had no roundness requirements for the individual sand grains.

MATERIAL INTERACTIONS

Sand/Smooth-HDPE Geomembrane Interfaces. Recent studies of interface friction mechanisms for a sand/smooth geomembrane interface provide rational basis for evaluating laboratory test data. Figure 1a shows the variation in peak secant friction coefficient resulting from tests on Ottawa 20/30 sand and smooth geomembrane (Dove and Frost, 1999). It may be inferred that the failure envelope for this material combination is non-linear. At normal stresses below 50 kPa, the peak secant friction coefficient decreases with increasing normal stress. The shear mechanism up to about 50 kPa is grain sliding with contact conditions between fully elastic and fully plastic. The decrease in friction coefficient is caused by the small rate of increase in real contact with increasing applied normal stress. The real contact area governs the interface shear force, therefore by definition, the friction coefficient must decrease and the failure envelope is concave downward.

Above a normal stress of about 50 kPa for Ottawa 20/30 sand, the plowing mechanism becomes important. Plowing has been referred to as "scouring" or "polishing" in previous studies. Plowing results when the normal stress reaches a level where the sand grains plastically indent the geomembrane surface. The grains remove the polymer as shear stress is applied thus requiring greater shear force to reach peak state. This increase in shear strength is proportional to normal stress resulting in a concave up failure envelope. The consequence of plowing is that the friction coefficient increases over sliding alone and the geomembrane is permanently scratched or grooved, depending on the shape of the soil particle. The increase in smooth geomembrane surface roughness after shear can be related to the degree of plowing.

Dove and Frost (1999) indicate that particle shape has an important influence on the peak and residual interface friction angles and on which mechanism controls friction behavior. Figure 1b shows that highly angular blasting sand exhibits plowing at all normal stresses with peak interface friction values of up to 28 degrees. However, spherical glass beads exhibited peak friction values of 11 degrees in a sliding shear mode. Subrounded sands exhibited intermediate friction angles of about 21 degrees. Based on the information obtained from these tests, it was inferred that natural sands with subrounded to rounded grains might exhibit favorable peak and residual interface friction behavior for designing the weak interface layer.

Woven Geotextile vs. Textured HDPE Geomembrane Interfaces. Little data could be found by the authors regarding either the peak or residual interface behavior between a woven geotextile and the textured surface of an HDPE geomembrane. However, GRI (1998) data included test results from a single interface direct shear test between a woven geotextile and a smooth HDPE geomembrane. This combination produced a peak interface friction angle of 10 degrees. The interface between a woven geotextile and a textured HDPE geomembrane was selected for further testing for the following reasons:

- A preliminary review of test results from similar projects indicated that the range of peak friction angles expected for the interface between a typical nonwoven geotextile and a textured HDPE geomembrane (25 to 30 degrees) would be too high to permit a nonwoven geotextile to be used as a RPS interface above the liner system;

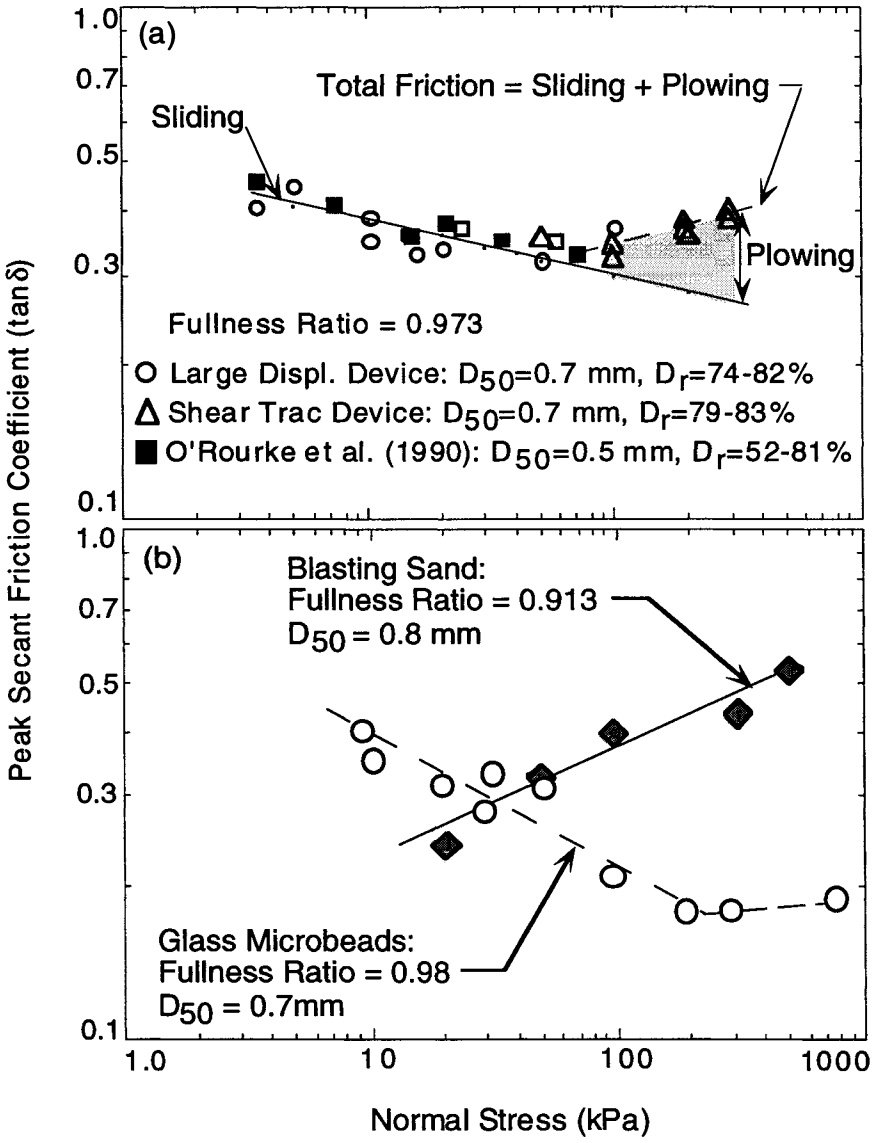

Figure 1. Behavior of Sand/Smooth Geomembrane Interfaces: (a) Ottawa 20/30 Sand; (b) Glass Microbeads and Blasting Sand (after Dove and Frost, 1999)

- A similar review of other test data indicated that the expected peak and residual friction angles for the interface between a typical nonwoven geotextile and a smooth-HDPE geomembrane (typically 9-13 degrees) would be too low to satisfy the project's minimum stability needs; and

- No other combination of geosynthetic interfaces previously known to have been tested (such as a geonet vs. nonwoven geotextile or nonwoven geotextile vs. double-sided geocomposite) appeared to exhibit the appropriate combination of moderately high peak- and relatively high residual-friction angles for this project.

EXPERIMENTAL STUDIES

Sand/Smooth HDPE Geomembrane Interface. A series of three point interface direct shear tests were conducted to evaluate the peak and residual interface behavior of four candidate sands when placed in contact with the smooth HDPE geomembrane surface. Interface tests were initially performed at a testing laboratory in California using a commercially available 300 mm square shear box at normal loads of 47.9 kPa (1,000 psf), 143.7 kPa (3,000 psf), and 287.4 kPa (6,000 psf). Index data for the sands are given in Table 1. The Fullness Ratio (FR) is a measure of grain shape that was determined using a microscope coupled to an image analyzer (D'Andria 1996). For comparison, a FR value of 1.0 is a perfectly round sphere; FR decreases with increasing angularity. One drawback to FR is that it is somewhat dependent on the particle D_{50} and grain size distribution. For two equally angular particles of different size the smaller particle would have the larger FR since the magnification would effectively be lower and would appear more spherical. The sands used herein have relatively small variation in D_{50} thus FR gives a general index of grain shape. The differences in FR would be greatest for angular particles of different sizes with differences decreasing with increasing roundness.

Table 1. Soil Index Data

Sand	D_{50} (mm)	$\gamma_{d\ max}$, kN/m^3 (pcf)	Opt. Moisture (%)	Cu	Fullness Ratio
Arroyo Seco	0.70	16.9 (108.1)	5.3	4.3	0.889
Kaiser-Felton Plant	0.62	18.0 (114.7)	5.7	4.4	0.871
Granite Rock-Quail Hollow	0.64	16.9 (108.1)	5.3	4.4	0.912
RMC-Lapis Plant	0.50	16.0 (102.1)	5.4	2.1	0.953

The sands were placed in the shear box at 90 percent of maximum dry density at optimum moisture content using ASTM Method D 698. The geomembrane was stapled to the back of the shear box in order to constrain the geomembrane and force the failure to occur along a uniform, smooth geomembrane surface. The shearing rate used in each test was 1 mm per minute (0.04 inches per minute). From top to bottom, the test section consisted of: a layer of the selected sand; 60 mil smooth/textured HDPE geomembrane (smooth side against the sand); and a concrete board used as the substrate.

A system performance test using RMC Lonestar-fill sand was conducted at a second laboratory at the same normal loads using a 300 mm square shear box. In this test series, the sand was compacted to 75% percent of maximum dry density at optimum moisture content (ASTM Method D 698). The entire liner system consisting of, a pre-hydrated specimen of double-nonwoven, needle punched GCL, an overlying 60-mil smooth/textured HDPE geomembrane, and an overlying layer of the test sand were included in the shear box test specimen assemblage. The geomembrane was left in a free condition (i.e., the geomembrane was not attached to the shear box in any way). The sand was first soaked for about 30 minutes under no load. Then the entire section was consolidated for 24 hours under each pressure and the entire section was sheared immediately thereafter at 1 mm per minute (0.04 inches per minute).

Woven Geotextile/Textured HDPE Geomembrane Interface. Two woven geotextiles were chosen for laboratory testing: Geotex 315 ST, a polypropylene slit-tape-woven geotextile

manufactured by Synthetic Industries, Chattanooga, Tennessee; and SRW 300, an orthogonal weave, polyester/polypropylene woven geotextile manufactured by TC Mirafi, Pendergrass, Georgia. Each geotextile had a fabric weight of approximately 200 g/m^2. A 300 mm square shear box designed and constructed by one of the authors was used. Tests were performed at a shearing rate of 1 mm per minute.

A series of three point direct shear tests were performed using the 315 ST and the SRW 300 geotextiles against the textured side of a double-sided textured HDPE geomembrane (Geomembrane No. 1). The roughness of the geomembrane was not assessed, however similar specimens of Geomembrane No. 1 have a typical average roughness, R_a, of 0.055 mm (Dove and Harpring, 1999).

To subjectively assess the influence of texturing on interface strength, additional single-point tests were conducted on both woven geotextiles using a HDPE geomembrane (Geomembrane No. 2) at a normal stress of 287.4 kPa (6,000 psf). Similar specimens of Geomembrane No. 2 have a typical average roughness, R_a, of 0.087 mm (Dove and Harpring, 1999).

A system performance test was conducted on the entire liner system to examine shear behavior of the composite section. The base layer consisted of a pre-hydrated specimen of double nonwoven, needle-punched GCL overlain by a 1.5 mm thick smooth/textured HDPE geomembrane.

In all of these woven geotextile/textured geomembrane interface test assemblages, a 50 mm thick layer of poorly graded fine-to-medium grained, angular to subangular sand was included as a superstrate layer over the geotextile. This material was used to simulate expected as-built field conditions, which would include a minimum 0.3 m thick sand drainage layer placed directly over the HDPE geomembrane. During each test, the geomembrane was attached to the back of the lower shear box, and the geotextile was left in a free condition (unattached to the shear box).

RESULTS

Sand/Smooth HDPE Geomembrane Interface Shear Strengths. Strength envelopes from the sand/smooth HDPE geomembrane interface testing are shown on Figure 2. Table 2 provides values of friction and adhesion determined by a conventional linear regression analysis of the data. This interpretation yields friction and "adhesion" values as the slope and intercept, respectively.

The RMC Lonestar fill sand exhibited the lowest peak friction coefficient of the candidate sand materials tested in the higher normal stress ranges. Therefore, this type of sand was found to be favorable for providing moderately low peak friction angles.

An interpretation of the test data using secant friction coefficients is shown on Figures 3 and 4. The secant friction coefficient is determined as the slope of a line connecting the origin of the strength diagram and each stress point. This interpretation permits evaluation of the changes in friction angle and shear mechanism with increasing normal stress. Figure 3 shows the logarithmic plot of peak secant friction coefficient versus normal stress of Figure 1a along

with the data collected from the four sands tested in this study. For comparison, the angular blasting sand used by Dove and Frost (1999) from Figure 1b is included.

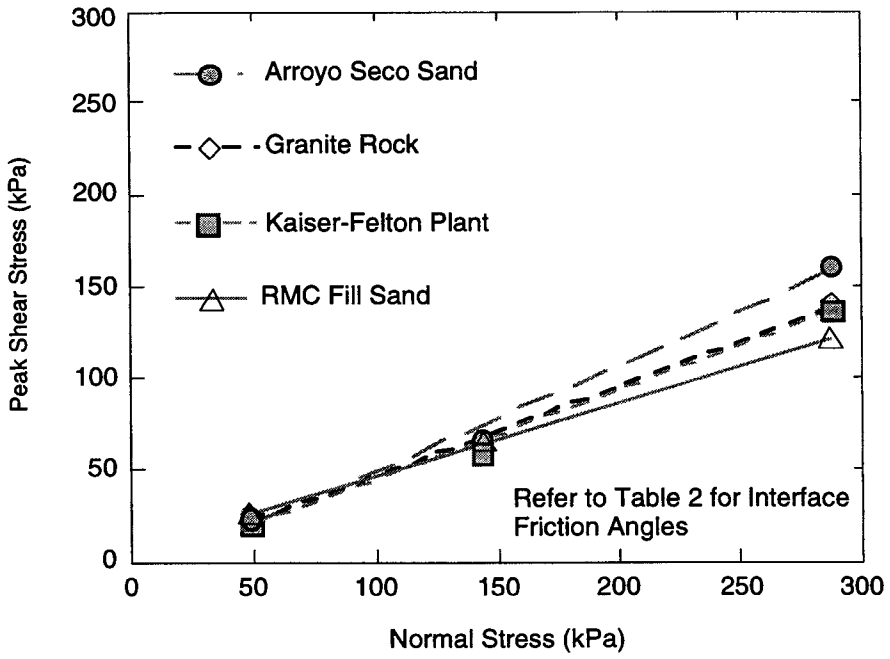

Figure 2. Peak Strength Envelopes from Sand/Smooth Geomembrane Tests

Table 2. - Interface Testing Results For Four Sands Vs. Smooth HDPE Geomembrane Interface (Conventional Interpretation)

Sand/Smooth Geomembrane	Peak Friction Angle (degrees)	Peak "Adhesion" (kPa)	Residual Friction Angle (degrees)
Arroyo Seco	28	0	25
Kaiser -Felton Plant	25	0	19
Granite Rock (Quail Hollow)	26	0	18
RMC Lonestar Fill Sand	22	6.7	14
RMC Lonestar Fill Sand (System test)	21	4.5	20

The candidate sands have FR values ranging from approximately 0.871 to 0.953. Even though the angular blasting sand had FR of 0.913, it is visually more angular than the candidate materials. This discrepancy is probably due to differences in effective magnification with varying D_{50}, as discussed earlier. The FR and the D_{50} of each sand given in Table 1 are also shown on Figure 3.

The friction coefficient of the materials tested in this study exhibit behavior similar to the Ottawa 20/30 sand, as shown in Figure 1a. The decreasing friction coefficient is due to unequal changes in contact area with increasing normal stress as discussed earlier. The slope of a line

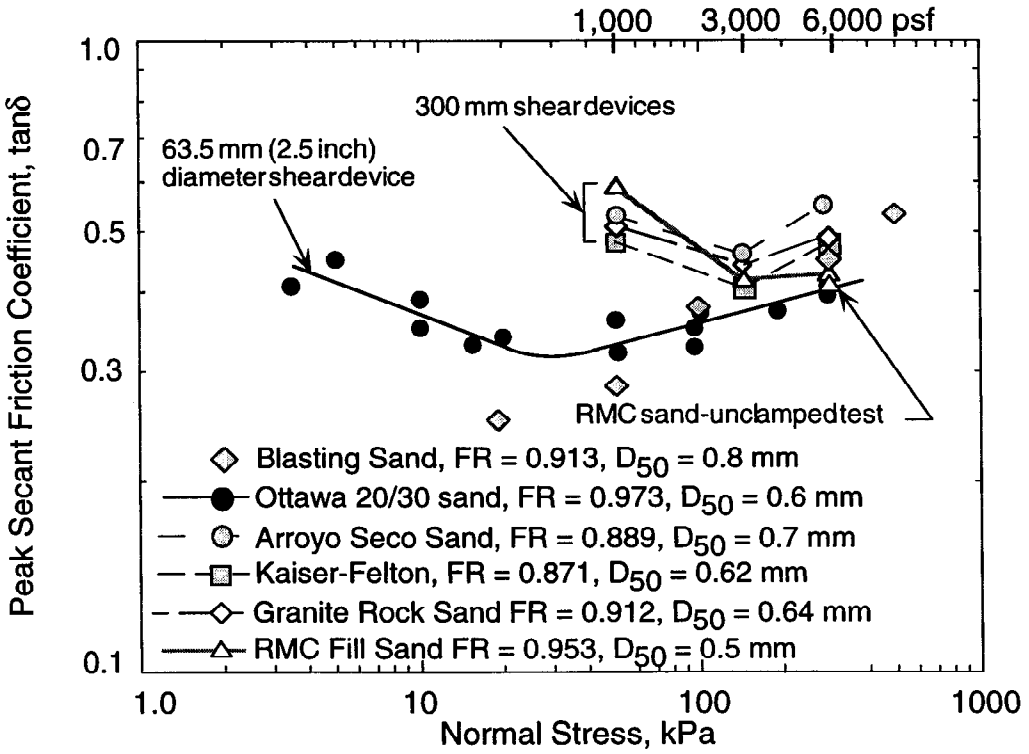

Figure 3. Behavior of Sand/Smooth HDPE Geomembrane Interfaces

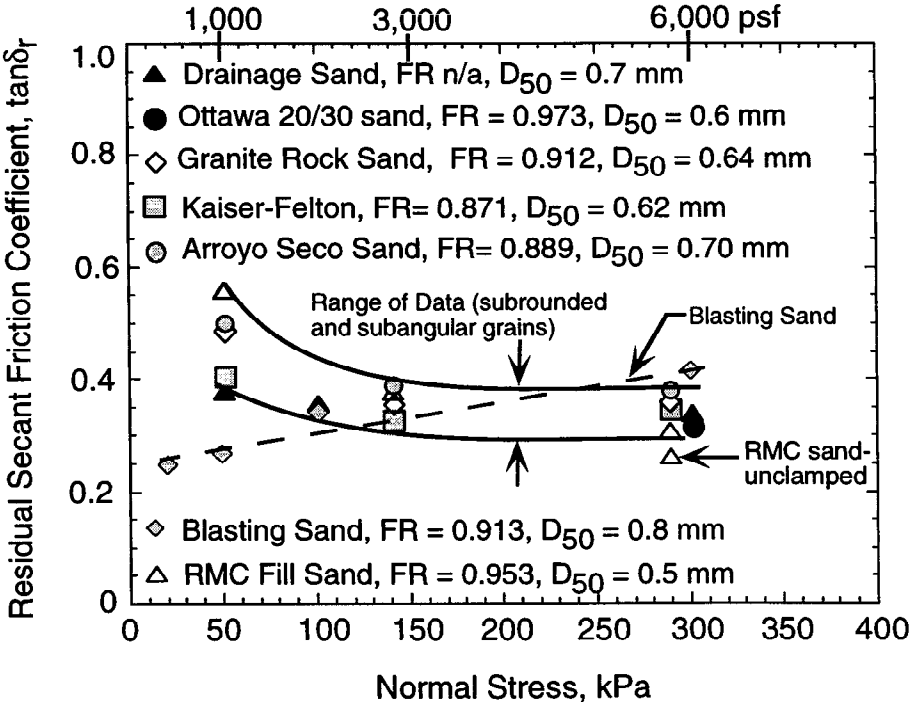

Figure 4. Secant Residual Friction Coefficients

through the data plotted on a logarithmic failure envelope is referred to as the "load index", n. (Dove and Frost, 1999).

The slopes of the sliding portions of the curves shown on Figure 3 is n-1 and ranges from -0.16 to-0.13 for Arroyo Seco, Kaiser, and Granite Rock sands, respectively. The curve for Ottawa 20/30 sand has a slope of -0.12. These slopes indicate that contact conditions are between fully elastic and fully plastic. In contrast, the sliding portion of the RMC fill sand curve of Figure 3 has a slope of -0.32. This means the load index equals 0.68 which corresponds to Hertz theory for elastic spheres. Thus the RMC sand contact conditions below 143.7 kPa are fully elastic, which would be expected with a more spherical particle. Except for the RMC Lonestar fill sand, the materials tested in this study exhibit plowing at higher normal stresses as shown on Figure 3.

Plowing requires additional energy input over that needed for adhesive sliding and results in a higher friction coefficient. Factors controlling the location of the sliding to plowing inflection point are being investigated but are likely related to polymer surficial shear strength and grain contact area. Plowing is discussed in more detail later in this paper.

The RMC fill sand does not exhibit plowing. The nearly constant friction coefficient between 143.7 kPa (3,000 psf) and 287.4 kPa (6,000 psf) is likely due to insufficient particle roughness to tear the polymer. The constant friction coefficient is typical of "plastic" contact conditions where the increase in contact area is directly proportional to normal load. The coefficient of friction in plastic contact will remain constant as long as plowing does not occur.

Figure 4 shows an arithmetic plot of the residual secant friction coefficient vs. normal stress for the sand/smooth HDPE geomembrane interfaces. It shows that grain shape has significant influence on residual friction. For subangular to subrounded sands, residual strengths decrease with increasing normal stress to a fairly narrow range of values at approximately 287.3 kPa. Greater residual strengths are observed at lower normal stresses analogous to peak-state behavior. Behavior of angular-blasting sand is shown for contrast. As normal stress increases, the residual-friction coefficient increases.

The value in examining the system behavior in plots such as Figures 3 and 4 is that the shear mechanism operating for a given particle, geomembrane and normal stress can be determined. Knowledge of the shear mechanism allows the engineer to better anticipate and model expected behavior of the interfaces. Greater benefit is achieved from being able to engineer the materials that produce a desired behavior.

The test results of Figures 3 and 4 indicate that a sand/smooth HDPE geomembrane reduced peak strength interface will likely be limited to sand particles that exhibit a relatively high FR and low angularity. The acceptability of a specific sand/smooth geomembrane interface also may depend on other factors such as geomembrane surface hardness, geomembrane polymer characteristics, field durability of sand grains, and/or the grain-size distribution of the sand particles used. This possibility requires additional interface testing of subrounded to rounded granular materials with different sizes (e.g., gravel). Because of variability in geosynthetic materials and the interface's sensitivity to material surfaces, specific testing should be performed when construction materials are selected. With the ability to quantify and control geomembrane roughness (see Dove and Harpring, 1999), the choice of geomembrane could be made rationally.

Woven-Geotextile/Textured-HDPE-Geomembrane Interface Shear Strengths. Interface-testing results for each geotextile with two differently textured HDPE geomembranes are summarized in Table 3. Friction angles for three-point tests were determined by regression analysis. Friction angles for the single-point tests were obtained by connecting a line from the stress point at 287.3 kPa (6,000 psf) to the plot origin.

Three-point tests on the 315 ST woven slit tape geotextile and Geomembrane No. 1 (less textured) interface resulted in peak and residual friction angle values of 19 and 17 degrees, respectively. When used with the overlying sand drainage layer, these data indicate this geotextile meets the range of friction angles for the engineered weak interface above the GCL-based composite liner system. This material combination could also be used for similar design applications under similar loading conditions.

Table 3 – Test Results-Woven Geotextile/Textured HDPE Geomembrane Interfaces

Woven Geotextile/Textured HDPE Geomembrane	Peak Friction Angle (degrees)	Peak "Adhesion" (kPa)	Residual Friction Angle (degrees)
315 ST slit-tape (3-point test-Gm. No. 1)	19	0	17
315 ST slit-tape (1-point test-Gm. No. 2)	21	0	18
SRW 300 (3-point test- Gm. No. 1)	21	10.8	19
SRW 300 (1-point test- Gm No. 2)	27	0	24

Results of the single-point interface testing conducted using the 315 ST slit-tape geotextile on the highly textured Geomembrane No. 2 gave 21 degree peak and 18 degree residual friction angles, respectively. This suggests this geotextile might be suitable for use with a variety of textured HDPE geomembranes exhibiting widely different degrees of texturing. Additional testing appears to be warranted to determine the peak and residual interface friction behavior of this type of woven geotextile when placed in contact with different textured HDPE geomembranes and using a variety of granular materials having varying grain shapes and sizes and loads as the superstrate layer.

The peak interface friction angle 21 degrees for the three-point system testing on the SRW 300 polyester/polypropylene woven geotextile and Geomembrane No. 1 interface is sufficiently high to meet stability requirements. It is also sufficiently low to permit underlying liner system components to be designed with stronger interface or internal shear strengths. The 19 degree residual friction angle determined for this interface also provides additional resistance to potential seismically induced deformation that might occur along this interface.

The 27 degree peak friction angle and 24 degree residual friction angle of the single point interface test using SRW 300 polyester/polypropylene woven geotextile and Geomembrane No. 2 suggest that this geotextile is not suitable for use with more aggressively textured HDPE geomembranes for the range of normal stresses studied in this investigation. This is because it may be difficult to design all elements of the liner system to be stronger than this interface. To assess peak and residual interface friction behavior, additional interface

testing of this type of woven geotextile in contact with different lightly to moderately textured HDPE geomembranes, is warranted for this application.

It was observed after testing that the finer-grained sand particles penetrated the more loosely woven polyester/polypropylene geotextile material to a greater degree when Geomembrane No. 1 (less textured) was tested than when Geomembrane No 2 (more textured) was used instead. It is possible that the greater abundance of granular particles along the surface of the more textured geomembrane could, to some extent, have affected the resulting interface friction angle values. Additional interface testing of this geotextile using different geomembrane textures and coarser and/or finer grained granular materials is an area for additional study.

System Performance Test. Results of system interface direct shear tests performed using the RMC Lonestar Fill sand/smooth HDPE geomembrane interface are shown on Figure 5. The values of peak interface friction angle obtained for the sand/smooth geomembrane interface fell within the range of values sought for the design. Specifically, the peak interface friction value was sufficiently high to meet stability requirements but also sufficiently low to permit all underlying liner-system components to be designed with stronger interface or internal shear strength properties. Therefore, this value was compatible with a design that forces any potential seismically-induced deformation to occur above, rather than within, the liner system. The relatively high residual interface friction value of 20 degrees helps limit the magnitude of any seismically induced deflections.

DISCUSSION

Evaluation of Plowing. An investigation was made to examine the plowing component of shear resistance. An index of surface roughness was determined perpendicular to the scratches remaining in the geomembrane samples after shear. The scratches begin forming at peak state and can be related to shear strength. Sets of smooth geomembranes used for the sand/geomembrane interface tests were profiled using a Taylor-Hobson Talysurf stylus profilometer. The profiles were 40 mm in length and were filtered to eliminate waviness. The Average Roughness parameter, R_a, was used as the roughness index since it is a standard measure of average profile height. Average spatial and geometric parameters for characterizing geomembranes are more fully discussed in Dove and Harpring (1999).

The average value of R_a for virgin geomembrane surface is 1.7 μm (microns). Increasing normal stress increases the depth and number of surface scratches thereby increasing the value of average roughness, R_a. It may be seen on Figure 6a that angular sands produce the greatest surface roughness. The less angular RMC Lonestar sand causes smaller increase in surface roughness. The data shown on Figure 6b are changes in R_a from the virgin state. From a normal stress of 47.9 kPa (1,000 psf) to 147.3 kPa (3,000 psf) the increase in R_a for the angular sands ranges from 0.3 μm to 0.8 μm. However, from 147.3 kPa (3,000 psf) to 287.3kPa (6,000 psf) the increase for these sands ranges from 1 μm to about 1.5 μm. In contrast, the RMC sand produces only about 0.6 μm total change in R_a, illustrating the influence of grain shape.

By referring to Figures 3 and 4, it may be seen that the degree of increase in surface roughness is related to the secant friction coefficients. Peak friction in sliding was discussed

earlier. Peak friction in plowing is due to initiation of grooves in the geomembrane with higher normal stresses causing deeper penetration and higher initial resistance to displacement.

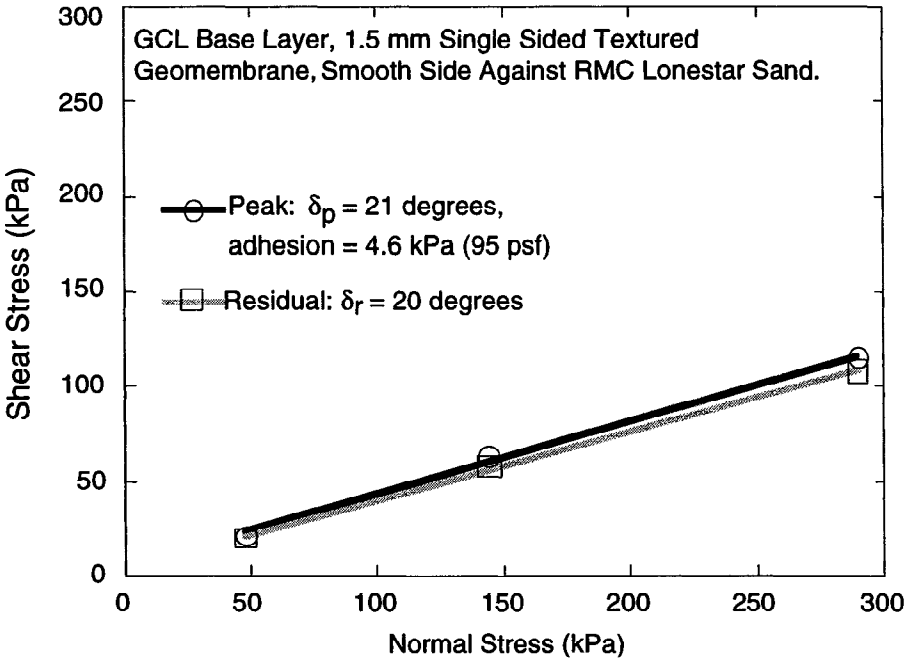

Figure 5. System Performance Test Results

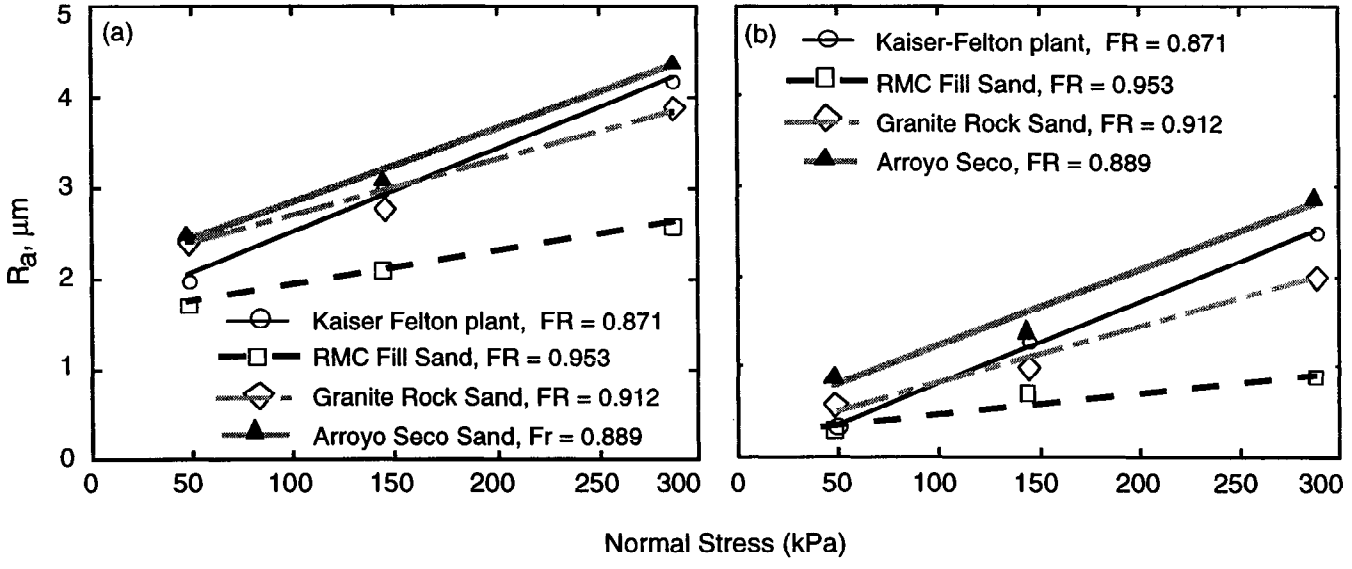

Figure 6. Large Displacement Roughness: (a) After Shear; (b) Change from Initial State

The residual friction coefficient may be controlled by attainment of equilibrium scratch geometry at relatively small shear displacements, contact area changes, and filling of scratches with finer particles. Equilibrium scratch geometry is reached as the vertical contact stresses from the particles are balanced by elastic resistance of the polymer. Once equilibrium scratches are initiated at peak state by leading sand grains, trailing sand grains in the same path do not

shear through the polymer but travel in or closely adjacent to the pre-formed path. Thus post-peak strain softening is pronounced when shear resistance rapidly decreases to a steady value when grooves meet and overlap as displacement increases. The steady state value is determined by the shear strength of the geomembrane within the upper few microns of the surface. This indicates that the most important variable determining system shear strength in the plowing mode is the shear strength of the softer material itself. The cause of the decreasing residual friction with increasing normal stress shown on Figure 4 is not known but is possibly related to variable contact area or test procedures. The plowing process is not fully understood and is the subject of current research.

Inter-laboratory Variations. Differences in peak interface friction and residual interface friction angles of 1 degree and 6 degrees, respectively were observed for the RMC Lonestar fill sand/smooth geomembrane interface between the two testing laboratories. The minor difference in reported peak values is considered to be within the expected range of inter-laboratory variability. The reported difference in residual interface shear strength appeared to be large compared to the typical range of inter-laboratory differences.

Possible reasons include: differences in the height of the gap maintained within the shear box during the interface testing, differences in the type of loading devices used or other apparatus-related factors, and/or differences in testing approaches used by the two laboratories. A larger gap permits a larger amount of sand to extrude from the shear box, which could influence the magnitude and distribution of applied normal load during at large displacements. The first laboratory used a simplified three-layer test specimen test approach whereas the second laboratory used a system performance test approach with all containment system components incorporated. Additional comparative tests by different laboratories using the same test approach would help resolve the importance of the reported differences in peak and residual interface shear strength.

CONCLUSIONS

The following systems were found to be appropriate for a reduced peak strength interface above a composite liner incorporating a GCL at the range of normal loads used herein: (1) woven slit-tape polypropylene geotextile with textured HDPE geomembrane; (2) polyester/polypropylene woven geotextile with textured geomembrane; and, (3) subrounded to rounded sands placed in direct contact with smooth HDPE geomembranes.

An ability to characterize the earth and manufactured materials, and rationally evaluate laboratory data are critical for designing optimum interface strengths for landfill applications. Values of peak and residual interface friction angle for each of the two interfaces of this study allows for: (1) design of a deeper disposal cell cut than originally conceived in preliminary design; (2) a higher interim refuse fill height than previously contemplated; and, (3) the possibility for greater utilization of interim landfill airspace. When properly evaluated, use of either of these interfaces could be used for other waste disposal facilities.

ACKNOWLEDGMENTS

The Georgia Tech research is sponsored by the National Science Foundation under Grant No. CMS-9800291. This support is gratefully acknowledged.

REFERENCES

D'Andria, G.G. (1996). "Development of an Index Test for Granular Materials-The Flow Index Test". Master of Science Thesis, School of Civil and Environmental Engineering, Georgia Institute of Technology, 149 p.

Daniel, D.E., Koerner, R.M., Bonaparte, R., Landreth, R.E., Carson, D.E., and Scranton, H.B. (1998). Slope Stability of Geosynthetic Clay Liner Test Plots. Journal of Geotechnical and Geoenvironmental Engineering, ASCE Vol. 124, No. 7, pp. 628-637.

Day, R.W. (1998). "Discussion: Earth Slide on Geomembrane", Journal of Geotechnical and Geoenvironmental Engineering, Vol. 124, No.7, p. 650.

Dove, J.E. and Frost, J.D. (1999). "Particle-Geomembrane Peak Interface Friction Behavior-Theoretical Considerations and Experimental Results", Journal of Geotechnical and Geoenvironmental Engineering, ASCE, In Press.

Dove, J.E. and Harpring, J.C. (1999). "Average Spatial and Geometric Parameters for Analysis of Geomembrane Surfaces", Proceedings of Geosynthetics '99, Boston, MA, IFAI, In Press.

Eid, and Stark, T. (1997). Shear Strength Behavior of an Unreinforced Geosynthetic Clay Liner. Geosynthetics International, IFAI, St. Paul, Vol. 4, No. 6, pp. 645-659.

Fox, P.J., Rowland, M.G., and Scheithe, J.R. (1998). "Internal Shear Strength of Three Geosynthetic Clay Liners". Journal of Geotechnical and Geoenvironmental Engineering, Vol. 124, No. 10, pp. 933-944.

Geosynthetics Research Institute. (1998). Unpublished GRI test data (07/98).

Gilbert, R.B., Fernandez, F., and Horsfield, D.W. (1996). "Shear Strength of Reinforced Geosynthetic Clay Liner". Journal of Geotechnical Engineering, Vol. 122, No. 4, pp. 259-266.

Hewitt, R.D., Soydemir, C., Stulgis, R.P., and Coombs, M.T. (1997). "Effect of Normal Stress During Hydration and Shear on the Shear Strength of GCL/Textured Geomembrane Interfaces." In: Testing and Acceptance Criteria for Geosynthetic Clay Liners, STP 1308, L.W. Well, Ed., ASTM, pp. 55-70.

Richardson, G.N. (1997). "GCL Internal Shear Strength Requirements". Geotechnical Fabrics Report, IFAI, St. Paul, MN, Vol. 15, No. 2, pp. 20-25.

Richardson, G.N., Thiel, R., and Mackey, R. (1998). "Designing with Needlepunched Reinforced GCLs: Stability Fundamentals". Geotechnical Fabrics Report, IFAI, St. Paul, Mn, Vol. 16, No. 8, pp. 22-27.